



Therapeutic application of PPE2 protein of *Mycobacterium tuberculosis* in inhibiting tissue inflammation

Ravi Pal^{1,2} , Madhu Babu Battu¹ & Sangita Mukhopadhyay^{1,*} 

Abstract

There is an increasing need to develop biological anti-inflammatory agents that are more targeted, effective, and with lesser side effects as compared to conventional chemical drugs. In the present study, we found that *Mycobacterium tuberculosis* protein PPE2 and a synthetic derivative peptide can suppress the mast cell population and inhibit several vasoactive and fibrogenic mediators and pro-inflammatory cytokines induced by mast cells in formalin-induced tissue injury. PPE2 was found to inhibit transcription from the promoter of stem cell factor, important for mast cell maintenance and migration. Thus, PPE2/peptide can be used as a potent nonsteroidal therapeutic agent for the treatment of inflammation and tissue injury.

Keywords fibroblast; inflammation/tissue injury; mast cell; PPE2 protein/peptide; SCF

Subject Categories Immunology; Pharmacology & Drug Discovery

DOI 10.15252/emmm.202114891 | Received 22 July 2021 | Revised 20 June 2022 | Accepted 23 June 2022

EMBO Mol Med (2022) e14891

Introduction

Inflammation is a generic protective biological response toward a harmful stimulus (pathogens, damaged cells, or irritants). Tissue inflammation results in vasodilation followed by the immigration of leukocytes and plasma, resulting in redness, swelling, and pain. Inflammation helps to eliminate the initial causes and clears out necrotic cells and tissues. Local inflammatory responses are beneficial, but at times, they might be harmful to the body. Chronic inflammation leads to greater immigration of immune cells followed by the destruction of tissues, resulting in a pathological condition. Some classical examples of chronic inflammation are rheumatoid arthritis, periodontitis, atherosclerosis, and even cancer (e.g., gallbladder carcinoma).

In most of cases, steroidal and nonsteroidal anti-inflammatory drugs (NSAIDs) are used for treating inflammation. Steroids, mainly

glucocorticoids, represent the standard therapy for inflammatory diseases such as asthma, rheumatoid arthritis, inflammatory bowel disease, and autoimmune disorders. Glucocorticoids bind to glucocorticoid receptors and upregulate transcription of anti-inflammatory genes, for example, *il-10* and *il-1 β* (Barnes, 1998). NSAIDs, like Aspirin, and Diclofenac suppress inflammation by inhibiting cyclooxygenase activity (Inoue *et al*, 2013). Both steroidal and nonsteroidal anti-inflammatory drugs are quite effective but are associated with adverse side effects, especially when used for longer (Marcum & Hanlon, 2010; Wong, 2019).

Irrespective of the cause of inflammation (physical, chemical, or biological), tissue-resident cells are the first ones to sense the abnormality in the microenvironment and signals for generating appropriate responses. Neighboring mast cells are the first cells to sense injury and necrotic tissue (Lunderius-Andersson *et al*, 2012). The role of mast cells in inflammation has been studied extensively (Krystel-Whittemore *et al*, 2015). Necrotic cells activate mast cells by secreting IL-33 (Enoksson *et al*, 2011). Once activated, mast cells release/degranulate anaphylactic mediators/compounds into the local microenvironment (Theoharides *et al*, 2012), which promotes extravasation of leukocytes and plasma, causing redness, swelling, and pain. Mast cell-deficient mice fail to develop arthritis (Nigrovic & Lee, 2005), indicating its important role in inflammation. Therefore, reduction of mast cell activity or mast cell population could be an effective strategy to treat inflammation and its related disorders.

In this study, we show that the administration of recombinantly purified PPE2 protein (rPPE2) or the synthetic peptide derived from PPE2 was able to reduce formalin-induced paw inflammation in Balb/c mice. We observed that rPPE2/peptide administration depletes the mast cell population and thereby reduces mast cell-specific mediators in inflamed paw tissues. We showed that PPE2 inhibits the transcription of the stem cell factor (SCF), which is indispensable for *in situ* survival of tissue-resident mast cells (Finotto *et al*, 1997) as well as for their immigration from the peripheral blood into the tissues (Huang *et al*, 2008). To the best of our knowledge, we, for the first time, have identified a protein and/or peptide that suppress inflammation by inhibiting the mast cell in the paw tissue. As the biologics and immune selective anti-inflammatory derivatives are the promising drug classes that will

¹ Laboratory of Molecular Cell Biology, Center for DNA Fingerprinting and Diagnostics (CDFD), Hyderabad, Telangana, India

² Graduate Studies, Manipal Academy of Higher Education, Manipal, Karnataka, India

*Corresponding author. Tel: +91 40 27216134; E-mail: sangita@cdfd.org.in

play the main role in the market, the present study may be important in identifying a novel molecule with a potent effect in suppressing inflammatory symptoms and tissue injury.

Results

rPPE2 subsides paw inflammation in mice

Earlier we have shown that PPE2 reduces the mast cell population in a murine model of infection (Pal & Mukhopadhyay, 2021). Since the role of mast cells is prominent in tissue inflammation (Lee *et al*, 2002), we hypothesized that recombinantly purified PPE2 protein (rPPE2) can be used as a novel anti-inflammatory drug candidate. To test our hypothesis, we used a formalin-induced paw inflammation model system. A subplantar injection of 5% formalin (20 μ l) was administered in the hind paw of Balb/c mice, and an equal volume of PBS was injected in another paw as control. After 1 h of formalin injection, mice were administered intraperitoneally with a single dose of either rPPE2 (various concentrations) or PBS (vehicle control). Paw inflammation was quantified by measuring edema/swelling for the next three consecutive hours. We observed that rPPE2 was able to reduce redness and swelling in the inflamed paw in a dose-dependent manner, and the best effect was observed with a 3 mg/kg dose (Fig 1A and B). Diclofenac sodium at 10 mg/kg (administered intraperitoneally) was used as a standard control NSAID drug (Yin *et al*, 2016). Next, after 3 h of rPPE2 administration, paw tissues were harvested and tissue sections were stained with hematoxylin and eosin (H&E) stain. We observed marked necrotic debris and cellular infiltration in paw tissues of mice administered with PBS as vehicle control, whereas mice administered with rPPE2 showed lesser necrotic debris and cellular infiltration (Fig 1C and D). A pathology score was calculated in these groups considering swelling, redness, tissue damage, and cells infiltrated in the formalin-injected paw, and the data reveal a reduction in the score in mice treated with rPPE2 as compared to vehicle control (Fig 1E). After 3 h of rPPE2 administration, we examined levels of pro-inflammatory cytokines like TNF- α and IL-6 in paw tissues derived from all the groups by real-time PCR (qPCR) and enzyme immunoassay (EIA). A reduction at the transcript level (Fig 1F and

G), as well as at the protein level (Fig 1H and I) of both TNF- α and IL-6 cytokines, was observed in the paw tissues of rPPE2-administered mice as compared to the vehicle control group. Also, there was a significant decrease in the serum levels of TNF- α and IL-6 cytokines (Appendix Fig S1). Mast cells are essential for neutrophil extravasation in localized inflammation and ablation of mast cell-derived TNF- α abrogates cellular infiltration of leukocytes (neutrophils; Dudeck *et al*, 2021). Among the immigrating leukocytes a heme-containing enzyme, myeloperoxidase (MPO) is released mainly by neutrophils, which is regarded as a biomarker for inflammation (Loria *et al*, 2008). Therefore, next, we compared MPO activity in the paw tissue samples and observed that rPPE2-treated mice had lesser MPO activity as compared to the vehicle control (Fig 1J). This indicates that PPE2 inhibits the recruitment of neutrophils to the inflamed tissue. When rPPE2 (3 mg/kg) was administered at 3, 24, and 48 h after formalin injection, it was found to suppress tissue inflammation at all time points (Fig 1K), suggesting a therapeutic effect of rPPE2 to treat inflammation.

We next investigated the anti-inflammatory activity of rPPE2 in carrageenan-induced paw inflammation. Carrageenan is a plant polysaccharide, and it induces inflammation by activating toll-like receptors (TLRs). Therefore, 1% of lambda (λ)-carrageenan was injected into the hind paw of Balb/c mice via the subplantar route. The same volume of PBS was injected into the other hind paw. After 5 h of carrageenan injection, mice were administered with either PBS (vehicle control) or rPPE2 (3 mg/kg) via intraperitoneal route, and after 3 h, swelling/edema was measured. We observed that rPPE2 suppressed redness and swelling in inflamed paws as compared to PBS (Fig EV1A and B). Next, paw tissue was harvested, and tissue sections were stained with H&E stain. We observed that similar to formalin-induced inflammation, paw tissues from rPPE2-treated mice showed lesser cellular infiltration and edema as compared to paw tissues from PBS-treated mice (Fig EV1C and D).

Formalin induces inflammation by causing necrosis in the tissues. If left untreated, inflammation becomes chronic and causes heavy tissue damage, leading to organ immobility. We observed in the earlier section that rPPE2 (3 mg/kg) administration can suppress inflammation when administered as early as 3 h. Next, we examined the long-term effect of rPPE2 (3 mg/kg) on the suppression of inflammation. To test this, a subplantar injection of 5% formalin

Figure 1. PPE2 subsides paw inflammation in mice.

- A–J A subplantar injection of 5% of formalin (20 μ l) was given in the right hind paw of Balb/c mice, and an equal volume of PBS was injected in the left hind paw. After 1 h of development of edema, mice were administered intraperitoneally with a single dose of either PBS (vehicle control) or Diclofenac (10 mg/kg) or different concentrations of rPPE2 (1 or 2 or 3 mg/kg). (A) Graphical representation of percentage inflammation in paw (paw thickness) was shown. Data were analyzed using one-way ANOVA with Bonferroni *post hoc* test. (B) Representative photographs of inflamed paws after 3 h of treatment. (C) Also, after 3-h post-treatment, mice were sacrificed; the paw sections were prepared and stained with hematoxylin and eosin. Photographs of representative sections were visualized at 20 \times magnification (scale bar = 100 μ m). The solid line represents thickness/edema (B, bone; Ep, epidermis). (D) The cells were counted using ImageJ software and plotted as cells per mm² (cells/mm²). (E) Formalin (20 μ l) was injected in the hind paw of Balb/c mice. After 1 h of development of edema, mice were administered intraperitoneally with a single dose of either PBS (vehicle control) or Diclofenac (10 mg/kg) or rPPE2 (3 mg/kg) and pathology score was calculated after 3 h. (F, G) Three-hour post-rPPE2/Diclofenac/PBS treatment, paw tissue samples were collected for all groups and used for tissue lysate preparation and cDNA synthesis. Next, qPCR was performed to observe transcription levels of TNF- α (F) and IL-6 (G). GAPDH transcript level was used as an internal control. Also, lysates were prepared from paw tissues from all groups, and an equal amount of lysate (500 μ g) from each group was used to determine the levels of TNF- α (H) and IL-6 (I) cytokines by EIA. Same lysates were tested for MPO activity (J), and absorbance at 460 nm was measured. Data are Mean \pm SEM of eight mice per group.
- K A subplantar injection of 5% of formalin (20 μ l) was administered in the right hind paw of Balb/c mice, and an equal volume of PBS was injected in the other paw. After 3 or 24 or 48 h of formalin injection, mice were administered intraperitoneally with a single dose of either rPPE2 (3 mg/kg) or PBS (vehicle control) and after 3 h percentage inflammation in paw was recorded. Data are Mean \pm SEM of six mice per group.

Data information: For (D–K), unpaired *t*-test was applied to calculate *P* values.

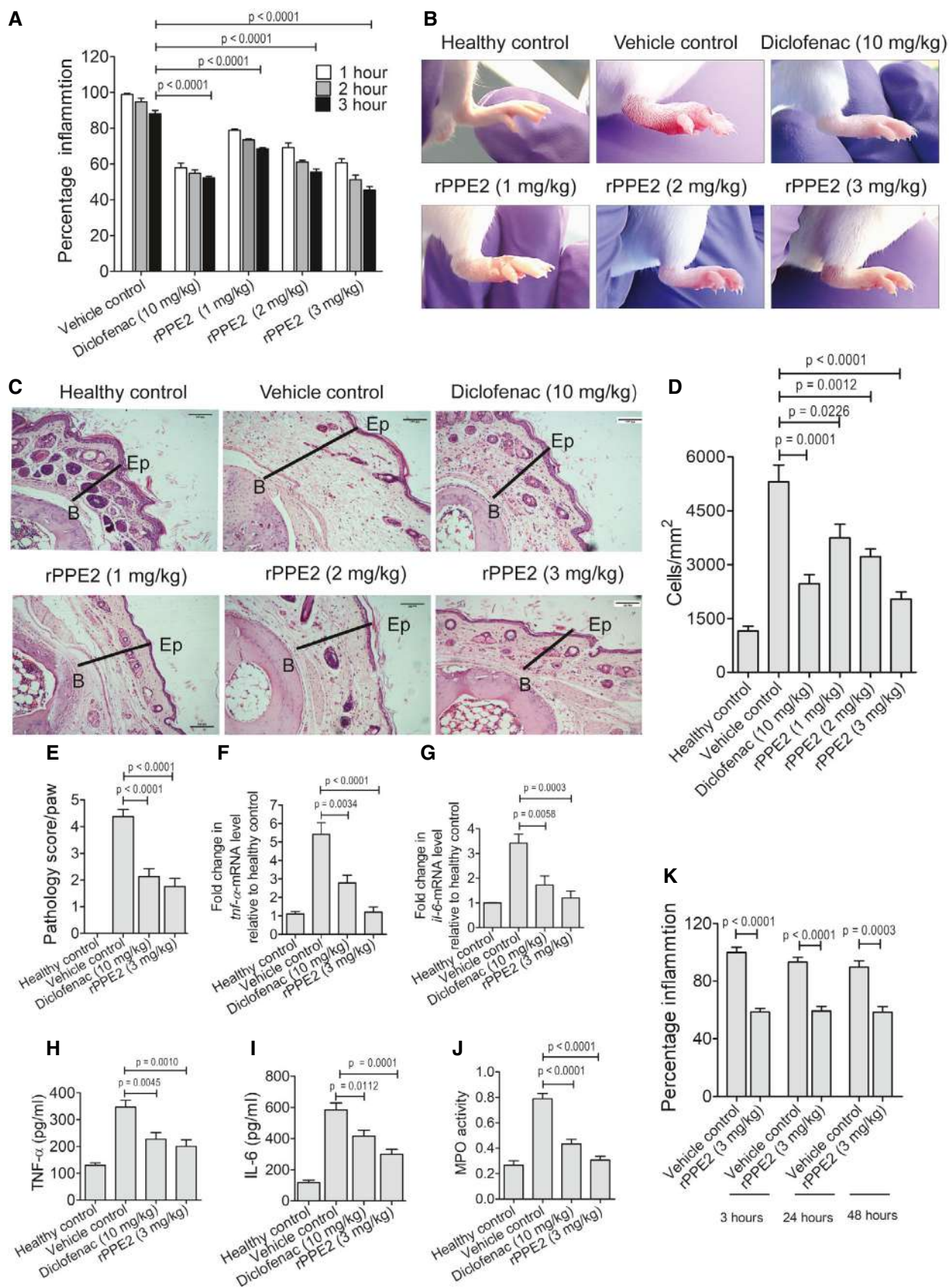


Figure 1.

(20 μ l) was administered in the right hind paw of Balb/c mice and an equal volume of PBS was injected in another paw. After 1 h of formalin injection, a single dose of 3 mg/kg of rPPE2 or equal volume of PBS (vehicle control) was administered intraperitoneally and paw swelling was measured for the next 21 days. Diclofenac at both 3 and 10 mg/kg was used as positive control drug. We observed that mice administered with rPPE2 at 3 mg/kg showed a gradual reduction in paw inflammation (Fig 2A and B). Notably, mice treated with PBS showed severe damage to the paw tissues due to sustained inflammation, whereas rPPE2 administration brought down paw inflammation back to almost normal condition. Diclofenac when used at 3 mg/kg did not have any significant effect on the reduction of swelling of paw tissue; however, at a higher dose (10 mg/kg), it was able to reduce the swelling though not as efficiently as rPPE2 (Fig 2A and B). H&E staining of the paw tissue sections from the various groups revealed that rPPE2-administered mice showed minimal tissue damage or inflammation, whereas mice administered with PBS alone (vehicle control) or 3 mg/kg of Diclofenac showed the extensive presence of necrotic tissues (Fig 2C). Our data indicate that the effect of a single dose of rPPE2 at 3 mg/kg was long-acting and sufficient to subside inflammation and also showed better results as compared to treatment with 10 mg/kg Diclofenac. These results indicate that rPPE2 has both long-term and short-term anti-inflammatory effects.

NSAIDs are often considered as the first line of drugs to treat inflammation (Ong *et al*, 2007). Despite their quick and effective response, usage of NSAIDs often presents various side effects and significantly increases the risks for gastrointestinal bleeding and hepatic and renal malfunctions (Davis & Robson, 2016). To test whether rPPE2 also causes organ cytotoxicity, we injected Balb/c mice with either PBS or PPE2 (3 mg/kg) via the intraperitoneal route for 8 continuous days. Since Diclofenac with only 10 mg/kg dosage was able to subside inflammation to a similar extent as that of 3 mg/kg dose of rPPE2 (Fig 2), we used Diclofenac sodium with 10 mg/kg as a standard NSAID control drug (Gupta *et al*, 2015) for toxicity studies. On day 9, mice from all the groups were sacrificed, and the blood serum was collected to check the levels of aspartate aminotransferase (AST or SGOT), alanine aminotransferase (ALT or SGPT), alkaline phosphatase (ALP) as a measure of liver function, and levels of creatinine, BUN, urea, albumin, and total protein as a measure of kidney function. It was observed that PBS- and rPPE2-administered mice did not show any changes in the levels of the blood biochemical parameters (Fig EV2A–H). Also, the rPPE2-administered group showed no change in any of the clinical features, whereas, as expected, the Diclofenac-treated mice showed significant changes in all the tested parameters. Diclofenac-administered mice showed ruffled fur coats, loss in body weight, and reduced activity upon stimulation. These observations indicate that rPPE2 is safe and does not impart any liver and kidney abnormality even when used for a longer duration.

rPPE2 depletes mast cell population in the inflamed tissue

Mast cells are important for the generation of inflammatory responses. We have shown earlier that PPE2 reduces the mast cell population in a mouse model of mycobacterial infection (Pal & Mukhopadhyay, 2021). Since PPE2 inhibits inflammation, we next

investigated the mast cell population in the paw tissue after rPPE2 treatment. Formalin (5%) was injected into the hind paw of Balb/c mice to induce inflammation. After 1 h of formalin injection, mice were administered with a single dose of either rPPE2 (3 mg/kg) or PBS (vehicle control) via the intraperitoneal route. Diclofenac (10 mg/kg) was used as a standard anti-inflammatory positive control drug. After 3 h of rPPE2 treatment, mice were sacrificed and the paw tissues were harvested. Paw tissues were fixed, stained with Toluidine blue, and the mast cell population in paw in the tissues were counted for each group as described earlier (Sasaki *et al*, 2015). We observed that paw tissues from rPPE2-treated mice showed a significant decline in the mast cell population as compared to those received PBS (vehicle control; Fig 3A and B). Diclofenac did not have any significant effect on the mast cell population (Fig 3A and B). When the cell population from the paw tissues were isolated and analyzed by flow cytometry, we observed a decrease in the mast cell population (CD117⁺, FcεRI⁺) in rPPE2-treated mice as compared to the vehicle control group and Diclofenac-treated mice (Fig 3C and D). This corroborates our histological observations made in Toluidine blue-stained tissue section. We also observed that the paw tissues of rPPE2-administered mice had reduced degranulation in mast cells as compared to the vehicle control (Fig 3E), which is also indicative of the lower inflammation in rPPE2-treated mice.

We have shown earlier that another PE/PPE family protein PPE18 activates IL-10 cytokine and has an anti-inflammatory property (Nair *et al*, 2009; Ahmed *et al*, 2018). The recombinantly purified PPE18 protein (rPPE18) was shown to interact with TLR2 and inhibit LPS-induced TNF- α and IL-12 production with simultaneous upregulation of IL-10 (Nair *et al*, 2009, 2011). Therefore, we tested the ability of rPPE18 to suppress formalin-induced paw tissue inflammation. We observed that rPPE18 (3 mg/kg) was not as effective as rPPE2 (3 mg/kg) to reduce formalin-induced paw inflammation and significantly failed to reduce the mast cell population in the inflamed tissue (Appendix Fig S2). These observations indicate that the anti-inflammatory property of PPE2 lies in its ability to reduce the population of mast cells in the inflamed tissue.

Activated mast cells secrete several mediators into the tissue microenvironment, which include mediators like histamine, serotonin β -hexosaminidase, mast cell proteases, chemokines like MCP-3 (CCL7), mast cell proteases like Mcpt4, kinins, etc., stored in granules as well as mediators, which are *de novo* synthesized like MCP-1, TNF- α etc. (Theoharides *et al*, 2012). Since we found rPPE2 administration reduced mast cell population in the inflamed tissue, we next measured β -hexosaminidase activity and the transcript levels of MCP-3 and Mcpt4 in these tissues. Inflammation was induced in mice hind paws using formalin, and after 1 h, rPPE2 (3 mg/kg) or PBS (vehicle control) was administered. Again after 3 h, mice were sacrificed and paw tissues were analyzed for β -hexosaminidase activity as well as transcript levels of MCP-3 and Mcpt4. We observed that paw tissues from rPPE2-treated mice showed a significant reduction in β -hexosaminidase activity (Fig 3F). Transcript levels of MCP-3 and Mcpt4 were also found to be lower in rPPE2-treated mice as compared to PBS-treated mice (Fig 3G and H). These results indicated that inflammatory mediators were reduced in paw tissues of mice treated with rPPE2. To further demonstrate that PPE2 suppresses formalin-induced tissue inflammation specifically through inhibition of mast cells, we

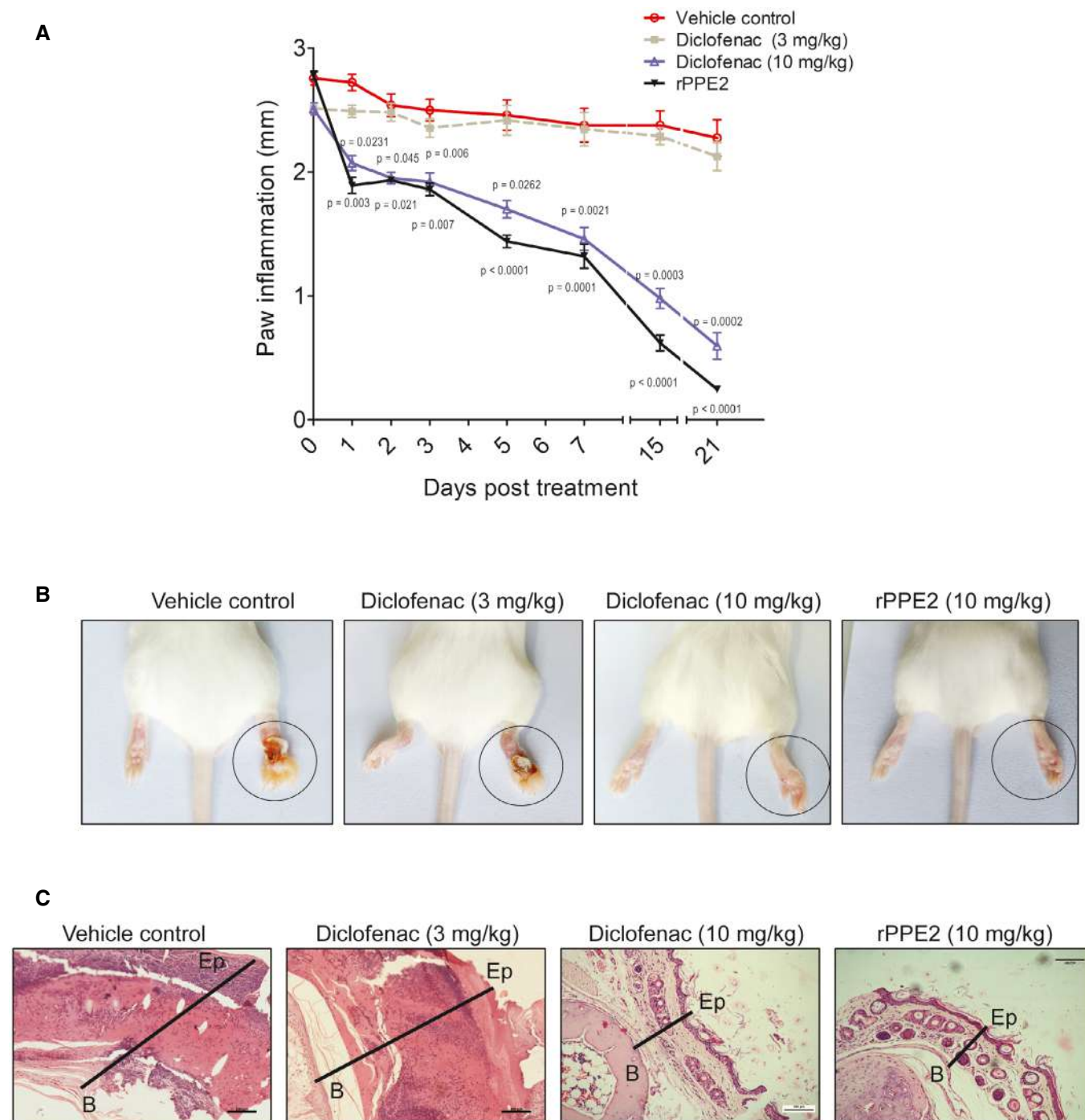


Figure 2. Single dose of rPPE2 prevents chronic inflammation in mice.

A subplantar injection of 5% of formalin (20 μ l) was done in the right hind paw of Balb/c mice, and an equal volume of PBS was injected in the left hind paw. After 1 h of formalin injection, a single dose of rPPE2 (3 mg/kg) or Diclofenac (3 or 10 mg/kg) or PBS (vehicle control) was administered and paw swelling was measured for next 21 days.

A Graphical representation of inflammation (mm) in paws of mice treated with either PBS or Diclofenac or rPPE2. Data shown are Mean \pm SEM of five mice. Statistical analysis was performed between groups treated with rPPE2 versus vehicle control and group treated with Diclofenac versus vehicle control, unpaired t-test was applied to calculate *P* values.

B The representative photographs of inflamed paws after 21 days of post-treatment were shown.

C After 21 days, mice were sacrificed, and the paw tissue sections were prepared and stained with hematoxylin and eosin and photographs of representative sections were visualized at 20 \times magnification (scale bar = 100 μ m). The solid line represents thickness/edema (B, bone; Ep, epidermis).

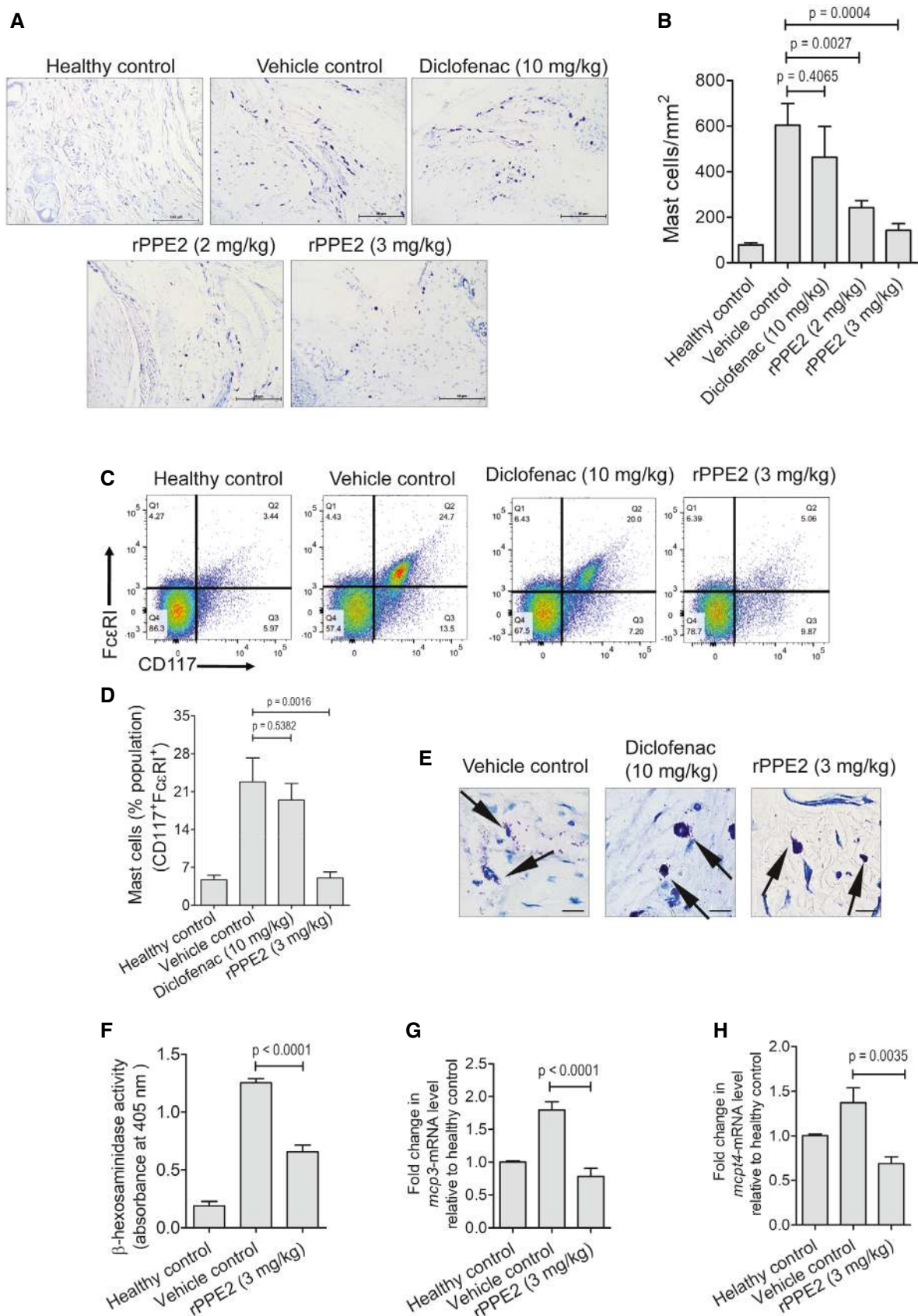


Figure 3.

Figure 3. PPE2 depletes mast cell population in inflamed paw tissue.

A–E A subplantar injection of 5% of formalin (20 μ l) was administered in the right hind paw of Balb/c mice, and an equal volume of PBS was injected in left hind paw. After 1 h of formalin injection, Balb/c mice were treated with a single dose of either PBS (vehicle control) or Diclofenac (10 mg/kg) or different concentrations of rPPE2 (2 and 3 mg/kg) via intraperitoneal route, and after 3 h of treatment, mice were sacrificed and the paw sections were prepared and stained with Toluidine blue to quantify mast cell population. (A) Photographs of representative sections were visualized at 20 \times magnification (scale bar = 50 μ m). (B) Counting of mast cells was performed in Toluidine blue-stained paw sections using ImageJ software and was normalized per unit area (mm²). (C, D) In another experiment, subplantar injection of 5% of formalin (20 μ l) was carried out in the right hind paw of Balb/c mice and equal volume of PBS was injected in another paw. After 1 h of formalin injection, Balb/c mice were injected intraperitoneally with a single dose of either Diclofenac (10 mg/kg) or rPPE2 (3 mg/kg) or PBS (vehicle control), and after 3 h of treatment, mice were sacrificed and the paw tissues were collected and analyzed for mast cell population by flow cytometry using anti-CD117 Ab and anti-Fc ϵ RI Ab (C) and percentage population of mast cells was estimated from flow cytometry (D). (E) Photographs of representative tissue sections stained with Toluidine blue were visualized at 40 \times magnification to observe mast cell degranulation (scale bar = 100 μ m). The arrow indicates the morphology (degranulation) of mast cells.

F–H (F) Lysates from paw tissue were prepared and analyzed for β -hexosaminidase activity at 405 nm optical density (OD). Also, paw tissues from all groups were collected and used for cDNA synthesis; qPCR was performed to observe transcription levels of MCP-3 (G) and Mcpt4 (H). GAPDH transcript levels were used as control.

Data information: Data shown are Mean \pm SEM of eight mice. For (B, D, F–H), unpaired t-test was applied to calculate *P* values.

performed a mast cell transplantation experiment, where bone marrow-derived mast cells (BDMCs) were purified (with > 95% purity, Fig 4A) and injected into the paw of rPPE2-treated mice via subplantar route as described elsewhere (Lee *et al*, 2002; Patel *et al*, 2016; Habuchi *et al*, 2021). When the percentage of inflammation in paw tissue was measured, an increased inflammation was observed in rPPE2-treated mice that were injected with bone marrow-derived mast cells when compared to rPPE2-treated mice that did not receive any mast cells (Fig 4B and C). It appears that subplantar injection of excess BDMCs to the site of inflammation overwhelmed the protective effect of rPPE2. This indicates that rPPE2 specifically targets mast cells for its anti-inflammatory properties. As expected, elevated levels of TNF- α (Fig 4D) and IL-6 (Fig 4E) cytokines, as well as increased MPO (Fig 4F) and β -hexosaminidase activities (Fig 4G), were observed in rPPE2-treated mice that received mast cells when compared to rPPE2-treated mice receiving no mast cells. These studies together confirmed that PPE2 suppressed inflammation by specifically targeting the mast cells to the inflamed tissue.

To further investigate whether rPPE2 has any direct effect on the activation of mast cells, we used a mast cell line, RBL-2H3, and measured β -hexosaminidase activity, and MCP-3, Mcpt4 transcript levels in the presence or absence of rPPE2. For this, RBL-2H3 cells were activated by lipopolysaccharide (LPS; Yang *et al*, 2012), and after 1 h, cells were treated with rPPE2 (3 μ g/ml) for 3 h. Cells were harvested, stained with Toluidine blue, and observed under a light microscope. No significant visible difference in the degranulation of LPS-activated mast cells was observed in the presence or absence of rPPE2 (Fig EV3A). Also, no significant changes in the β -hexosaminidase activity, as well as transcript levels of MCP-3 and

Mcpt4, were observed in rPPE2-treated cells when compared to the untreated controls (Fig EV3B–D). These results indicate that rPPE2 does not have a direct effect on mast cell activation. Also, MTT assay results showed that rPPE2 did not have any direct cytotoxic effect on the mast cells (Fig EV3E and F).

rPPE2 is present at the site of injury and localizes to the nucleus of fibroblasts

To test the physical presence and localization of rPPE2 in the inflamed paw tissues, we injected rPPE2 (3 mg/kg) intraperitoneally in mice and after 1 h of administration of rPPE2, paw tissues were harvested and analyzed for localization of PPE2 by confocal microscopy. We observed positive staining for PPE2 (green) predominantly in the dermal and hypodermal region of the inflamed paw tissue, which are rich in fibroblast cells (Fig 5A). PBS-injected mice were used as vehicle control. This indicates that PPE2 is present at the site of inflammation after its administration. Notably, PPE2 was seen in the nucleus (red) of the majority of the cells of the paw tissue.

We had reported earlier that PPE2 protein has a leucine zipper DNA-binding motif and a functional nuclear localization signal (Bhat *et al*, 2017). In the present study, PPE2 localization was observed in the hypodermal and dermal regions of the paw tissue (Fig 5A), which happens to be the anatomical location of the tissue fibroblasts. Also, PPE2 was found to be localized in the nucleus (red) of the majority of the cells of the paw tissue. Therefore, next, we used NIH-3T3 fibroblasts to observe the nuclear localization of PPE2. NIH-3T3 fibroblasts were treated with rPPE2, and after 45 min, cells were harvested and analyzed for PPE2 localization by

Figure 4. Subplantar injection of mast cells restores inflammation in rPPE2-treated mice.

A Mast cells were enriched from the bone marrow of the Balb/c mice in the presence of SCF and IL-3.

B A subplantar injection of 5% of formalin (20 μ l) was carried out in the right hind paw of Balb/c mice, and an equal volume of PBS was injected in another paw. After 1 h of formalin injection, Balb/c mice were treated with a single dose of either Diclofenac (10 mg/kg) or rPPE2 (3 mg/kg) or PBS (vehicle control) via intraperitoneal route. After 3 h of treatment, about 1×10^6 mast cells were injected via subplantar route. After 3 h of mast cell injection, the percentage inflammation was measured and the paw tissues were harvested. Representative photographs of inflamed paws after 3 h of mast cell injection.

C Graphical representation of percentage inflammation in paw (paw thickness) was shown.

D–G Next, tissue lysates (500 μ g) were prepared and the levels of TNF- α (D), IL-6 (E) were measured by EIA. In the same lysate samples, MPO activity (F) and β -hexosaminidase activity (G) were measured.

Data information: Data shown are Mean \pm SEM of eight mice. For (C–G), unpaired t-test was applied to calculate *P* values.

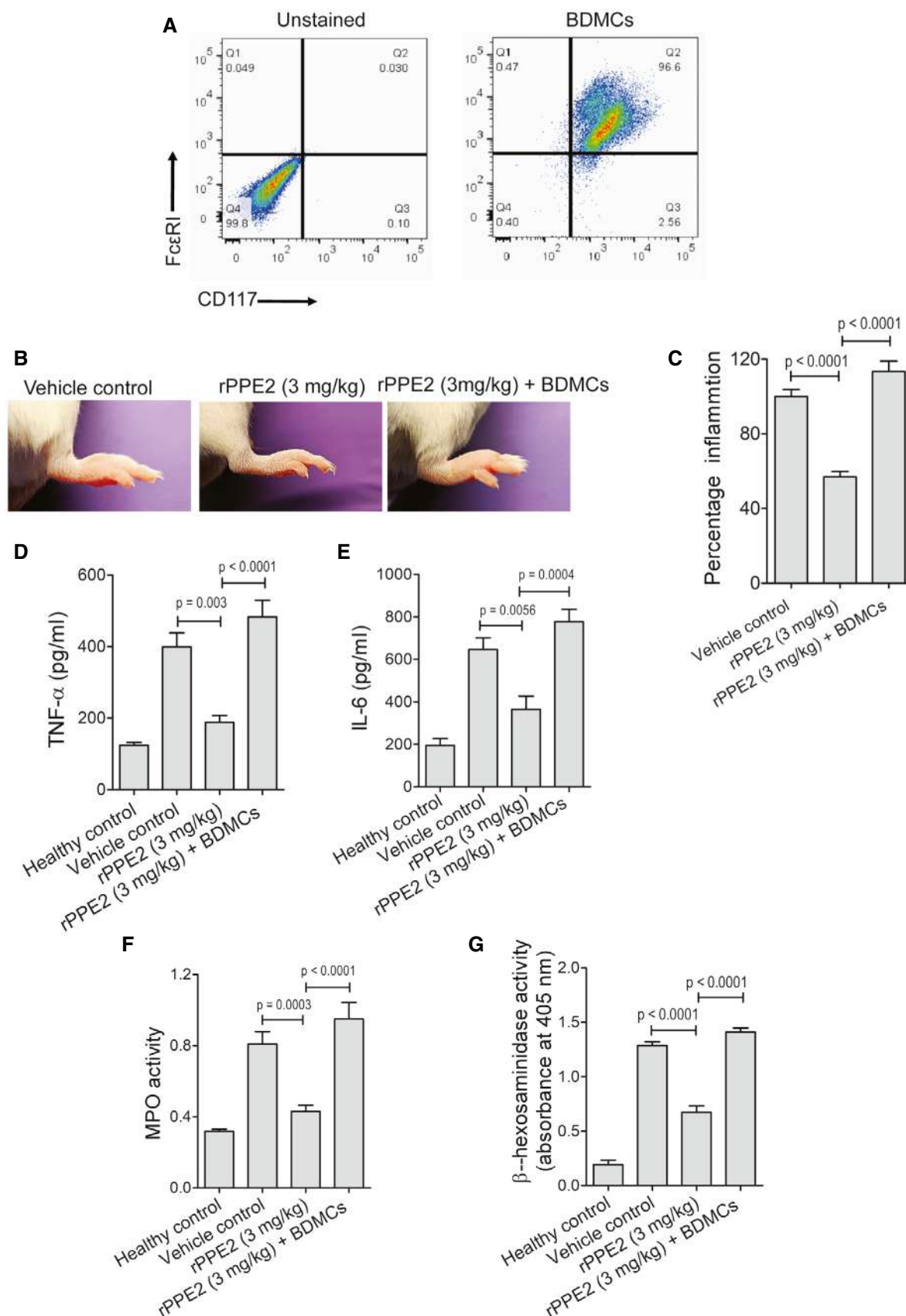


Figure 4.

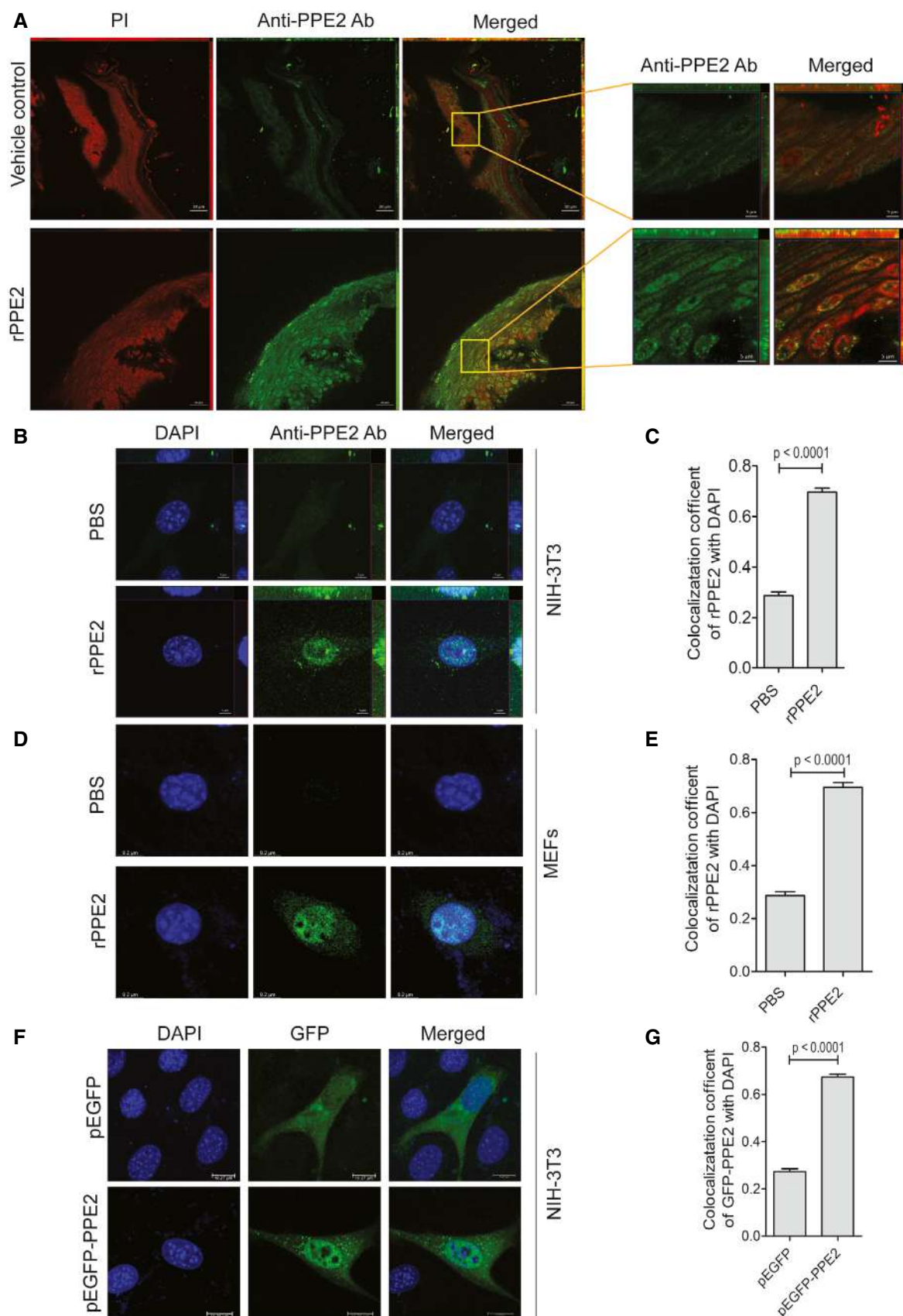


Figure 5.

Figure 5. PPE2 localizes to fibroblast nucleus.

- A A subplantar injection of 5% of formalin (20 μ l) was done in the right hind paw of Balb/c mice, and an equal volume of PBS was injected in left hind paw. After 1 h of formalin injection, mice were administered with either PBS (vehicle control) or rPPE2 (3 mg/kg, single dose) via the intraperitoneal route. After 1 h of rPPE2 treatment, mice were sacrificed and the paw sections were prepared. Next, paw tissue samples were deparaffinized, subjected to antigen retrieval, and were stained with anti-PPE2 Ab, and observed under a confocal microscope. Propidium iodide (PI) was used to stain the nucleus. (scale bar = 20 μ m).
- B–E In another experiment, NIH-3T3 cells (B, C) or MEFs (D, E) were incubated with either PBS or rPPE2 (3 μ g/ml). After 45 min of rPPE2 treatment, cells were fixed, permeabilized, and stained with anti-PPE2 Ab. DAPI was used to stain the nucleus. Nuclear localization of rPPE2 in NIH-3T3 (C) and MEFs (E) was measured by calculating the colocalization coefficient.
- F, G (F) NIH-3T3 cells were transiently transfected with either pEGFP or pEGFP-PPE2. After 24 h of transfection, cells were fixed and observed under a confocal microscope. DAPI was used to stain the nucleus. (G) Nuclear localization of rPPE2 was measured by calculating colocalization coefficient.
- Data information: Data represent Mean \pm SEM of more than 50 cells of three independent experiments. For (C, E and G), unpaired t-test was applied to calculate P values.

confocal microscopy. We observed that PPE2 was translocated to the nucleus of NIH-3T3 fibroblast (Fig 5B and C). Similarly, PPE2 was also found to translocate into the nucleus of another fibroblast cell line, mouse embryonic fibroblasts (MEFs) indicating that PPE2 can get translocated into the nucleus of fibroblast (Fig 5D and E). Similar results were also observed when NIH-3T3 cells were transfected with plasmid-carrying PPE2 fused with GFP (pEGFP-PPE2) as EGFP-tagged PPE2 showed enhanced localization in the nucleus as compared to cells transfected with pEGFP alone (Fig 5F and G).

rPPE2 inhibits *scf* transcription by binding to *scf* promoter

Fibroblast-mast cell communication is important for *in situ* survival and function of mast cells (Majety *et al.*, 2015). Tissue-resident fibroblasts secrete SCF (stem cell factor), which binds to SCF receptor (SCFR) present on the mast cells surface. SCF and SCFR interaction is essential for the survival of tissue-resident mast cells. SCF is also crucial for the migration of mast cells from peripheral blood to the tissue (Okayama & Kawakami, 2006). Since rPPE2 administration was able to reduce mast cell population, we next investigated the levels of SCF transcripts by qPCR in formalin-injected paw tissues of mice treated with rPPE2. A significant decrease in the SCF transcripts levels was observed in the paw tissues of mice treated with rPPE2 as compared to mice received PBS (vehicle control) as well as Diclofenac (Fig 6A).

To further ascertain whether PPE2 actually inhibits SCF induction in fibroblast cells, we used NIH-3T3 fibroblast cell line and

measured the levels of SCF transcripts by qPCR. Accordingly, NIH-3T3 fibroblasts were pre-treated with LPS for 30 min and then either left untreated or treated with rPPE2 (3 μ g/ml) for 3 h. We observed that cells co-treated with LPS and rPPE2 had reduced levels of SCF transcript as compared to the cells treated with LPS alone (Fig 6B). These results confirm that PPE2 actually inhibits SCF in fibroblast cells.

In the earlier section, we demonstrated that rPPE2 was able to localize in the nucleus of NIH-3T3 fibroblasts and suppress SCF transcription. In our earlier study, we found that PPE2 sterically inhibits *inos* transcription by directly interacting with the GATA-1 elements present proximal to the TATA box in the *inos* promoter (Bhat *et al.*, 2017). Therefore, we next checked the promoter activity of SCF in presence of PPE2. The eukaryotic promoter database (EPD) was used to predict the promoter region of the *scf* gene (Périer *et al.*, 2000). EPD predicted a 60 bp of DNA (chr10:100,015,778–100,015,837) as the putative core promoter region. To include additional regulatory elements, we selected promoter fragments of 600 bp (–500 bp, +100 bp), 400 bp (–300 bp, +100 bp), and 200 bp (–100 bp, +100 bp) surrounding the transcription start site (TSS). These promoter fragments were cloned separately into a promoter-less vector, pGL3 (basic vector), and co-transfected with pEGFP into NIH-3T3 fibroblast for analyzing promoter activity via luciferase activity. We observed that all three constructs showed positive luciferase activity as compared to the vector control (Fig EV4A and B). Cell lysates from these groups were also used to check the expression levels of GFP protein by Western

Figure 6. PPE2 inhibits *scf* transcription by binding to *scf* promoter.

- A A subplantar injection of 5% of formalin (20 μ l) was done in the right hind paw of Balb/c mice, and an equal volume of PBS was injected in left hind paw. After 1 h of formalin injection, mice were administered with either a single dose of Diclofenac (10 mg/kg) or rPPE2 (3 mg/kg) or PBS (vehicle control) via intraperitoneal route. After 3 h, paw tissues were harvested and used for cDNA synthesis. Next, qPCR was performed to observe transcription levels of SCF. GAPDH transcript level was used as an internal control. Data shown here are Mean \pm SEM of eight mice.
- B NIH-3T3 cells were activated by LPS (1 μ g/ml) and after 30 min, cells were treated with rPPE2 (3 μ g/ml) for 3 h. Cells were then harvested for cDNA synthesis and qPCR was performed to observe transcription levels of SCF. GAPDH transcript level was used as an internal control. Data shown are Mean \pm SEM of three independent experiments.
- C NIH-3T3 cells were co-transfected with pGL3-SCF and pEGFP. After 24 h of transfection, cells were treated with rPPE2 (3 μ g/ml)/PBS. The control group received the empty vector (pGL3) alone. After 3 h of treatment with rPPE2/PBS, cells were harvested and analyzed for luciferase activity. Data shown are Mean \pm SEM of three independent experiments.
- D Lysates prepared from the same samples used in C were resolved on SDS–PAGE and checked for GFP expression by Western blotting using anti-GFP Ab. GAPDH was used as a loading control.
- E Varying concentrations of rPPE2 protein were incubated with [γ - 32 P]-ATP oligonucleotides of 60 bp spanning SCF promoter. DNA-protein complexes were resolved on 7% native polyacrylamide gel. In cold competition reactions, equimolar cold/unlabeled 60 bp oligonucleotides were used (arrow represents PPE2-oligo complex). The data shown are representative of three independent experiments.

Data information: For (A–C), unpaired t-test was applied to calculate P values.

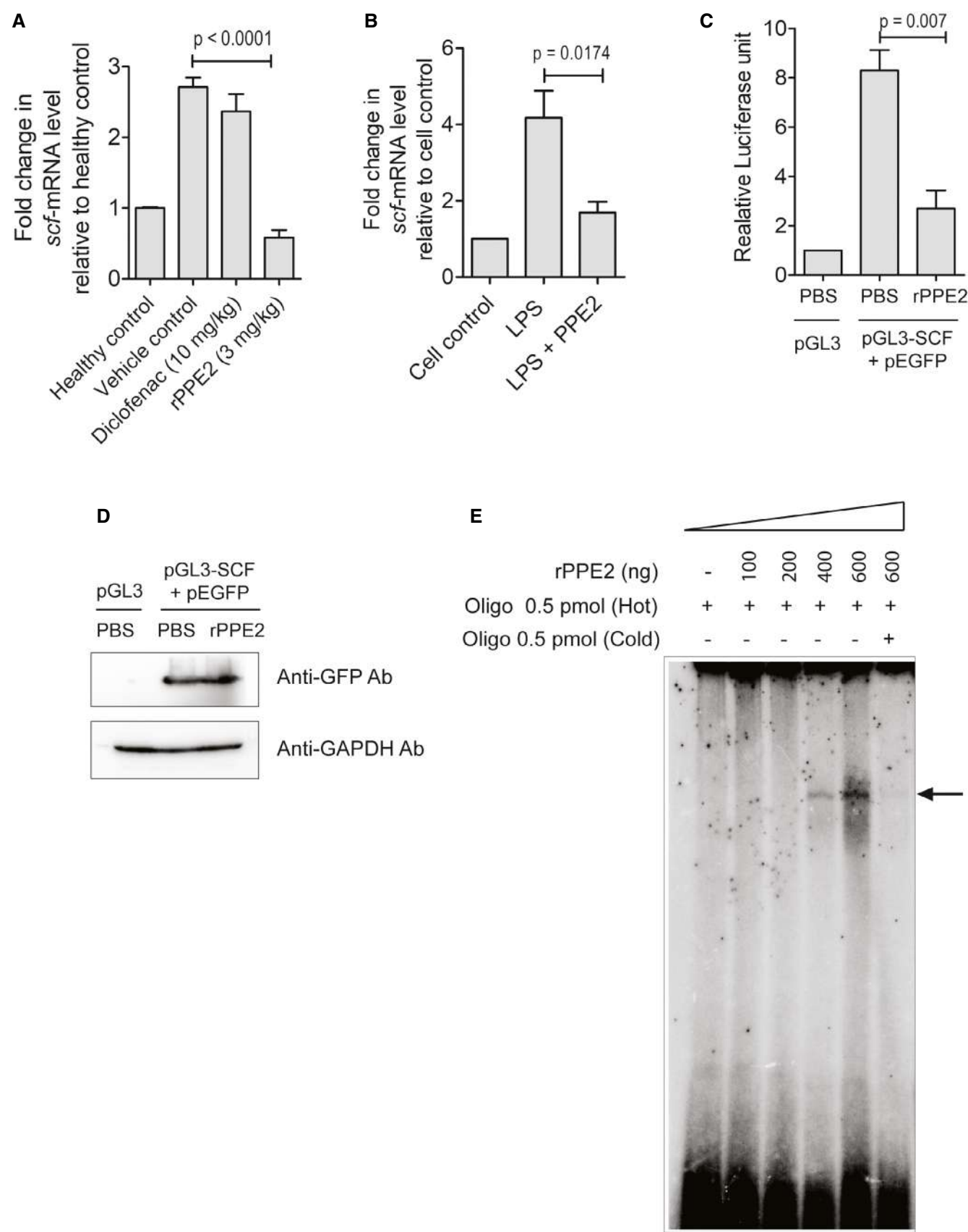


Figure 6.

blotting using an anti-GFP antibody (Ab) to ensure that all the groups had equal transfection efficiency (Fig EV4C). We proceeded with the shortest 200 bp (pGL3-SCF) promoter region for our next experiments. To see the effect of PPE2 on SCF promoter activity, we co-transfected NIH-3T3 fibroblasts with pGL3-SCF and pEGFP. The control group received the pGL3 empty vector alone. After 24 h, pGL3-SCF transfected cells were treated with either PBS or rPPE2 (3 µg/ml) for 3 h. Cells were next harvested and analyzed for luciferase activity. We found that cells treated with rPPE2 showed reduced luciferase activity as compared to PBS control (Fig 6C). Cell lysates from these groups were used to check the levels of GFP protein by Western blotting using anti-GFP Ab, which indicates equal transfection efficiency (Fig 6D). Taken together, these studies indicate that PPE2 inhibits the promoter activity of SCF. Since earlier we found that PPE2 binds to the *inos* promoter, we speculated a similar mechanism of transcriptional inhibition for the *scf* promoter also. Therefore, we next examined whether PPE2 physically interacts with the exact core 60 bp promoter predicted by the EPD using electrophoretic mobility shift assay (EMSA). An increasing concentration of recombinantly purified PPE2 was incubated with 60 bp radiolabeled duplex oligonucleotides encompassing the core promoter element and loaded onto the gel. We observed that rPPE2 binds to the 60 bp core promoter region in a concentration-dependent manner (Fig 6E), indicating that rPPE2 inhibits *scf* promoter activity in a way similar to that of *inos* promoter. Therefore, we speculate that rPPE2 enters into the nucleus of the fibroblast and sterically inhibits promoter activity of SCF by directly interacting with its core promoter and hence its transcription.

A synthetic peptide derived from PPE2 subsides paw inflammation in mice

Next, we aimed to design a short peptide sequence from PPE2 for easy cellular delivery. According to the ScanProsite tool (<https://prosite.expasy.org/scanprosite/>), PPE2 possesses a putative leucine zipper. Based on the nuclear localization ability and DNA-binding activity of PPE2 to *scf* promoter, we designed a synthetic peptide of 36 amino acids by combining putative leucine zipper (KTLLEQ-TLALLPAALPLLAAPLPLTL) and nuclear localization signal (RRRRPKIKQ; Fig EV5A and B). To further gain insight into the DNA-binding ability of the peptide, we performed *in silico* analysis. The peptide was modeled based on the homology using MODELLER 9.23 (Webb & Sali, 2016). The model was validated by the

Ramachandran plot (Fig EV5C and D) showing that all the residues fall in the allowed regions. The modeled peptide was docked with the 60 bp of SCF promoter DNA sequences using the online tool HDock (Yan et al, 2017; Fig EV5E).

The anti-inflammatory activity of PPE2-derived synthetic peptide was assessed using paw inflammation as a model system. Balb/c mice were injected with 5% formalin in the right hind paw. After 1 h of formalin injection, a single dose of the peptide or PBS (vehicle control) was administered to the mice via the intraperitoneal route at varying concentrations (1, 4, and 8 mg/kg). Paw edema/swelling was measured after 3 h of peptide administration. We observed that similar to the recombinant PPE2 protein, the peptide was also able to reduce edema and redness as compared to the PBS (vehicle control) in a dose-dependent manner and the best effect was observed with an 8 mg/kg dose (Fig 7A and B). Next, the paw tissues were harvested from control- and peptide- (8 mg/kg) treated groups, and tissue sections were stained with H&E dye. We observed that necrotic debris and infiltration of cells were lesser in mice treated with peptide as compared to mice treated with PBS (vehicle control; Fig 7C). Paw tissues were also harvested to check the levels of TNF-α and MPO activity as hallmarks of inflammation. We observed a significant reduction in the mRNA levels of TNF-α, and also MPO activity was found to be significantly low in mice treated with the peptide as compared to the vehicle control (Fig 7D and E).

The long-term effect of the peptide on suppressing inflammation was also studied. Therefore, Balb/c mice with formalin-induced edema were injected intraperitoneally with either PBS (vehicle control) or peptide (8 mg/kg), and paw swelling was measured for the next 21 days. Mice administered with peptide showed a gradual and significant reduction in paw inflammation (Fig 7F and G) as compared to vehicle control. Only a single dose of the peptide was found to be sufficient to subside inflammation for a longer duration. Taken together, it was concluded that the peptide derived from PPE2 also possesses anti-inflammatory activity and can suppress inflammation in both acute and chronic inflammation conditions.

The synthetic peptide derived from PPE2 suppresses SCF transcription and mast cell population in paw tissue

Next, we studied whether the PPE2-derived peptide can also target *scf* gene transcription in the mast cell. Therefore, 5% formalin was injected in the hind paw of Balb/c mice to induce paw inflammation in the absence or presence of 8 mg/kg peptide. After 3 h of peptide

Figure 7. PPE2-derived synthetic peptide subsides paw inflammation in mice.

- A–E A subplantar injection of 5% of formalin (20 µl) was administered in the right hind paw of Balb/c mice, and an equal volume of PBS was injected in the left hind paw. After the development of edema at 1 h time point, mice were administered intraperitoneally with a single dose of either PBS or different concentrations of peptide. (A) After 3 h, mice were examined for paw thickness, and percentage inflammation was plotted. (B) Representative photographs of inflamed paws after 3 h of peptide (8 mg/kg) treatment were shown. (C) These mice were next sacrificed and the paw sections were prepared and stained with hematoxylin and eosin, and photographs of representative sections were visualized at 20× magnification (scale bar = 100 µm). The solid line represents thickness/edema (B, bone; Ep, epidermis). (D) Three hours post-PBS/peptide treatment, paw tissue samples were collected and used for cDNA synthesis. Next, qPCR was performed to observe transcription levels of TNF-α. GAPDH transcript level was used as an internal control. (E) Also, lysates were prepared from paw tissues and 50 µg of tissue lysate was used for testing MPO activity, and absorbance was measured at 460 nm. Data shown are Mean ± SEM of eight mice per group. For (A, D and E) unpaired *t*-test was applied to calculate *P* values.
- F, G In another experiment, a subplantar injection of 5% of formalin (20 µl) was given in the right hind paw of Balb/c mice, and an equal volume of PBS was injected in left hind paw. (F) After 1 h of formalin treatment, peptide (8 mg/kg) was administered and paw swelling was measured for the next 21 days. (G) Representative photographs of inflamed paws after 21 days of peptide treatment. Data shown here are Mean ± SEM of five mice. For (F) paw inflammation following treatment with peptide versus PBS at various days was compared using one-way ANOVA with Bonferroni *post hoc* test.

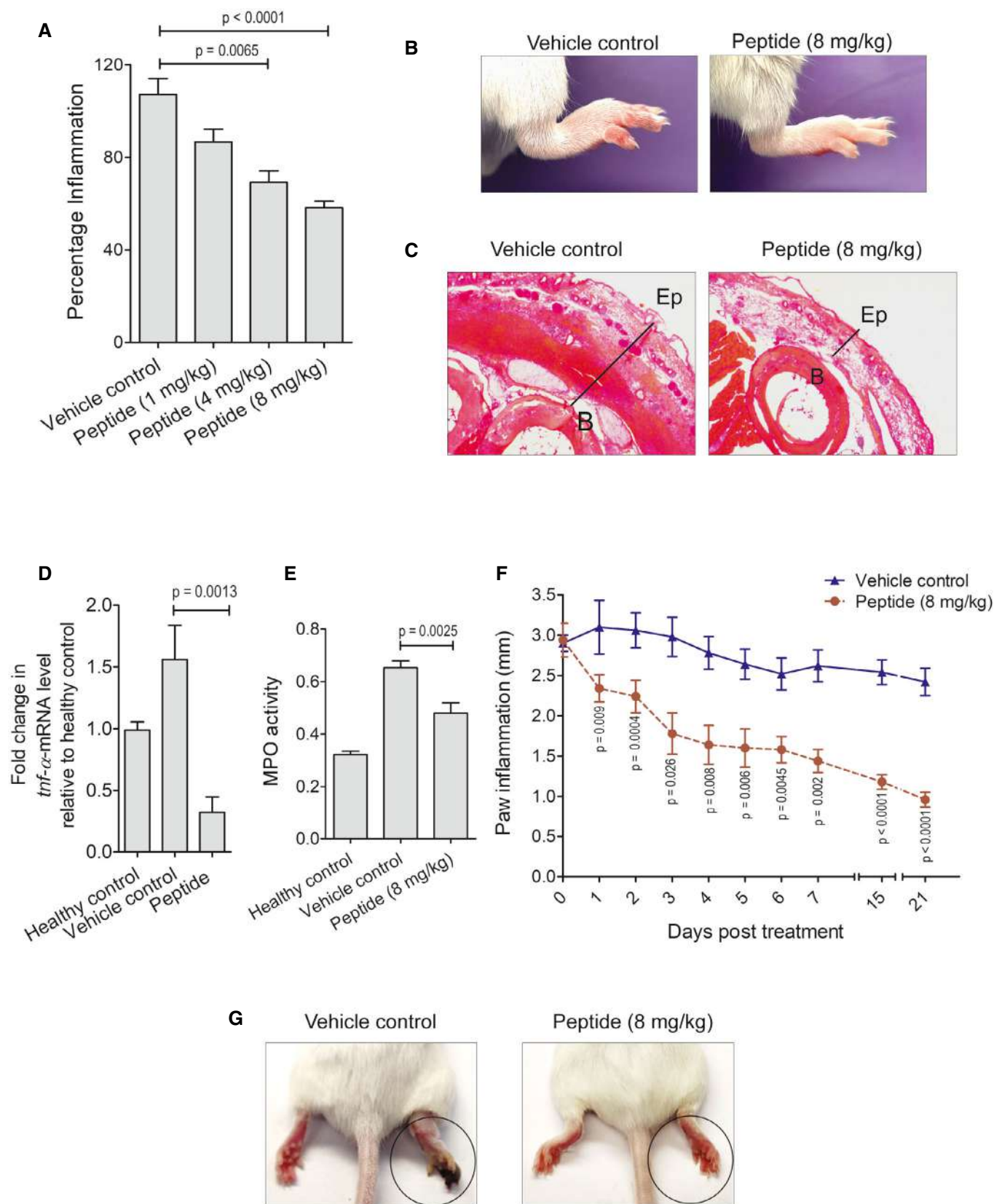


Figure 7.

treatment, mice were sacrificed and the paw tissue samples were harvested. SCF transcript level was quantified by qPCR. We observed a significant decrease in SCF transcripts in the peptide-treated paw tissues when compared to the paw tissues of vehicle control (Fig 8A). In Toluidine blue-stained paw tissue sections, the mast cell population was also found to be reduced in peptide-treated mice as compared to vehicle control (Fig 8B and C). Also, when

β -hexosaminidase activity, as well as transcript levels of MCP-3 and Mcpt4, were measured, it was found that peptide-treated mice had reduced β -hexosaminidase activity and lower MCP-3 and Mcpt4 transcript levels as compared to vehicle control (Fig 8D–F). These results indicate that the administration of PPE2-derived synthetic peptide can also reduce the mast cell population and its mediators in the inflamed tissues.

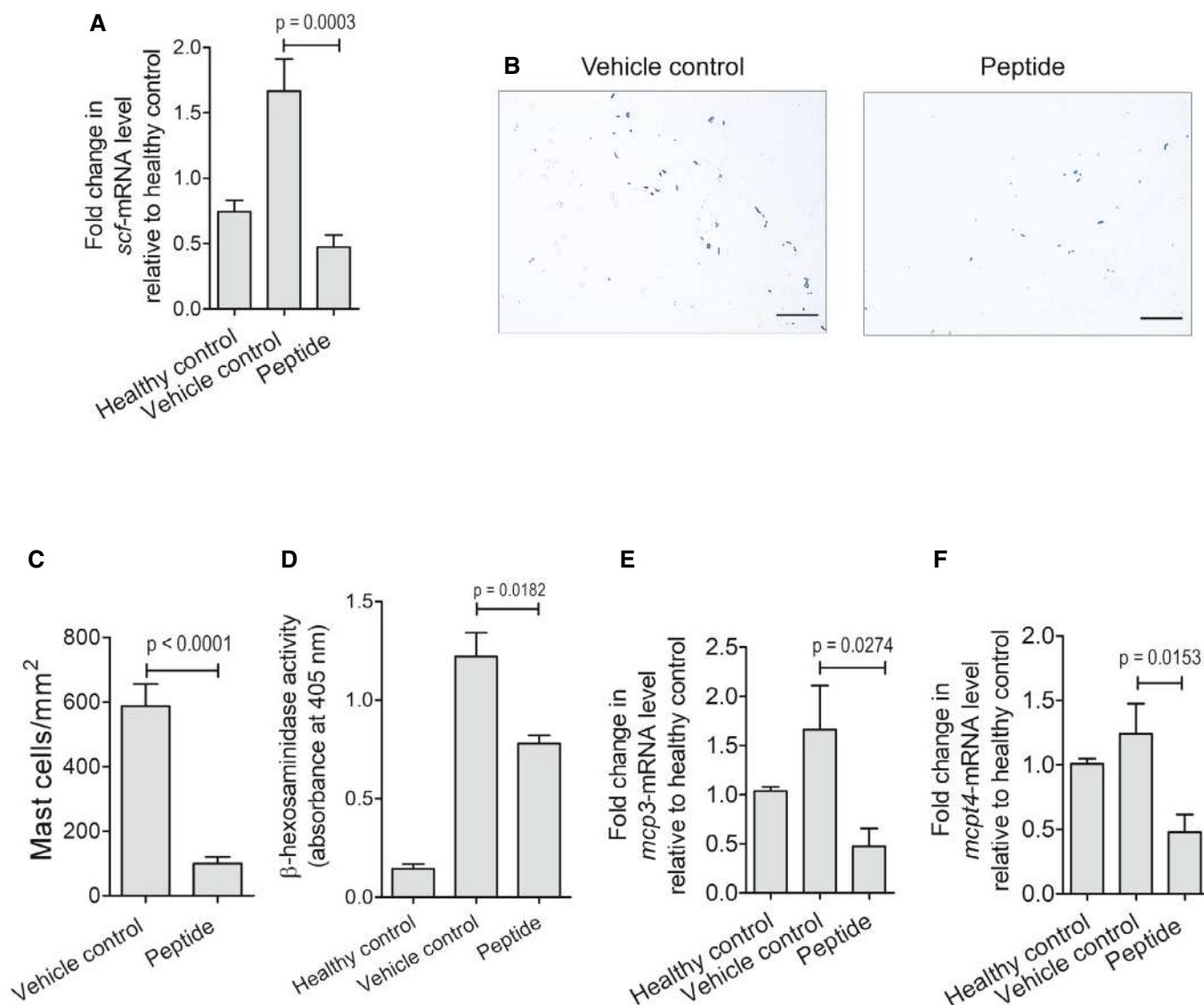


Figure 8. Synthetic peptide derived from PPE2 suppresses SCF transcription and mast cell population in paw tissue.

A subplantar injection of 5% of formalin (20 μ l) was administered in the right hind paw of Balb/c mice, and an equal volume of PBS was injected in left hind paw. After induction of inflammation, Balb/c mice were treated with PBS or peptide (8 mg/kg) via the intraperitoneal route. After 3 h, paw tissues were harvested and used for cDNA synthesis.

A, B (A) qPCR was performed to observe transcription levels of SCF. GAPDH transcript levels were used as an internal control. In another experiment, paw tissues from formalin-injected mice treated with PBS/peptide were collected to prepare tissue sections. (B) Next, Toluidine blue staining was done to check the mast cell population. Photographs of representative sections were visualized at 20x magnification (scale bar = 100 μ m).

C Counting of mast cells was performed in Toluidine blue-stained paw sections using ImageJ software and was normalized per unit area (mm^2).

D Tissue lysate (50 μ g) from each group was analyzed for β -hexosaminidase activity and absorbance was measured at 405 nm.

E, F Three-hour post-peptide (8 mg/kg) treatment, paw tissue samples were collected for all groups and used for cDNA synthesis. qPCR was performed to observe transcription levels of MCP-3 (E) and Mcpt4 (F). GAPDH transcript levels were used as control.

Data information: Data shown are Mean \pm SEM of eight mice. For (A, C–F) unpaired *t*-test was applied to calculate *P* values.

Discussion

Inflammation is characterized by the activation and recruitment of immune cells in response to infection and tissue injury. Under normal physiological conditions, inflammation is tightly upregulated in the presence of a threat and resolves once the threat fades away. However, an excess unregulated inflammation or inability to resolve an inflammatory response often leads to the development of diseases like atherosclerosis, cancer, and autoimmunity (Netea *et al*, 2017). Biologic therapeutics often employs engineered proteins/antibodies that target specific players in a disease process and is emerging rapidly due to their actions on selective targets and thereby have fewer side effects. The immune system, especially in the context of inflammation, has been the focus of the development of biological therapeutics over the last few decades. Several monoclonal antibody-based therapeutics have been approved targeting TNF- α to control inflammation in inflammatory diseases like rheumatoid arthritis and Crohn's disease (Molinelli *et al*, 2016).

Earlier we reported that a mycobacterial protein PPE2 interferes with myelopoiesis leading to the reduction in the population of myeloid cells in the peripheral blood without affecting the population of lymphoid cells (Pal & Mukhopadhyay, 2021). PPE2 appears to be a multifunctional protein that could affect the production of nitric oxide (NO) by binding to the *inos* promoter and also inhibited the production of reactive oxygen species (ROS) by destabilizing NADPH-oxidase complex in the phagosome (Pal *et al*, 2021).

Mast cells are credited to provide a "jump start" of immune responses to the site of injury by fast recruitment of inflammatory cells because of their ability to release preformed mediators immediately as well as rapid elaboration of lipid mediators (Nigrovic & Lee, 2005). The role of the mast cells in inflammation appears to be critical as mast cell knockout mice failed to develop joint inflammation/arthritis, but susceptibility was restored when these mice were engrafted with mast cells (Lee *et al*, 2002). Since PPE2 was found to affect myeloid cell population that includes mast cells, we speculated that recombinantly purified PPE2 may be used to suppress inflammation and potentially be used as an anti-inflammatory biologic. Therefore, in the present study, we used formalin-induced tissue injury in the hind paw of mice as a model of inflammation and investigated the effect of PPE2 on this model. Interestingly, we found that a single dose of 3 mg/kg of rPPE2 administered through the intraperitoneal route could bring down paw edema by more than 50% within 3 h of its administration and is comparable to that of Diclofenac sodium used as a control drug. Levels of inflammation markers like TNF- α and IL-6 in paw tissue as well as in serum were found to be significantly low in rPPE2-treated mice as compared to the vehicle control and comparable to mice administered with Diclofenac. Interestingly, rPPE2 was found to be effective to inhibit inflammation even when administered at 48 h post-tissue injury indicating its ability to act on an established full-fledged inflammation.

Continuous usage of steroidal or nonsteroidal anti-inflammatory drugs is associated with hepatic and renal toxicities. Although NSAIDs are quick and effective, they offer limited usage due to various side effects. We administered Diclofenac sodium (10 mg/kg) every day for the same duration of 8 days, and as expected, Diclofenac has deteriorated liver and kidney functions, which manifested into clinical symptoms of ruffling of fur coats, reduced activity on

stimulation, and reduced body weight. On the contrary, when administered continuously for 8 days, rPPE2 (3 mg/kg) did not show any side effects on the kidney and liver functions. This indicates that prolonged usage of rPPE2 is probably safer than Diclofenac. Additionally, proteins are molecules with a fixed structural conformation and therefore, unlike typical small-molecule chemical drugs, proteins are highly specific and, thus, result in decreased toxicity and other adverse side effects (Bruno *et al*, 2013).

Formalin administration causes acute inflammation characterized by mast cell degranulation and swelling (Rosland *et al*, 1990). Mast cells are considered as sensors of tissue damage and are recruited to the site of tissue injury (Enoksson *et al*, 2011). Mast cells also play a role in recruiting neutrophils to the damaged tissue essential for mounting efficient innate immunity (Schramm & Thorlacius, 2004). When we compared the mast cell population in the paw tissues in all the groups, we found that a single-dose administration of rPPE2 (3 mg/kg) significantly reduced the mast cell population and levels of mast cell-specific mediators (β -hexosaminidase, MCP-3, and Mcpt4). Interestingly, rPPE2 has no direct effect on mast cell activation or viability, indicating that PPE2 possibly targets mast cell population indirectly in the inflamed tissue. Subplantar injection of mast cells in the paw tissue was able to restore the inflammation in mice treated with rPPE2, indicating that PPE2 specifically targets the mast cells for its anti-inflammatory effect.

Earlier we reported that another mycobacterial protein, PPE18, belonging to the same PPE family, can inhibit sepsis-induced inflammation (Ahmed *et al*, 2018). Therefore, we compared the efficacy of rPPE18 with rPPE2 in suppressing formalin-induced paw inflammation. However, we observed that the administration of rPPE18 did not suppress inflammation as efficiently as rPPE2. Interestingly, it was found that population of mast cells to the inflamed tissue was not significantly different in the presence of rPPE18 as compared to vehicle control, unlike PPE2 where a significant decrease was observed. Interestingly, Diclofenac did not have a significant effect on the reduction of mast cell population although its ability to reduce paw inflammation was slightly less to that of rPPE2. Diclofenac is known to inhibit prostaglandin synthesis through inhibition of cyclooxygenase-1 (COX-1) and cyclooxygenase-2 (COX-2) activity (Gan, 2010; Inoue *et al*, 2013) to suppress inflammation. Therefore, the anti-inflammatory property of PPE2 appears to be predominantly due to its ability to reduce the mast cell population at the site of inflammation.

When we examined the physical presence of rPPE2 at the site of inflammation, it was found that rPPE2 is predominantly localized in the fibroblastic cells of the dermal and hypodermal regions. Using mouse embryonic fibroblasts and NIH-3T3 fibroblastic cell lines, nuclear localization of PPE2 was observed as PPE2 contains a functional NLS (Bhat *et al*, 2017). Since PPE2 also contains a DNA-binding motif and is known to inhibit transcription from the *inos* promoter (Bhat *et al*, 2017), we speculated that it may interfere with some factors present in the fibroblastic cells essential for mast cell recruitment to the site of injury, which may explain a decrease in the mast cell population observed in the paw edema upon PPE2 administration. Interestingly, we found that PPE2 did not directly affect either viability or functions of the mast cells. Interaction of mast cells with the neighboring cells appears to be critical for its expansion and viability (Hogaboam *et al*, 1998). The stem cell factor (SCF) produced by the fibroblasts plays an important role for

mast cell survival by suppressing apoptosis (Iemura *et al*, 1994; Jensen *et al*, 2008). The level of SCF receptor (c-kit) and SCF is known to be upregulated in cases of Mastocytosis and mast cells associated cancers (Pittoni *et al*, 2011). SCF secreted by the fibroblasts also enhances blood to tissue migration of mast cells and their migration within the tissue (Okayama & Kawakami, 2006). Therefore, we speculated that PPE2 may affect *scf* transcription by virtue of its ability to localize into the nucleus and DNA-binding properties. Expectedly, we found a significant reduction in the *scf* transcript both in the inflamed tissue and in NIH-3T3 fibroblasts in the presence of rPPE2. Inhibition of functional *scf* promoter activity was further confirmed using a *scf* promoter-driven reporter assay. Mechanism of inhibition appears to be similar to that of *inos* promoter as the minimal *scf* promoter containing a 60 bp core region around the TATA box was found to specifically interact with purified PPE2 as observed in EMSA. Therefore, PPE2-mediated suppression of *scf* transcription appears to be the reason for the low mast cell count observed in rPPE2-administered mouse paw tissue.

One of the major problems of protein-based therapeutics is their tendency to trigger an unwanted immune response against themselves. One of the strategies to overcome this problem would be designing smaller peptides to avoid immune surveillance. Thus, we designed a PPE2-derived synthetic peptide by combining its putative leucine zipper DNA-binding motif and nuclear localization signal (NLS). Based on homology modeling and peptide-DNA docking score, we synthesized a peptide and used it to analyze its anti-inflammatory activity in paw inflammation. It was found that the peptide containing the NLS and DNA-binding domain together was enough to replicate the PPE2 functions and reduce the mast cell population in a similar way. The peptides/smaller molecules are more stable, easy to chemically synthesize, and tend to have a longer shelf-life than macromolecules. Proteins/peptides are of great therapeutic value because these biomolecules have a specific 3-dimensional geometry that enables them to act either as enzymes, hormones, interferons, or antibodies with high competency and accuracy as compared to drug molecules. Therefore, this class of therapeutic drugs is emerging as an important class of medicines in novel therapies.

Mast cells are unique as compared to other inflammatory cells. Mast cells are the only cells that store pro-inflammatory cytokines like TNF- α and IL-6 in preformed granules and release them upon activation to initiate inflammation instantly. Many FDA-approved drugs inhibit mast cell activity by neutralizing the mast cell mediators, and most of them lower the inflammation as well (Finn & Walsh, 2013). However, the beneficial therapeutic effects of neutralization of one or a few mast cell mediators are often limited due to a lack of cell specificity (Harvima *et al*, 2014). Therefore, selective suppression of mast cells may provide better and broad-spectrum relief. In fact, targeting SCF-c-Kit signaling axis has been suggested as a potential therapeutic strategy to reduce mast cell population at least in some pathological conditions (Siebenhaar *et al*, 2018). Some drugs like imatinib (Cahill *et al*, 2017), nilotinib, and dasatinib, which target the tyrosine kinase activity of c-Kit, are being evaluated for mast cell-driven diseases (Harvima *et al*, 2014) but suffer from off-target effects on other tyrosine kinases beyond mast cell population.

To the best of our knowledge, in this study, we report a protein and a peptide derivative that can reduce the mast cell population by targeting *scf* transcription in fibroblasts. Also, the anti-inflammatory effect of a single-dose administration is long-lasting and also

essentially non-toxic in a mouse model. Though our findings are limited to formalin-induced paw edema, it will be interesting to examine the efficacy of PPE2 and the derived peptide in other mast cell-driven diseases in future. Thus, PPE2 and the derived peptide may constitute an important nonsteroidal biological molecule to be used successfully in the treatment of several mast cell-driven inflammatory diseases in humans.

Materials and Methods

Animals

Balb/c mice of 6–8 weeks of age were used for this study. Mice were maintained at the animal house facility of Centre for DNA Fingerprinting and Diagnostics, Hyderabad, and the experimental protocols were performed as per the guidelines of the Institutional Animal Ethics Committee (IAEC).

Protein purification

BL21 (DE3)pLysS strain of *Escherichia coli* was transformed with a pRSET-A vector containing *ppe2* gene as described earlier (Bhat *et al*, 2017). In brief, single transformed colonies were used to set up primary culture. The primary culture was inoculated into 1,000 ml of terrific broth in the presence of antibiotics [chloramphenicol (35 μ g/ml) and ampicillin (100 μ g/ml)]. The culture was grown in a shaker incubator at 37°C. At an O.D. of 0.5–0.7, protein expression was induced by adding β -D-1-thiogalactopyranoside (IPTG; VWR Life Sciences, USA) to a final concentration of 1 mM and was incubated for another 4 h at 37°C. Bacterial cells were harvested by centrifugation. For protein isolation, pellets were suspended in a lysis buffer [PBS containing 5% glycerol, 0.3% sodium lauroyl sarcosine, 1 mM PMSF, protease inhibitor (Sigma-Aldrich)] and lysed using sonication. The lysate was centrifuged at 13,800 g for 30 min, and the supernatant was allowed to bind with the TALON resin (Takara, USA) for 30 min. The beads were next washed with a washing buffer (PBS containing 5% glycerol and 20 mM imidazole) and eluted using elution buffer (PBS containing 5% glycerol and 200 mM imidazole). Elutes were run on an SDS-PAGE gel to assess the purity of the protein. Next, the protein was dialyzed against PBS to remove imidazole from the protein samples. Dialyzed protein was passed through a column packed with Polymyxin-B agarose beads (Sigma-Aldrich, USA) to remove residual LPS. The concentration of the purified protein was estimated using Micro BCA™ Protein Assay Kit (Thermo Fisher Scientific, USA) following the manufacturer's instructions.

Formalin-induced inflammation/tissue injury

A subplantar injection of 0.02 ml of 5% formalin (Sigma-Aldrich, USA) was administered to the right hind paw. The same volume of phosphate buffer saline (PBS) was injected into the left hind paw as vehicle control. A single dose of rPPE2 or Diclofenac was injected intraperitoneally, and induction of inflammation was confirmed at various time points by swelling in the right hind paw using a Vernier caliper. In some experiments, formalin-injected mice were treated intraperitoneally with a PPE2-derived synthetic peptide, and

inflammation was recorded. Based on *in silico* analysis, the synthetic peptide (KTLLEQTLALLPAALPLAAPLTLRRRRPKIKQ) was designed and purchased from Biotech Desk Pvt Limited, India. The peptide obtained was mass spectrometer validated and HPLC purified with > 90% purity.

Measurement of paw thickness

Paw thickness was measured using electronic digital Vernier caliper (Aerospace, India) at various time points. Percentage inflammation was calculated using the following formula:

$$\frac{\text{Post} - \text{drug treated (right hind paw)} - \text{left hind paw}}{\text{Pre} - \text{drug treated (right hind paw)} - \text{left hind paw}} \times 100$$

Histopathology

Mice were sacrificed, and paw samples were collected for all the groups and were fixed in 10% neutral buffered formalin followed by decalcification in 24.4% formic acid, and 0.5 N sodium hydroxide for 5 days. Tissue samples were embedded in paraffin wax and sectioned (3 ~ 5 µm) for further staining. For Toluidine blue staining, the sections were deparaffinized in xylene followed by hydration in distilled water. Further, the sections were stained in the Toluidine blue solution [0.5% Toluidine blue in 1% NaCl (pH - 2.3)] for 2–3 min. Slides were washed with distilled water, dehydrated using 100% Ethanol, and mounted on the slides for image acquisition. For hematoxylin and eosin (H&E) staining, the sections were deparaffinized and hydrated in distilled water. Further, sections were stained with hematoxylin (30 s), washed in distilled water, and counterstained with eosin (1% in distilled water for 30 s). Slides were washed, dehydrated, and mounted on the slides for imaging. Tissue section images were acquired using Nikon ECLIPSE Ni-U light upright microscope.

Histopathological severity of tissue damage was scored in a blinded fashion. The histological severity of tissue was graded as follows: 1 = minimal inflammation, minimal cellular infiltration; 2 = mild inflammation, cellular infiltration and tissue damage; 3 = moderate inflammation, cellular infiltration and necrosis; 4 = extensive inflammation, tissue damage, and necrosis.

Isolation of mast cells from paw tissue and analysis by flow cytometry

Cells from the paw tissues were isolated as described elsewhere (Regan-Komito *et al*, 2020). Briefly, the skin was removed, and the paw tissue was chopped into 4–5 small pieces. Next, tissue pieces were incubated in 1 ml of RPMI-1640 supplemented with DNase I (0.1 mg/ml, Sigma-Aldrich, USA) and Liberase (0.3 mg/ml, Roche, USA) for 90 min at 37°C. Digested soft tissue was passed through a 70 µm strainer (BD Biosciences, USA) to obtain a single-cell suspension. For flow cytometry, cells were washed with PBS and stained with anti-CD117 Ab conjugated to FITC (BioLegend, USA, 0.6 µg per million cells) and anti-FcεRI Ab conjugated to APC (BioLegend, USA, 0.25 µg per million cells) diluted in staining buffer (1% BSA [bovine serum albumin] in 1× PBS containing 0.01% sodium azide) for 1 h on ice. Cells were next analyzed for mast cell population by flow cytometry (BD LSR Fortessa; BD Biosciences).

Mouse bone marrow-derived mast cell culture

Balb/c mice of 6–8 weeks of age were used for isolation of mast cells as described elsewhere (Meurer *et al*, 2016). Briefly, mice were sacrificed by CO₂ asphyxiation and the femurs were removed under sterile conditions. Next, the bone marrow was isolated via flushing the bones with a syringe using complete RPMI-1640 medium [supplemented with 10% fetal bovine serum (Gibco, USA), 1× Glutamax (Invitrogen, USA), and 1× Anti-Anti (Invitrogen, USA)]. The bone marrow cells were further cultured for 25 days in the presence of SCF (30 ng/ml, Peprotech, USA) and IL-3 (20 ng/ml, Peprotech, USA). The purity of the bone marrow-derived mast cells was confirmed by flow cytometry using anti-CD117 Ab and anti-FcεRI Ab.

Mammalian cell culture

NIH-3T3 fibroblasts (ATCC) and mouse embryo fibroblasts (MEFs) were maintained in Dulbecco's Modified Eagle Medium (DMEM) supplemented with 10% fetal bovine serum (FBS), 1× Glutamax, and 1× Anti-Anti. Cell lines were routinely tested for mycoplasma contamination.

Beta-hexosaminidase assay

Beta-hexosaminidase (β-hexosaminidase) activity in the paw tissue was measured as described earlier (Fukuishi *et al*, 2014). Briefly, the paw tissues were homogenized in a 50 mM phosphate buffer with 1% Triton X-100. Equal amounts of tissue lysates were incubated with 200 µl of 1 mM P-nitrophenyl N-acetyl-beta-D-glucosamine (Sigma-Aldrich, USA) dissolved in 0.05 M citrate buffer (pH 4.5). After 1 h of incubation at 37°C, absorbance was measured at 405 nm.

Quantification of TNF-α and IL-6 in tissue lysates by EIA

Levels of TNF-α and IL-6 cytokines in tissue lysates were quantified by sandwich EIA using Invitrogen kit (Thermo Fisher Scientific, USA) according to the manufacturer's protocol. Absolute concentration of TNF-α/IL-6 cytokine was measured using a standard curve provided by the manufacturer.

Myeloperoxidase (MPO) assay

Myeloperoxidase (MPO) assay in the tissues was performed as described earlier (Pulli *et al*, 2013) with some modifications. Briefly, paw tissues were homogenized in a 20 mM phosphate buffer (pH 7.4) with 1% Triton X-100. Tissue lysates were incubated with 20 mM phosphate buffer containing 30 mM of O-dianisidine dihydrochloride (Sigma-Aldrich, USA), and 20 mM hydrogen peroxide (Sigma-Aldrich) at 37°C for 10 min, and the absorbance was measured at 460 nm.

Transplantation of bone marrow-derived mast cell in the paw tissue

A subplantar injection of 0.02 ml of 5% formalin (Sigma-Aldrich, USA) was administered to the right hind paw. The same volume of PBS was injected into the left hind paw. After 1 h, rPPE2 (3 mg/kg)

was injected intraperitoneally. After 3 h of rPPE2 treatment, about 1×10^6 mast cells were injected into the inflamed paw via subplantar route as described elsewhere (Patel *et al*, 2016). After 3 h of mast cell administration, inflammation in paw was observed and paw tissues were harvested for assaying MPO and β -hexosaminidase activity as well as for measuring TNF- α and IL-6 cytokines by EIA.

Transfection of NIH-3T3 cells

NIH-3T3 cells were transiently transfected using Lipofectamine 3000 (Invitrogen, USA) following the manufacturer's protocol. Briefly, 1 μ g of plasmid and 3 μ l of Lipofectamine 3000 mixture were diluted separately in 100 μ l of Opti-MEM (Invitrogen, USA) and incubated at room temperature. After 20 min of incubation, the mixture was added to NIH-3T3 cells cultured with Opti-MEM. After 6 h of transfection, cells were replenished with fresh complete DMEM medium, and after 24 h of transfection, cells were harvested for further experiments.

RNA isolation, cDNA synthesis, and real-time PCR

For RNA isolation, cells or paw tissues were homogenized in the Trizol solution (Amersham), and chloroform was added. The samples were centrifuged, and the transparent supernatant was collected. An equal amount of isopropanol was added, and the mixture was centrifuged for 30 min at 18,800 g (4°C). The pellets were washed twice with 70% ethanol at 18,800 g (4°C) for 15 min. The pellet was air-dried and dissolved in nuclease-free water. The RNA quantity and quality were analyzed by NanoDrop (Thermo Scientific, USA). The cDNA synthesis was carried out using Moloney Murine Leukemia Virus (MMLV) reverse transcriptase as per the manufacturer's protocol (Invitrogen, USA). Real-time PCR was carried out with a specific set of primers (Appendix Table S1) using CFX96 Real-time PCR system (Bio-Rad, USA) with DyNamo Flash SYBR GREEN qPCR master mix (Invitrogen, USA) for detection. A comparative Ct method ($2^{-\Delta\Delta Ct}$) was used to calculate the relative change in mRNA levels using expression from untreated control as base (one fold) as described elsewhere (Livak & Schmittgen, 2001). Briefly, ΔCt is the Ct value for the gene of interest normalized to the Ct value of the respective GAPDH control. $\Delta\Delta Ct$ values were calculated as a relative change in ΔCt of the target gene in all the groups with respect to healthy control. Fold changes in the mRNA levels were expressed as $2^{-\Delta\Delta Ct}$. The data were analyzed using CFX Maestro software (Bio-Rad, USA).

Confocal microscopy

For studying PPE2 localization, cells were treated with 3 μ g/ml of rPPE2 for 45 min. Cells treated with PBS were used as control. Cells were harvested and washed with PBS and fixed using 4% paraformaldehyde. Cells were permeabilized using Triton X-100 (0.1%) and incubated with anti-PPE2 Ab [in-house raised (Bhat *et al*, 2017); 1:500] for overnight at 4°C. Next, cells were washed and incubated with Alexa Fluor 488-conjugated anti-mouse secondary Ab (Thermo Fisher Scientific, USA; 1:1,000) for 60 min. Cells were washed and mounted with a mounting medium containing DAPI (VECTASHIELD, Vector labs, USA) and observed under LSM 700

The paper explained

Problem

Inflammation is a generic immune response generated to protect the body against harmful agents such as bacteria and viruses. It occurs when the inflammatory cells arrive at the barrier site of infection/injury. The actual problem arises when the inflammation becomes chronic, and the own protective inflammatory response eventually starts damaging healthy cells, tissues, and organs. There are anti-inflammatory drugs available on the market but are associated with side effects during prolonged usage. Therefore, there is a need to develop anti-inflammatory drugs/molecules with better efficiency and the least/no side effects.

Results

We identified a novel *Mycobacterium tuberculosis* protein, PPE2, which can be used as an anti-inflammatory drug. We observed that a single dose of PPE2 protein/peptide was effective in subsiding the inflammation for a longer duration. PPE2 exerts its anti-inflammatory activity by affecting fibroblast-mast cell communication. PPE2 downregulates SCF production in the fibroblasts and diminishes the in situ mast cell population at the site of injury. Reduction of mast cells in the tissues results in reduced mast-mediators and cues of inflammation and hence suppresses inflammation. PPE2 did not show any liver and kidney toxicity. PPE2-derived synthetic peptide imparts similar anti-inflammatory activity by suppressing the mast cell population.

Impact

The market-available anti-inflammatory drugs are laden with side effects when used for a longer duration. We hereby report PPE2 protein and a peptide derivative that reduce the mast cell population and the mast cell-driven inflammatory signaling by targeting scf transcription in fibroblasts. These findings are likely to help develop drugs to treat mast cell-centric diseases.

Zeiss confocal microscope (Carl Zeiss Micro-Imaging, Germany). Cells transfected with pEGFP/pEGFP-PPE2 were harvested after 24 h, washed with PBS, and fixed using 4% paraformaldehyde. Next, cells were washed and mounted with a mounting medium containing DAPI. Cells were visualized under Leica SP8 confocal microscope (Leica Microsystems, USA).

For tissues, paraffin-embedded sections were obtained on the pre-coated slide (Fisher Scientific, USA). The tissue sections were deparaffinized by washing with xylene (Sigma-Aldrich, USA) followed by hydration in gradient ethanol solution (95, 75, and 50%). Next, for antigen retrieval, sections were then boiled in 10 mM sodium citrate (pH 6) for 10 min. The sections were then washed, permeabilized with Triton X-100 (0.1%), and stained with anti-PPE2 Ab for overnight at 4°C followed by staining with Alexa Fluor 488-conjugated anti-mouse secondary Ab for 60 min at room temperature. Next, sections were washed and mounted with propidium iodide (VECTASHIELD, Vector labs, USA). Images were acquired on a Zeiss LSM 700 confocal microscope equipped with 405, 488, and 555 nm lasers, and fitted with a 63 \times , 1.4 NA objective.

Cloning of SCF promoter

NIH-3T3 cells were used to isolate the genomic DNA via organic extraction. Approximately, 5×10^7 cells were lysed in 1 ml of lysis buffer [10 mM Tris (pH 8.0), 10 mM EDTA, 0.5% SDS, RNase]. After lysis of cells, Proteinase-K (1 mg/ml; Sigma-Aldrich, USA) was

added and incubated for 12–16 h at 50°C. Next, an equal volume of phenol:chloroform:isoamyl alcohol (25:24:1) was added and gently vortexed. The sample was centrifuged at 18,800 g at room temperature, and the aqueous phase was collected. To this aqueous phase, 0.2 volumes of 10 M Ammonium acetate and 2 volumes of ethanol were added to precipitate the genomic DNA. The pellet was washed with 70% ethanol and dissolved in nuclease-free water. Genomic DNA concentration was checked by NanoDrop, and quality was checked by running it on 0.7% agarose gel. From isolated genomic DNA, the putative promoter regions were amplified and cloned into the pGL3 basic vector (Promega, USA) at XhoI and MluI restriction sites using a specific set of primers (Appendix Table S1). The promoter activity of these clones was checked by transfecting NIH-3T3 cells using the Luciferase kit (Promega, USA).

Electrophoretic mobility assay (EMSA)

For EMSA analyses, the 60-bp nucleotide (Appendix Table S1) was used. The reverse and forward complementary oligomers were annealed by incubating at 95°C for 10 min in 100 mM NaCl and gradually cooling to room temperature. The annealed oligonucleotides were end-labeled with [γ - 32 P]-ATP using T4 polynucleotide kinase (New England Bio Labs) for 1 h at room temperature. For competition studies, equimolar excess of the unlabeled oligonucleotides was incubated with the labeled probes. Varying amounts of rPPE2 were incubated with 1 ng of 32 P-end-labeled oligonucleotide in a binding buffer (20 mM HEPES, 0.5 mM DTT, 0.5 mM EDTA, and 5% glycerol) for 30 min at room temperature. The protein-DNA complex was resolved on a 7% native polyacrylamide gel using running buffer (25 mM Tris, 190 mM Glycine, 1 mM EDTA, pH 8.3) at 4°C. The specificity of the binding was determined by competition with equimolar excess of unlabeled probes. After the run, the gel was dried at 80°C for 1 h and exposed to an imaging plate (Fujifilm, USA) overnight. The imaging was done using a phosphor imager (GE, health care, USA).

Generation of peptide using homology modeling and Peptide-DNA interaction

The putative “leucine zipper” spanning region (KTLLEQTLALL-PAALPLLAAPLAPLTL) of PPE2 was modeled using Ba3-cytochrome-c oxidase (1EHK) as a template using MODELLER 9.23. Based on the DOPE and GA score, the best model was selected. The resulting model was validated using PROCHECK. Ramachandran plot for the modeled peptide showed all the residues falling in the favorable and allowed regions. Next, modeled peptide structure was docked with the SCF promoter DNA sequence (predicted by EPD database) using HDock. The docked structure was further visualized by PyMOL.

Statistical analysis

GraphPad Prism software, version 5.0, was used for determining the significance of the difference in the mean between the samples. Student's *t*-test was performed to calculate the significance between two samples. For multiple group comparison, one-way ANOVA with Bonferroni *post hoc* test was performed. *P* < 0.05 was considered to be significant.

Data availability

This study has no data that require deposition in a public database.

Expanded View for this article is available online.

Acknowledgements

The authors thank Dr. Rashna Bhandari, CDFD, Hyderabad, for providing RBL-2H3 cells. Author thanks Mr. Chilakala Gangi Reddy and Ms. Kiranmai, Lab of Computational Biology, CDFD, for helping with the modeling and docking experiments. This work was supported by grants from the Science and Engineering Research Board (SERB), Department of Science and Technology (DST), Government of India (DST/SERB/CRG/2019/000239), TATA Innovation Fellowship, DBT (BT/HRD/35/01/03/2018), Department of Biotechnology (DBT), Govt of India (BT/PR35722/BRB/10/1837/2019) and a core grant from the Centre for DNA Fingerprinting and Diagnostics by the Department of Biotechnology (DBT) to Sangita Mukhopadhyay.

Author contributions

Ravi Pal: Data curation; formal analysis; validation; investigation; visualization; writing—original draft. **Madhu Babu Battu:** Conceptualization. **Sangita Mukhopadhyay:** Conceptualization; formal analysis; supervision; funding acquisition; project administration; writing—review and editing.

In addition to the [CRediT](#) author contributions listed above, the contributions in detail are:

RP and SM conceived, designed the experiments, and analyzed the data. RP performed all the experiments. MBB helped in mice inflammation experiments. RP and SM wrote the manuscript. SM corrected and edited the manuscript.

Disclosure and competing interests statement

A patent application based on the results described in this paper is being filed by the Centre for DNA Fingerprinting and Diagnostics, in which SM and RP and MBB are listed as inventors.

References

- Ahmed A, Dolasia K, Mukhopadhyay S (2018) *Mycobacterium tuberculosis* PPE18 protein reduces inflammation and increases survival in animal model of sepsis. *J Immunol* 200: 3587–3598
- Barnes PJ (1998) Anti-inflammatory actions of glucocorticoids: molecular mechanisms. *Clin Sci (Lond)* 94: 557–572
- Bhat KH, Srivastava S, Kotturu SK, Ghosh S, Mukhopadhyay S (2017) The PPE2 protein of *Mycobacterium tuberculosis* translocates to host nucleus and inhibits nitric oxide production. *Sci Rep* 7: 39706
- Bruno BJ, Miller GD, Lim CS (2013) Basics and recent advances in peptide and protein drug delivery. *Ther Deliv* 4: 1443–1467
- Cahill KN, Katz HR, Cui J, Lai J, Kazani S, Crosby-Thompson A, Garofalo D, Castro M, Jarjour N, DiMango E *et al* (2017) Kit inhibition by imatinib in patients with severe refractory asthma. *N Engl J Med* 376: 1911–1920
- Davis A, Robson J (2016) The dangers of NSAIDs: look both ways. *Br J Gen Pract* 66: 172–173
- Dudeck J, Kotrba J, Immler R, Hoffmann A, Voss M, Alexaki VI, Morton L, Jahn SR, Katsoulis-Dimitriou K, Winzer S *et al* (2021) Directional mast cell degranulation of tumor necrosis factor into blood vessels primes neutrophil extravasation. *Immunity* 54: 468–483

- Enoksson M, Lyberg K, Möller-Westerberg C, Fallon PG, Nilsson G, Lunderius-Andersson C (2011) Mast cells as sensors of cell injury through IL-33 recognition. *J Immunol* 186: 2523–2528
- Finn DF, Walsh JJ (2013) Twenty-first century mast cell stabilizers. *Br J Pharmacol* 170: 23–37
- Finotto S, Mekori YA, Metcalfe DD (1997) Glucocorticoids decrease tissue mast cell number by reducing the production of the c-kit ligand, stem cell factor, by resident cells: in vitro and in vivo evidence in murine systems. *J Clin Invest* 99: 1721–1728
- Fukuishi N, Murakami S, Ohno A, Yamanaka N, Matsui N, Fukutsuji K, Yamada S, Itoh K, Akagi M (2014) Does β -hexosaminidase function only as a degranulation indicator in mast cells? The primary role of β -hexosaminidase in mast cell granules. *J Immunol* 193: 1886–1894
- Gan TJ (2010) Diclofenac: an update on its mechanism of action and safety profile. *Curr Med Res Opin* 26: 1715–1731
- Gupta AK, Parasar D, Sagar A, Choudhary V, Chopra BS, Garg R, Ashish KN (2015) Analgesic and anti-inflammatory properties of gelsolin in acetic acid induced writhing, tail immersion and carrageenan induced paw edema in mice. *PLoS ONE* 10: e0135558
- Habuchi H, Izumi M, Dan J, Ushida T, Ikeuchi M, Takeuchi K, Habuchi O (2021) Bone marrow derived mast cells injected into the osteoarthritic knee joints of mice induced by sodium monoiodoacetate enhanced spontaneous pain through activation of PAR2 and action of extracellular ATP. *PLoS ONE* 16: e0252590
- Harvima IT, Levi-Schaffer F, Draber P, Friedman S, Polakovicova I, Gibbs BF, Blank U, Nilsson G, Maurer M (2014) Molecular targets on mast cells and basophils for novel therapies. *J Allergy Clin Immunol* 134: 530–544
- Hogaboam C, Kunkel SL, Strieter RM, Taub DD, Lincoln P, Standiford TJ, Lukacs NW (1998) Novel role of transmembrane SCF for mast cell activation and eotaxin production in mast cell-fibroblast interactions. *J Immunol* 160: 6166–6171
- Huang B, Lei Z, Zhang GM, Li D, Song C, Li B, Liu Y, Yuan Y, Unkeless J, Xiong H et al (2008) SCF-mediated mast cell infiltration and activation exacerbate the inflammation and immunosuppression in tumor microenvironment. *Blood* 112: 1269–1279
- Iemura A, Tsai M, Ando A, Wershil BK, Galli SJ (1994) The c-kit ligand, stem cell factor, promotes mast cell survival by suppressing apoptosis. *Am J Pathol* 144: 321–328
- Inoue T, Anai S, Onishi S, Miyake M, Tanaka N, Hirayama A, Fujimoto K, Hirao Y (2013) Inhibition of COX-2 expression by topical diclofenac enhanced radiation sensitivity via enhancement of TRAIL in human prostate adenocarcinoma xenograft model. *BMC Urol* 13: 1
- Jensen BM, Akin C, Gilfillan AM (2008) Pharmacological targeting of the KIT growth factor receptor: a therapeutic consideration for mast cell disorders. *Br J Pharmacol* 154: 1572–1582
- Krystel-Whittemore M, Dileepan KN, Wood JG (2015) Mast cell: a multi-functional master cell. *Front Immunol* 6: 620
- Lee DM, Friend DS, Gurish MF, Benoist C, Mathis D, Brenner MB (2002) Mast cells: a cellular link between autoantibodies and inflammatory arthritis. *Science* 297: 1689–1692
- Livak KJ, Schmittgen TD (2001) Analysis of relative gene expression data using real-time quantitative PCR and the 2^{(-Delta Delta C(T))} Method. *Methods* 25: 402–408
- Loria V, Dato I, Graziani F, Biasucci LM (2008) Myeloperoxidase: a new biomarker of inflammation in ischemic heart disease and acute coronary syndromes. *Mediators Inflamm* 2008: 135625
- Lunderius-Andersson C, Enoksson M, Nilsson G (2012) Mast cells respond to cell injury through the recognition of IL-33. *Front Immunol* 3: 82
- Majety M, Pradel LP, Gies M, Ries CH (2015) Fibroblasts influence survival and therapeutic response in a 3D co-culture model. *PLoS ONE* 10: e0127948
- Marcum ZA, Hanlon JT (2010) Recognizing the risks of chronic nonsteroidal anti-inflammatory drug use in older adults. *Ann Longterm Care* 18: 24–27
- Meurer SK, Neß M, Weiskirchen S, Kim P, Tag CG, Kauffmann M, Huber M, Weiskirchen R (2016) Isolation of mature (peritoneum-derived) mast cells and immature (bone marrow-derived) mast cell precursors from mice. *PLoS ONE* 11: e0158104
- Molinelli E, Campanati A, Ganzetti G, Offidani A (2016) Biologic therapy in immune mediated inflammatory disease: basic science and clinical concepts. *Curr Drug Saf* 11: 35–43
- Nair S, Pandey AD, Mukhopadhyay S (2011) The PPE18 protein of *Mycobacterium tuberculosis* inhibits NF- κ B/rel-mediated proinflammatory cytokine production by upregulating and phosphorylating suppressor of cytokine signaling 3 protein. *J Immunol* 186: 5413–5424
- Nair S, Ramaswamy PA, Ghosh S, Joshi DC, Pathak N, Siddiqui I, Sharma P, Hasnain SE, Mande SC, Mukhopadhyay S (2009) The PPE18 of *Mycobacterium tuberculosis* interacts with TLR2 and activates IL-10 induction in macrophage. *J Immunol* 183: 6269–6281
- Netea MG, Balkwill F, Chonchol M, Cominelli F, Donath MY, Giamarellos-Bourboulis EJ, Golenbock D, Gresnigt MS, Heneka MT, Hoffman HM et al (2017) A guiding map for inflammation. *Nat Immunol* 18: 826–831
- Nigrovic PA, Lee DM (2005) Mast cells in inflammatory arthritis. *Arthritis Res Ther* 7: 1–11
- Okayama Y, Kawakami T (2006) Development, migration, and survival of mast cells. *Immunol Res* 34: 97–115
- Ong CK, Lirk P, Tan CH, Seymour RA (2007) An evidence-based update on nonsteroidal anti-inflammatory drugs. *Clin Med Res* 5: 19–34
- Pal R, Ghosh S, Mukhopadhyay S (2021) Moonlighting by PPE2 protein: focus on mycobacterial virulence. *J Immunol* 207: 2393–2397
- Pal R, Mukhopadhyay S (2021) PPE2 protein of *Mycobacterium tuberculosis* affects myeloid hematopoiesis in mice. *Immunobiology* 226: 152051
- Patel KR, Aven L, Shao F, Krishnamoorthy N, Duvall MG, Levy BD, Ai X (2016) Mast cell-derived neurotrophin 4 mediates allergen-induced airway hyperinnervation in early life. *Mucosal Immunol* 9: 1466–1476
- Périer RC, Praz V, Junier T, Bonnard C, Bucher P (2000) The eukaryotic promoter database (EPD). *Nucleic Acids Res* 28: 302–303
- Pittoni P, Piconese S, Tripodo C, Colombo MP (2011) Tumor-intrinsic and -extrinsic roles of c-kit: mast cells as the primary off-target of tyrosine kinase inhibitors. *Oncogene* 30: 757–769
- Pulli B, Ali M, Forghani R, Schob S, Hsieh KL, Wojtkiewicz G, Linnoila JJ, Chen JW (2013) Measuring myeloperoxidase activity in biological samples. *PLoS ONE* 8: e67976
- Regan-Komito D, Swann JW, Demetriou P, Cohen ES, Horwood NJ, Sansom SN, Griseri T (2020) GM-CSF drives dysregulated hematopoietic stem cell activity and pathogenic extramedullary myelopoiesis in experimental spondyloarthritis. *Nat Commun* 11: 155
- Rosland JH, Tjølsen A, Mæhle B, Hole K (1990) The formalin test in mice: effect of formalin concentration. *Pain* 42: 235–242
- Sasaki H, Kurotaki D, Osato N, Sato H, Sasaki I, Koizumi S, Wang H, Kaneda C, Nishiyama A, Kaisho T et al (2015) Transcription factor IRF8 plays a critical role in the development of murine basophils and mast cells. *Blood* 125: 358–369
- Schramm R, Thorlacius H (2004) Neutrophil recruitment in mast cell-dependent inflammation: inhibitory mechanisms of glucocorticoids. *Inflamm Res* 53: 644–652
- Siebenhaar F, Redegeld FA, Bischoff SC, Gibbs BF, Maurer M (2018) Mast cells as drivers of disease and therapeutic targets. *Trends Immunol* 39: 151–162

- Theoharides TC, Alysandratos KD, Angelidou A, Delivanis DA, Sismanopoulos N, Zhang B, Asadi S, Vasiadi M, Weng Z, Miniati A et al (2012) Mast cells and inflammation. *Biochim Biophys Acta* 1822: 21–33
- Webb B, Sali A (2016) Comparative protein structure modeling using MODELLER. *Curr Protoc Bioinformatics* 54: 5.6.1–5.6.37
- Wong RSY (2019) Disease-modifying effects of long-term and continuous use of nonsteroidal anti-inflammatory drugs (NSAIDs) in spondyloarthritis. *Adv Pharmacol Sci* 2019: 5324170
- Yan Y, Zhang D, Zhou P, Li B, Huang SY (2017) HDock: a web server for protein-protein and protein-DNA/RNA docking based on a hybrid strategy. *Nucleic Acids Res* 45: W365–W373
- Yang C, Mo X, Lv J, Liu X, Yuan M, Dong M, Li L, Luo X, Fan X, Jin Z et al (2012) Lipopolysaccharide enhances FcεRI-mediated mast cell degranulation by increasing Ca²⁺ entry through store-operated Ca²⁺ channels: implications for lipopolysaccharide exacerbating allergic asthma. *Exp Physiol* 97: 1315–1327
- Yin ZY, Li L, Chu SS, Sun Q, Ma ZL, Gu XP (2016) Antinociceptive effects of dehydrocorydaline in mouse models of inflammatory pain involve the opioid receptor and inflammatory cytokines. *Sci Rep* 6: 27129



License: This is an open access article under the terms of the Creative Commons Attribution License, which permits use, distribution and reproduction in any medium, provided the original work is properly cited.



TRADE IN ANY FLOW CYTOMETER FOR
UP TO 25% OFF OF CYTEK PRODUCTS



LEARN MORE



***Mycobacterium tuberculosis* PPE2 Protein Interacts with p67^{phox} and Inhibits Reactive Oxygen Species Production**

This information is current as of September 29, 2019.

Shruti Srivastava, Madhu Babu Battu, Mehak Zahoor Khan, Vinay Kumar Nandicoori and Sangita Mukhopadhyay

J Immunol 2019; 203:1218-1229; Prepublished online 2 August 2019;

doi: 10.4049/jimmunol.1801143

<http://www.jimmunol.org/content/203/5/1218>

Supplementary Material <http://www.jimmunol.org/content/suppl/2019/08/01/jimmunol.1801143.DCSupplemental>

References This article **cites 80 articles**, 27 of which you can access for free at: <http://www.jimmunol.org/content/203/5/1218.full#ref-list-1>

Why *The JI*? [Submit online.](#)

- **Rapid Reviews! 30 days*** from submission to initial decision
- **No Triage!** Every submission reviewed by practicing scientists
- **Fast Publication!** 4 weeks from acceptance to publication

**average*

Subscription Information about subscribing to *The Journal of Immunology* is online at: <http://jimmunol.org/subscription>

Permissions Submit copyright permission requests at: <http://www.aai.org/About/Publications/JI/copyright.html>

Email Alerts Receive free email-alerts when new articles cite this article. Sign up at: <http://jimmunol.org/alerts>



Mycobacterium tuberculosis PPE2 Protein Interacts with p67^{phox} and Inhibits Reactive Oxygen Species Production

Shruti Srivastava,^{*,†} Madhu Babu Battu,^{*} Mehak Zahoor Khan,[‡] Vinay Kumar Nandicoori,[‡] and Sangita Mukhopadhyay^{*}

Mycobacterium tuberculosis employs defense mechanisms to protect itself from reactive oxygen species (ROS)–mediated cytotoxicity inside macrophages. In the current study, we found that a secretory protein of *M. tuberculosis* PPE2 disrupted the assembly of NADPH oxidase complex. PPE2 inhibited NADPH oxidase–mediated ROS generation in RAW 264.7 macrophages and peritoneal macrophages from BALB/c mice. PPE2 interacted with the cytosolic subunit of NADPH oxidase, p67^{phox}, and prevented translocation of p67^{phox} and p47^{phox} to the membrane, resulting in decreased NADPH oxidase activity. Trp236 residue present in the SH3-like domain of PPE2 was found to be critical for its interaction with p67^{phox}. Trp236Ala mutant of PPE2 did not interact with p67^{phox} and thereby did not affect ROS generation. *M. tuberculosis* expressing PPE2 and PPE2-null mutants complemented with PPE2 survived better than PPE2-null mutants in infected RAW 264.7 macrophages. Altogether, this study suggests that PPE2 inhibits NADPH oxidase–mediated ROS production to favor *M. tuberculosis* survival in macrophages. The findings that *M. tuberculosis* PPE2 protein is involved in the modulation of oxidative response in macrophages will help us in improving our knowledge of host–pathogen interactions and the application of better therapeutics against tuberculosis. *The Journal of Immunology*, 2019, 203: 1218–1229.

Tuberculosis, caused by *Mycobacterium tuberculosis*, is a global threat to public health claiming ~1.8 million lives every year (1). The innate immune system uses NADPH oxidase complex (2) to produce free radicals, commonly known as reactive oxygen species (ROS). As an innate defense mechanism, these free radicals generated by macrophages are critical for killing intracellular pathogens (3–5). Superoxide anions generated by NADPH oxidase complex subsequently generate different

oxidants primarily to kill the invading microorganisms (6–8). Inhibition of ROS generation has been an exploited mechanism of defense used by various microorganisms (9, 10). For example, YopE is an effector protein in *Yersinia pseudotuberculosis* that interacts with Rac2/Rac1 and inhibits ROS generation (10). In human cystic fibrosis, there is an inhibition of NADPH oxidase activity in macrophages, resulting in diminished ROS generation, which increased the survival of *Pseudomonas aeruginosa* (11). Similarly, mice deficient in p47^{phox} and gp91^{phox} subunits of NADPH oxidase complex are more susceptible to bacterial or fungal infections, such as *Staphylococcus aureus* and *Aspergillus fumigatus* (12, 13). Again, in the case of *Salmonella typhimurium*, the *Salmonella* pathogenicity island 2 does not allow the assembly of NADPH oxidase to prevent oxidative killing by macrophages (9).

The importance of ROS in curtailing *M. tuberculosis* infection is significantly highlighted in the pathological case study of chronic granulomatous disease patients in which mutation in one or multiple subunits of NADPH oxidase caused a reduction in ROS generation, increased susceptibility toward mycobacterial infection (14), and increased propensity toward recurrent bacterial infections (12, 14). Recently, in macrophages, a gene NRROS has been identified as a negative regulator of ROS. NRROS^{−/−}-deficient macrophages showed aggravated inflammation and bactericidal activity against *Escherichia coli* and *Listeria monocytogenes* (15). Initially, hydrogen peroxide (H₂O₂) was discovered as an effector molecule of macrophages responsible for the killing of *Mycobacterium* sp. in vitro, although its actual role in the pathogenesis of human tuberculosis remains controversial (16–18). It is assumed that H₂O₂ may inactivate critical metabolic enzymes and promote lipid peroxidation in mycobacteria via secondary reactive intermediates. Among the *M. tuberculosis* strains, CDC1551 and CB3.3 are known to be significantly more resistant to both H₂O₂ and acidified sodium nitrite, and higher resistance could be correlated to clinical virulence (19). It appears that because of early and more robust macrophage activation, intracellular CDC1551 bacilli confront higher levels of stress, leading to increased

^{*}Laboratory of Molecular Cell Biology, Centre for DNA Fingerprinting and Diagnostics, Hyderabad, Telangana 500039, India; [†]Graduate Studies, Manipal Academy of Higher Education, Manipal, Karnataka 576104, India; and [‡]National Institute of Immunology, Delhi 110067, India

ORCID: 0000-0002-5682-4178 (V.K.N.).

Received for publication August 20, 2018. Accepted for publication July 4, 2019.

This work was supported by grants from the Department of Biotechnology, Government of India (BT/PR12817/COE/34/23/20135), the TATA Innovation Fellowship (BT/HRD/35/01/03/2018), and a core grant from the Centre for DNA Fingerprinting and Diagnostics by the Department of Biotechnology (to S.M.). S.S. is the recipient of a fellowship from the Innovation in Science Pursuit for Inspired Research (IF140588), the Department of Science & Technology, Government of India. M.B.B. is supported by a Science and Engineering Research Board National Post-Doctoral Fellowship (PDF/2016/000741), Government of India. M.Z.K. is a recipient of a Senior Research Fellowship of the Council of Scientific and Industrial Research of India.

S.M. and S.S. designed the experiments and analyzed the data. S.S. performed all in vitro, mutagenesis experiments, and some *M. tuberculosis*–related experiments. M.B.B. carried out in silico prediction analysis and molecular biology–related experiments. V.K.N. and M.Z.K. generated complemented *M. tuberculosis* strains and M.Z.K. performed *M. tuberculosis*–related experiments. S.M., S.S., and M.B.B. wrote the manuscript. S.M. edited the manuscript.

Address correspondence and reprint requests to Dr. Sangita Mukhopadhyay, Laboratory of Molecular Cell Biology, Centre for DNA Fingerprinting and Diagnostics, Inner Ring Road, Uppal, Hyderabad 500039, India. E-mail address: sangita@cdfd.org.in

The online version of this article contains supplemental material.

Abbreviations used in this article: BCG, bacillus Calmette–Guérin; DCFH-DA, 2',7'-dichlorofluorescein diacetate; IdeR, iron-dependent repressor; ITC, isothermal calorimetry; MOI, multiplicity of infection; NII, National Institute of Immunology; PPE2:KO, *M. tuberculosis ppe2* null mutant; PPE2:KO:comp, complemented *M. tuberculosis* strain; PRR, proline-rich region; ROS, reactive oxygen species; siRNA, small interfering RNA; WT, wild-type.

Copyright © 2019 by The American Association of Immunologists, Inc. 0022-1767/19/\$37.50

upregulation of the bacterial stress response genes as compared with HN878 (20). It has been observed that the assembly of NADPH oxidase complex on *M. bovis* bacillus Calmette-Guérin (BCG) phagosomes is facilitated by IFN- γ cytokine (21), whereas TNF- α induces mitochondrial ROS production against *M. marinum* infection (22). A recent report by Paik et al. (23) suggests that upon phagocytosis of *M. smegmatis*, ROS activates an endoplasmic reticulum-mediated stress response in macrophages. Thus, inhibition of ROS production in macrophages is helpful for the survival of *M. smegmatis* (23). *M. tuberculosis* is also susceptible to oxidative damage generated by the antimycobacterial drug isoniazid and vitamin C (24, 25). During oxidative stress, macrophages produce glutathione and nitrosogluthathione, and *M. tuberculosis* H₃₇Rv is sensitive to glutathione and nitrosogluthathione in macrophages (26). β -Glucan from yeast induces ROS and inhibits the growth of *M. bovis* BCG in macrophages (27). Therefore, ROS appear to play a role in antimycobacterial toxicity (28). To counter the toxic effect of H₂O₂ and related molecules, *M. tuberculosis* is equipped with decent antioxidants, such as superoxide dismutase, catalase/peroxidase, thioredoxin reductase, alkyl hydroperoxide reductase, and peroxiredoxin (29–32). These antioxidants protect the bacilli against oxidative stress as the virulence of *M. tuberculosis* is dramatically attenuated when superoxide dismutase and related genes are deleted (33, 34). It has also been shown that a histone like protein Isr2 shields mycobacterial DNA from ROS stress but not NO stress (35). Mice knockout for p47^{phox} were also found to be less resistant to tuberculosis (36). These studies highlight the importance of ROS in restraining various microbial infections (16, 37). Although *M. tuberculosis* is known to inhibit ROS production, the factor(s) and the mechanisms of the inhibition of ROS production in macrophages are not understood well.

PPE2 belongs to the proline-glutamate/proline-proline-glutamate (PE/PPE) family in *M. tuberculosis*, a family mostly associated with virulence and evasion of host immune response (38). PPE2 expression was up in hypoxia and NO stress in *DosS* null mutant (39, 40). PPE2 was found to be translocated from the cytosol to the nucleus where it binds to the GATA-1 binding site of the *inos* promoter to inhibit *inos* gene expression and consequently reduced NO production (41). Because the functions of both ROS and NO are co-operative, we speculated PPE2 has a role in the inhibition of ROS generation. In this study, we found that the PPE2 protein inhibits ROS production by preventing the assembly of NADPH oxidase complex on the membrane by seizing up p67^{phox} in the cytosol.

Materials and Methods

Antibodies

Sources and dilutions of primary Abs used in the study were as follows: 1:500 diluted anti-p67^{phox} Ab (610912; BD Biosciences), 1:50 diluted anti-p47^{phox} Ab (ab795; Abcam), 1:100 diluted anti-p40^{phox} Ab (SAB2101554; Sigma-Aldrich), anti-Rac1 Ab (sc-514583; Santa Cruz Biotechnology), 1:1000 diluted anti-Na⁺-K⁺-ATPase Ab (ab76020; Abcam), 1:2000 diluted anti-GAPDH Ab (IMG6665A; IMGENEX), 1:2000 diluted anti- β -actin Ab (sc-4778; Santa Cruz Biotechnology), and 1:10,000 diluted anti-PPE2 Ab (in-house generated) (41). Secondary Abs used were either 1:2000 diluted HRP-conjugated rat anti-mouse IgG VeriBlot (ab131368; Abcam) or 1:10,000 diluted rabbit anti-goat HRP (A5420; Sigma-Aldrich) or goat anti-rabbit HRP (A0545; Sigma-Aldrich) or rabbit anti-mouse HRP (A9044; Sigma-Aldrich).

Sequence homology study of PPE2

Primary FASTA sequence for PPE2 was obtained from TubercuList and UniProtKB databases. p47^{phox} and p67^{phox} sequences were retrieved from UniProtKB. Multiple sequence alignment of the SH3 domains was achieved in Prime Application (Maestro Tool; Schrödinger).

The culture of bacterial strains

E. coli strain DH5 α used for cloning was grown in Luria-Bertani broth (Becton Dickinson, Difco Laboratories). *M. tuberculosis* wild-type (WT) CDC1551 (CDC1551), *M. tuberculosis* ppe2 null mutant (PPE2:KO), and complemented *M. tuberculosis* strains (PPE2:KO:comp) were maintained in the biosafety level 3 facility of National Institute of Immunology (NII) (Delhi, India). Mycobacterial strains were grown in Middlebrook 7H9 Broth supplemented with 10% albumin, dextrose, catalase, and NaCl (HiMedia Laboratories) along with 0.2% glycerol (Sigma-Aldrich) and 0.05% Tween-80 (Sigma-Aldrich). Hygromycin was used at 75 μ g/ml for mycobacteria and at 150 μ g/ml for *E. coli*. Kanamycin was used at 25 and 50 μ g/ml for *E. coli* and *M. tuberculosis*, respectively.

Generation of complementation strain

For generating the complementation strain, pVV16 vector expressing the ppe2 (pVV16-PPE2) (41) construct was electroporated into the electrocompetent cells of PPE2:KO *M. tuberculosis* strain to generate PPE2:KO:pVV16-PPE2 (PPE2:KO:comp). For electroporation, mycobacterial cells were washed three times and resuspended in 10% glycerol. About 100 ng of plasmid DNA was electroporated, and post-24-h revival, cells were plated on 7H11-oleic acid, albumin, dextrose, catalase, and NaCl (HiMedia Laboratories) plates containing hygromycin and kanamycin antibiotics.

Isolation of mouse peritoneal macrophages

BALB/c mice were maintained at the animal house facility of NII. Experiments were performed as per the guidelines of the Institutional Animal Ethics Committee of NII. About 6–8-wk-old BALB/c mice were given 1 ml i.p. injection of 4% thioglycollate medium. Three days postinjection, macrophages were harvested by peritoneal lavage as described earlier (41). Macrophages were cultured in RPMI 1640 medium (Invitrogen) containing 10% heat-inactivated FBS (Invitrogen), 1 \times antibiotic-antimycotic solution, and 1 \times MEM vitamin (all from Invitrogen).

Transfection

RAW 264.7 macrophages were maintained in DMEM (HyClone; Thermo Fisher Scientific) containing 10% FBS, 1 \times antibiotic-antimycotic solution, and 1 \times MEM vitamin. Cells were transfected with various plasmids using polyethylenimine reagent (Polysciences) according to the manufacturer's instructions. The transfection efficiency was found to be ~20–30%.

Determination of ROS generation

RAW 264.7 macrophages were transfected with various plasmid constructs and stimulated with PMA (10 ng/ml) for 90 min. Macrophages were washed and treated with 2',7'-dichlorofluorescein diacetate (DCFH-DA) dye (Sigma-Aldrich) for 60 min, and fluorescence associated with DCFH-DA was measured by flow cytometry (42). Also, peritoneal macrophages from 6–8-wk-old BALB/c mice were infected with different mycobacterial strains at 1:10 multiplicity of infection (MOI). After 4 and 24 h of infection, cells were washed with PBS and treated with 7 μ M of CellROX Deep Red Reagent for 30 min at 37°C followed by washing with PBS. Macrophages were then fixed with 4% paraformaldehyde and trypsinized, and ROS production was measured by flow cytometry.

Preparation of cytoplasmic and plasma membrane fractions from macrophages

RAW 264.7 macrophages were transfected with pEGFP-C1 vector or pEGFP-C1-PPE2 for 24 h followed by stimulation with PMA (10 ng/ml) for 90 min. Macrophages were washed with 1 \times PBS and lysed in HEPES buffer (50 mM HEPES [pH 7.5], 150 mM NaCl, 0.1% Nonidet P-40, 0.25% sodium deoxycholate, and 1 mM EDTA) supplemented with 1 mM leupeptin, 1 mM aprotinin, 1 mM sodium orthovanadate, and 1 mM PMSF for 30 min in ice with occasional vortexing. The lysate was clarified at 13,000 rpm at 4°C to obtain whole cell lysate. To separate cytoplasmic and plasma membrane fraction, whole cell lysate was subjected to ultracentrifugation at 41,000 rpm at 4°C for 60 min. The supernatant was collected as a cytoplasmic fraction, and the pellet was washed thrice with PBS, resuspended in RIPA buffer with 0.1% Nonidet P-40, and centrifuged at 14,000 rpm at 4°C for 60 min. Thus, the clear supernatant obtained after centrifugation was collected as a plasma membrane fraction. The concentration of protein was estimated using Micro BCA Protein Assay Kit (Thermo Fisher Scientific) following the manufacturer's instructions. Whole cell lysate, plasma membrane, and cytoplasmic fractions were stored at –80°C till further use.

Cloning of His-tagged fusion proteins of PPE2, p67^{phox}, and p47^{phox} and site-directed mutagenesis

The DNA fragments encoding N-terminal PPE2 (1–178 aa) and C-terminal PPE2 (179–556 aa) were amplified from WT PPE2 cloned in pRSET-A vector using gene-specific primers (mentioned in Table 1). Site-directed mutagenesis in WT pRSET-A-PPE2 or pCDNA3.1His-PPE2 was performed using the QuickChange Site-Directed Mutagenesis protocol (DpnI method) (StrataGene). Plasmids expressing pET15b-p67^{phox} and pET15b-p47^{phox} were obtained as kind gifts from Dr. L. Baciou.

Purification of recombinant full-length and mutant PPE2, p67^{phox}, and p47^{phox} proteins

The recombinant WT and mutant PPE2 proteins were purified as described earlier (41). For His-tagged p67^{phox} and His-tagged p47^{phox} proteins, plasmid pET15b-p67^{phox} and pET15b-p47^{phox} were transformed and amplified in Rosetta BL21(DE3) *E. coli* cells. Cells were induced with 1 mM isopropyl β -D-1-thiogalactopyranoside and further incubated for 3–4 h. Following induction, cells were harvested and resuspended in Tris Lysis Buffer (10 mM Tris, 150 mM NaCl, 5% glycerol, 0.3% sodium lauryl sarcosine, and 1 mM PMSF), sonicated, and centrifuged at 13,000 rpm at 4°C to remove cell debris. The clear supernatant was loaded onto TALON column for 60 min and washed with wash buffer (10 mM Tris, 150 mM NaCl, 5% glycerol, and 20 mM imidazole). TALON-bound proteins were eluted with elution buffer (10 mM Tris, 150 mM NaCl, 5% glycerol, and 250 mM imidazole). Eluted samples were loaded onto the SDS-PAGE gel to confirm the purity of proteins. Recombinant proteins were dialyzed against dialysis buffer (10 mM Tris, 150 mM NaCl, and 5% glycerol). The concentration of the purified protein was estimated using Micro BCA Protein Assay Kit (Thermo Fisher Scientific).

Pull-down assay

Approximately 1 mg of either whole cell lysate or cytoplasmic or plasma membrane fraction of macrophages was incubated overnight with 20- μ l bed volume of the TALON beads bound to recombinant full-length or mutant PPE2 proteins (41). The beads were collected by centrifugation and washed extensively (five to seven times) with PBS. The washed beads were eluted in the Laemmli buffer and boiled. About 20–40 μ g of the whole cell lysate or cytoplasmic or plasma membrane fraction was used for input. Western blotting was performed using the following Abs: anti-p67^{phox} Ab, anti-p47^{phox} Ab, anti-Na⁺-K⁺-ATPase Ab, anti-GAPDH Ab, anti- β -actin Ab, and anti-PPE2 Ab. This was followed by the use of appropriate combinations of secondary Abs.

Immunoprecipitation

Monolayer culture of RAW 264.7 macrophages was washed, lysed in HEPES buffer, and centrifuged at 13,000 rpm for 20 min at 4°C to get whole cell lysate. The lysate was incubated with 2 μ l of specific Abs overnight at 4°C, followed by incubation with 25 μ l of Protein A/G agarose beads for 1 h at 4°C. Protein A/G agarose beads were collected by centrifugation at 2500 rpm for 3 min, followed by washing in HEPES buffer with 25 mM imidazole and boiled in Laemmli SDS sample buffer. Samples were resolved by 10% SDS-PAGE and transferred onto PVDF membrane. The membrane was probed using appropriate combinations of primary and secondary Abs.

Protein–protein interaction by ELISA

Ninety-six-well microtiter plate was coated with recombinant proteins (specified in legends) diluted in carbonate buffer and incubated for overnight at 4°C. After blocking the wells with 5% FBS in PBS, target recombinant protein was added in 1:3 M ratio for overnight at 4°C. BSA was used as a control protein. After washing, the plate was incubated with mouse anti-p67^{phox} Ab or mouse anti-p47^{phox} Ab or anti-PPE2 Ab followed by incubation with HRP-conjugated anti-mouse secondary Ab. Binding was quantified after adding the substrate of tetramethylbenzidine (BD Biosciences). The reaction was stopped with 1N H₂SO₄, and the resulting absorbance was measured at 450/550 nm in an ELISA microplate reader. All the experiments were performed in triplicate, and mean \pm SEM was calculated after subtracting the control (43).

Isothermal calorimetry

Isothermal calorimetry (ITC) measurements were carried out using a Nano ITC (TA instruments) (44) with an operating cell volume of 170 μ l. The experiments were performed using a Tris buffer for both

protein solutions at a temperature of 25°C. The p67^{phox} protein (1 μ M in the cell) was titrated using 10 μ M PPE2 (dialyzed in Tris buffer). Each titration was performed with 20 injections of 2.5 μ l volume for each injection. The heat of dilutions was determined experimentally from blank titrations. The PPE2–p67^{phox} interaction was analyzed using basic thermodynamic relationships following the two-site binding model provided by the manufacturer in the TA NanoAnalyze software (version 3.7.5). All the recombinant proteins were used within 24 h after purification.

Small interfering RNA-mediated silencing of p67^{phox} in macrophages

RAW 264.7 macrophages were transfected with p67^{phox} small interfering RNA (siRNA) (sc-36164; Santa Cruz Biotechnology) or control siRNA (sc-37007; Santa Cruz Biotechnology) using MISSION siRNA transfection reagent (S1452; Sigma-Aldrich) following the manufacturer's protocol. Expression of p67^{phox} was checked by Western blotting using anti-p67^{phox} Ab.

Intracellular bacterial survival assay

RAW 264.7 macrophages were transfected with p67^{phox} siRNA or control siRNA. Macrophages were infected with CDC1551, PPE2:KO, and PPE2:KO:comp for 4 h at an MOI of 1:10. Postinfection, macrophages were washed with PBS/DMEM. Macrophages were then lysed in 0.1% SDS + 7H9 medium at various time points, and serial dilutions of lysates were plated on 7H11 plates supplemented with 10% oleic acid, albumin, dextrose, catalase, and NaCl (HiMedia Laboratories). Plates were incubated at 37°C, and colonies were counted after 3–4 wk (45).

Statistical analysis

For multiple group comparisons, one-way ANOVA test was performed. Individual statistical analyses of unpaired samples were performed by Student *t* test using Prism 5.02 (Graph Pad Software). A *p* value < 0.05 was considered significant.

Results

Expression of PPE2 in macrophages attenuates ROS generation

Increased PPE2 expression was observed in laboratory and clinical strains of *M. tuberculosis* during macrophage infection as well as in response to hypoxia and NO stress (39, 40). Therefore, to examine the effect of PPE2 on ROS generation, full-length PPE2 was cloned in pCDNA3.1-His vector as described earlier (41). RAW 264.7 macrophages were transfected with either pCDNA3.1-His (vector control) or pCDNA3.1-His expressing WT *ppe2* gene (pCDNA3.1-PPE2-WT). After 24 (Fig. 1A, 1B) and 48 h (Fig. 1C, 1D) of transfection, the cells were stimulated with PMA (10 ng/ml) (Sigma-Aldrich) (42, 43) and treated with a fluorescent dye, DCFH-DA (Sigma-Aldrich), to measure the surge in ROS generation (45). We found that macrophages expressing PPE2 had poorer ROS generation as compared with macrophages harboring pCDNA3.1-His vector alone.

Membrane localization of cytosolic p47^{phox} and p67^{phox} subunits are inhibited in macrophages expressing PPE2

NADPH oxidase is a multi-subunit enzyme complex consisting of two membrane-bound subunits (gp91^{phox} and p22^{phox}) and three cytosolic components (p67^{phox}, p47^{phox}, and p40^{phox}) and a low m.w. G protein (either Rac2 or Rac1) (2). Activation of NADPH oxidase complex is stimulus dependent and requires the recruitment of the cytoplasmic subunits p67^{phox}, p47^{phox}, and p40^{phox} as a complex to the membrane and interact with gp91^{phox} and p22^{phox} to form a functional NADPH oxidase complex (2, 46–48). The inhibition in ROS generation observed in the presence of PPE2 (Fig. 1A, 1C) could be a result of the reduced activity of NADPH complex. Hence, we first assessed whether PPE2 downregulated the activity of NADPH oxidase complex. In macrophages transfected with pEGFPC1 vector or

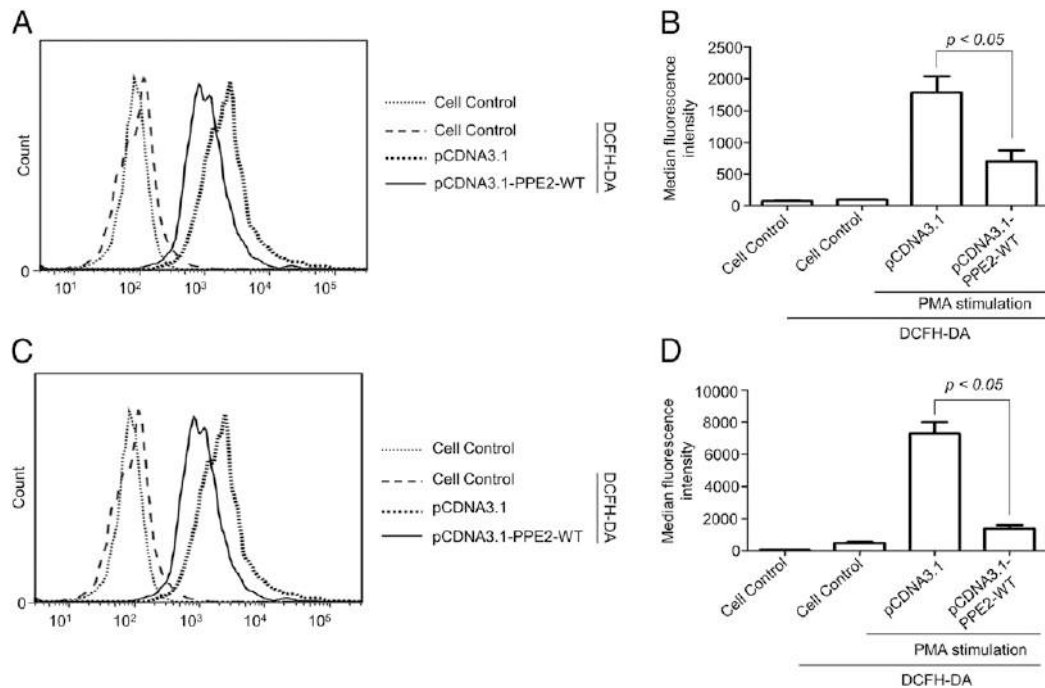


FIGURE 1. Expression of PPE2 significantly attenuates ROS generation in macrophages. RAW 264.7 macrophages were transfected with pCDNA3.1-His vector or pCDNA3.1-PPE2-WT. After 24 h (A and B) and 48 h (C and D) posttransfection, cells were stimulated with PMA (10 ng/ml) for 90 min followed by staining with DCFH-DA dye for 60 min. Fluorescence associated with DCFH-DA was measured in transfected macrophages by flow cytometry (A and C). Median fluorescence intensities of different experimental groups described in (A and C) were calculated, and the results shown are mean \pm SEM of three independent experiments (B and D).

pEGFPC1-PPE2, membrane fractions were separated, and NADPH oxidase activity was measured using a commercial kit (Abcam). It was found that in pEGFPC1-PPE2-transfected macrophages, the ratio of NADP/NADPH in plasma membrane fraction

was significantly lower as compared with that of cells transfected with backbone pEGFPC1 vector alone (Fig. 2A). Lower NADP/NADPH ratio is an indication of the inefficient assembly of NADPH oxidase complex in the presence of PPE2.

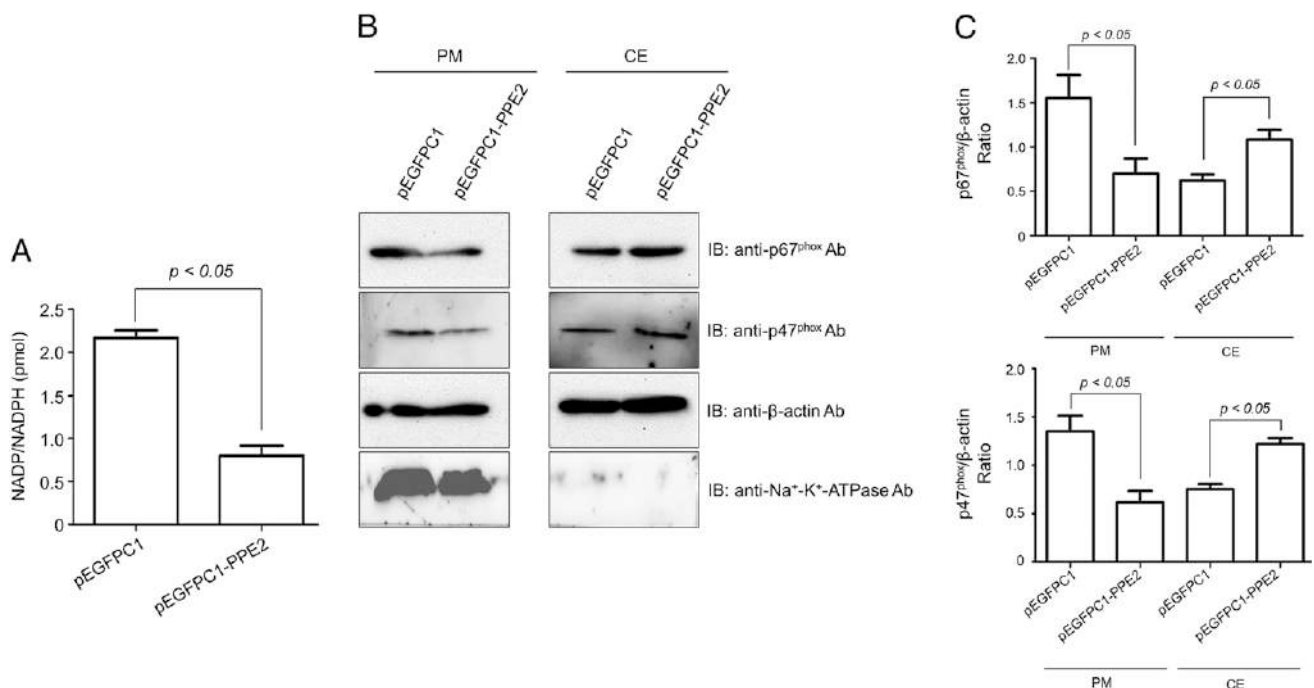


FIGURE 2. PPE2 inhibits membrane localization of cytosolic p47^{phox} and p67^{phox} subunits in macrophages. RAW 264.7 macrophages were transfected with pEGFPC1 vector or pEGFPC1-PPE2 and stimulated with PMA (10 ng/ml) for 90 min. (A) NADPH oxidase activity in plasma membrane fractions was measured using total NADP and NADPH assay kit, and data are shown as mean \pm SEM of three independent experiments. (B) The levels of p47^{phox} and p67^{phox} subunits in plasma membrane and cytoplasm fractions (CE) of transfected macrophages were analyzed by Western blotting. Data are representative of three different experiments. (C) Densitometric analysis of p67^{phox} and p47^{phox} expressions in macrophages was performed by ImageJ software. The graph summarizes densitometric analysis of three independent experiments.

Many intracellular pathogens (for example, *Listeria* and *Neisseria*) suppress ROS generation by causing the defective assembly of NADPH oxidase complex (48–52). To determine whether PPE2 also targets the assembly of NADPH oxidase complex, we examined the recruitment of p47^{phox} and p67^{phox} cytosolic subunits between the plasma membrane and cytosolic extract by Western blotting. We found that both p47^{phox} and p67^{phox} were unable to get recruited to the membrane in pEGFPC1-PPE2-transfected macrophages (Fig. 2B, 2C). Moreover, these results indicate that in the presence of PPE2, NADPH oxidase complex was not assembled properly on the membrane, resulting in the reduced activity of NADPH oxidase complex. In the absence of two key subunits, p47^{phox} and p67^{phox}, NADPH oxidase complex formation failed at the membrane, which compromised the generation of NADPH oxidase-mediated ROS in macrophages.

Interaction of PPE2 with p67^{phox} prevents the migration of p67^{phox}

Our observations from Fig. 2B suggest that p47^{phox} and p67^{phox} are sequestered in the cytoplasm and fail to be recruited to the plasma membrane in the presence of PPE2. To find out whether

PPE2 is affecting the membrane translocation of cytosolic p47^{phox} and p67^{phox} by physically interacting with these proteins, we performed pull-down experiments using whole cell lysate from unstimulated and PMA-stimulated macrophages. PMA stimulation is known to increase the expression and translocation of NADPH oxidase subunits as well as the activity of NADPH oxidase complex (53). Interestingly, when compared with PMA-stimulated macrophages, we observed that PPE2 was able to pull down p67^{phox} in unstimulated macrophages in significant quantities (Fig. 3A). Because PMA stimulation increases the NADPH activity, it is likely that most of the cytosolic p67^{phox} had already been migrated to the plasma membrane to form NADPH complex. Therefore, a lesser amount of free form of p67^{phox} was available for interaction with PPE2, and this probably explains the reduced level of PPE2–p67^{phox} interaction in PMA-stimulated macrophages, although its total expression level was significantly higher. Therefore, it appears that PPE2–p67^{phox} interaction occurred at the cytoplasm. To confirm our hypothesis, we repeated a series of pull-down experiments using TALON-bound PPE2 with cytoplasmic and plasma membrane fractions obtained from unstimulated and PMA-stimulated macrophages. We observed that PPE2

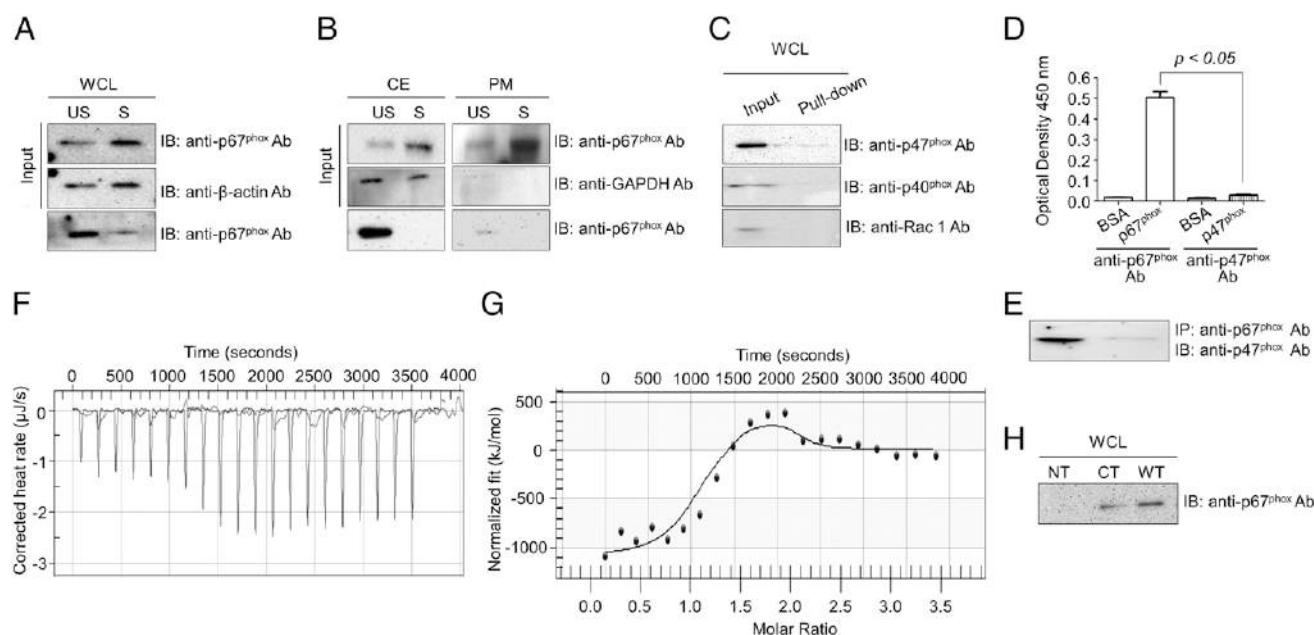


FIGURE 3. Interaction of PPE2 with p67^{phox} prevents its migration from cytosol to the membrane. **(A)** TALON-bound rPPE2 protein was incubated with whole cell lysate (WCL) prepared from either unstimulated (US) or PMA-stimulated (S) RAW 264.7 macrophages. Macrophages were stimulated with PMA (10 ng/ml) for 90 min. PPE2-bound p67^{phox} was probed by Western blotting using mouse anti-p67^{phox} Ab followed by incubation with HRP-conjugated rabbit anti-mouse secondary Ab. Levels of β -actin were checked as input control. **(B)** TALON-bound rPPE2 protein was incubated with either cytoplasmic extract (CE) or plasma membrane fractions separated from unstimulated and PMA-stimulated macrophages. PPE2-bound p67^{phox} was checked by Western blotting using anti-p67^{phox} Ab. **(C)** In another experiment, WCL from unstimulated macrophages was incubated with TALON-bound PPE2 protein. Interaction of PPE2 with p47^{phox} or p40^{phox} or Rac1 interaction was checked by Western blotting using either anti-p47^{phox} Ab or anti-p40^{phox} Ab or anti-Rac1 Ab. **(D)** Also, ELISA experiment was set up to check in vitro interaction of PPE2 with p67^{phox} or p47^{phox}. The 96-well microtiter plate was coated with rPPE2 protein and allowed to interact with either BSA or recombinant p67^{phox} protein or p47^{phox} protein in 1:3 M ratio for overnight at 4°C. Bound protein was detected by Western blotting using either anti-p67^{phox} Ab or anti-p47^{phox} Ab. **(E)** RAW 264.7 macrophages were transfected with pEGFPC1 vector or pEGFPC1-PPE2 and stimulated with 10 ng/ml PMA for 90 min. Transfected cells were lysed in HEPES buffer and subjected to ultracentrifugation to obtain cytoplasmic fraction. p67^{phox} was immunoprecipitated from cytoplasmic fraction with anti-p67^{phox} Ab overnight at 4°C, followed by the addition of protein A/G bead for 60 min at 4°C. Beads were collected by centrifugation and washed with HEPES buffer. Western blotting was performed using anti-p47^{phox} Ab to detect p47^{phox}-bound p67^{phox}. **(F and G)** Direct interaction of PPE2 with p67^{phox} was monitored using a Nano ITC. ITC measurements were carried out using a Nano ITC (TA instruments) with an operating cell volume of 170 μ l. The p67^{phox} protein (1 μ M in the cell) was titrated using 10 μ M PPE2 (dialyzed in Tris buffer). Each titration was performed by 2.5 μ l injection followed by 20 injections. The PPE2–p67^{phox} interaction was analyzed using basic thermodynamic relationships following two-site binding model provided by the manufacturer in the TA NanoAnalyze software (version 3.7.5). Representative images from ITC experiments are illustrated with raw data (F) and fitting curves (continuous lines) (G). The molar ratio and affinity of the PPE2 and p67^{phox} interaction were 2:1 and 12 nm, respectively. **(H)** Whole cell lysate from macrophages was incubated with TALON-bound N-terminal, C-terminal, or full-length PPE2 protein overnight at 4°C. Bound p67^{phox} was probed by Western blotting using anti-p67^{phox} Ab. Data are representative of three independent experiments.

was able to strongly interact with p67^{phox} present in the cytosolic fraction isolated from unstimulated macrophages (Fig. 3B). The interaction between PPE2 and p67^{phox} was further confirmed by a coimmunoprecipitation experiment in which PPE2 was overexpressed in RAW 264.7 macrophages. Endogenous p67^{phox} from transfected macrophages were immunoprecipitated using anti-p67^{phox} Ab, and the bound PPE2 was probed with anti-PPE2 Ab. We found that PPE2 can interact with p67^{phox} (Supplemental Fig. 1).

We also examined the interaction of PPE2 with p47^{phox}; however, no significant interaction was observed in either pull-down or ELISA experiments (Fig. 3C, 3D). Also, no interaction was observed between PPE2 and p40^{phox} as well as PPE2 and Rac1 (Fig. 3C). These results confirm that PPE2 protein interacts with p67^{phox} subunit of NADPH complex predominantly in the cytosol. The results shown in Fig. 3E indicate that interaction between p67^{phox} and p47^{phox} was inhibited in the presence of PPE2. We additionally performed an ITC experiment with recombinant PPE2 and p67^{phox} to get information about the strength of the PPE2–p67^{phox} interaction. We observed a dissociation constant (K_d) of ± 12 nM, indicating a fairly strong interaction between PPE2 and p67^{phox} (Fig. 3F, 3G). The data indicate that PPE2 interacts with p67^{phox} at a 2:1 ratio, approximately.

As a member of the PE/PPE family of proteins, PPE2 can be broadly divided into two regions: a conserved N-terminal (1–178 aa) and a variable C-terminal (179–556 aa) domain (38, 41). To delineate the region of PPE2 sufficient to interact with p67^{phox}, we generated N-terminal PPE2- and C-terminal PPE2-truncated mutants in pRSET-A vector and expressed them in *E. coli* BL21(DE3)pLysS as described earlier (41). In a pull-down experiment, TALON-bound

N-terminal PPE2 or C-terminal PPE2 or full-length PPE2 (WT) were incubated with whole cell lysate of unstimulated macrophages, and their interactions with p67^{phox} were examined by Western blotting. We found that N-terminal PPE2 was not able to interact with p67^{phox} from a whole cell lysate of macrophages, but both C-terminal and full-length PPE2 could do so (Fig. 3H). These observations suggest that the C-terminal of PPE2 is involved in the interaction with p67^{phox}.

PPE2 targets the p67^{phox} subunit to inhibit ROS generation in macrophages during M. tuberculosis infection

In our earlier sections, we observed that when PPE2 was transiently expressed in RAW 264.7 macrophages, it inhibited NADPH oxidase activity by its direct interaction with p67^{phox} and reduced ROS generation. Because PPE2 is a secretory protein (41), we next examined whether during *M. tuberculosis* infection PPE2 could inhibit ROS generation as successfully as we observed in *in vitro* experiments. Accordingly, peritoneal macrophages from BALB/c mice were infected with either WT *M. tuberculosis* CDC1551 (CDC1551) or *M. tuberculosis* PPE2-null mutant (PPE2:KO) or with a PPE2:KO:comp at an MOI 1:10. Expression of PPE2 in the mycobacterial strains used in the study was confirmed by Western experiment using anti-PPE2 Ab (Fig. 4A). ROS generation was measured after 4 (Fig. 4B, 4C) and 24 h (Fig. 4D, 4E) postinfection. We found a significant reduction in ROS generation in macrophages infected with WT *M. tuberculosis* CDC1551 as compared with PPE2:KO strain at the 24 h time point. When PPE2:KO strain was complemented with plasmid pVVI6 expressing WT full-length ppe2 (PPE2:KO:comp), ROS generation in macrophages was

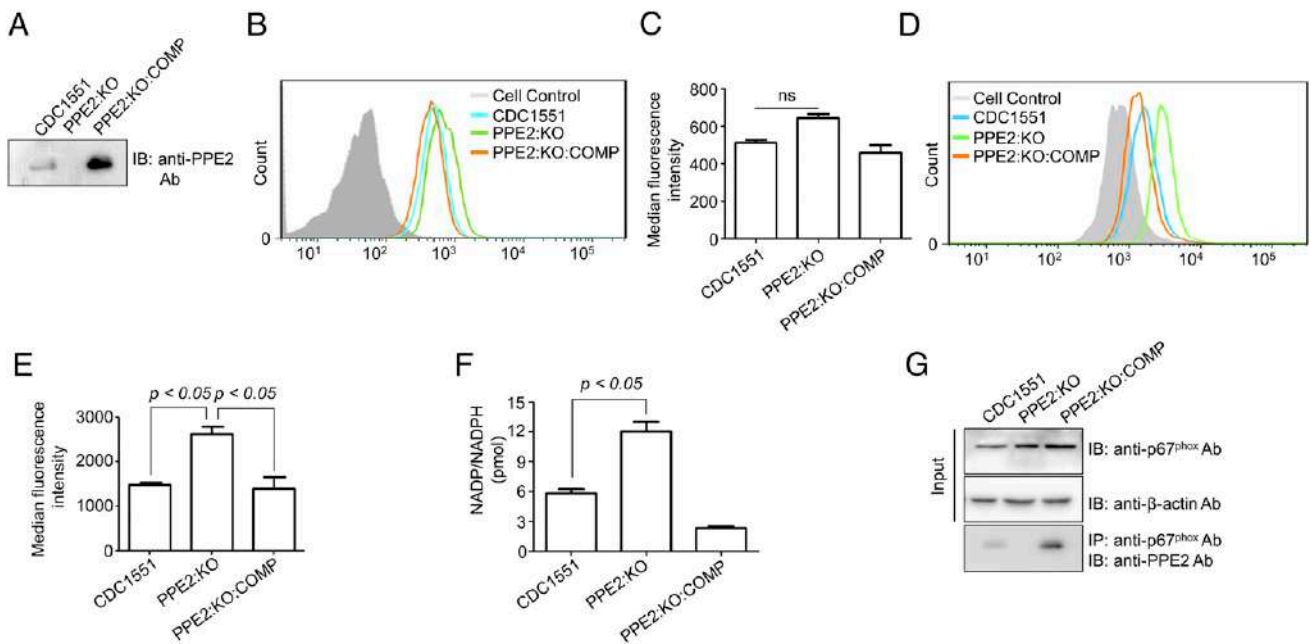


FIGURE 4. *M. tuberculosis* PPE2 targets p67^{phox} to inhibit ROS generation. (A) Expression of PPE2 was checked for mycobacterial strains used in this study. About 10 ml cultures of each mycobacterial strain were subjected to several rounds of bead beating using zirconia beads followed by centrifugation at 13,000 rpm \times g for 20 min at 4°C. PPE2 expression in *M. tuberculosis* was checked by Western blotting using anti-PPE2 Ab. (B–E) Peritoneal macrophages from BALB/c mice were infected with WT (CDC1551) or PPE2-deficient (PPE2:KO) or PPE2:KO:comp *M. tuberculosis* strains at an MOI of 1:10 for either 4 h (B and C) or 24 h (D and E). ROS generation was measured by staining the cells with CellROX Deep Red Reagent (Invitrogen), and the fluorescence was analyzed by flow cytometry. Median fluorescence intensities of different experimental groups described in (B and D) were calculated, and the results shown are mean \pm SEM of three independent experiments (C and E). ns, not significant. (F) RAW 264.7 macrophages were infected with either WT CDC1551 or PPE2:KO or PPE2:KO:comp *M. tuberculosis* strains for 24 h. Macrophages were lysed and subjected to ultracentrifugation for separating plasma membrane fractions. The NADPH oxidase activity in plasma membrane fractions was measured using Total NADP and NADPH assay kit. (G) RAW 264.7 macrophages infected for 24 h with either WT CDC1551 or PPE2:KO or PPE2:KO:comp *M. tuberculosis* strains were lysed in HEPES buffer, and immunoprecipitation was performed with anti-p67^{phox} Ab. The presence of PPE2 in the immunoprecipitated complexes was detected by Western blotting using mouse anti-PPE2 Ab and secondary mouse IgG Ab (VeriBlot). Data are representative of two independent experiments.

decreased as expected (Fig. 4B–D). We also examined NADPH oxidase activity in the plasma membrane fractions obtained from macrophages infected with either CDC1551 or PPE2:KO or PPE2:KO:comp *M. tuberculosis* strains. The presence of PPE2 was found to significantly lower NADPH oxidase activity (Fig. 4F). Additionally, we also investigated the PPE2–p67^{phox} interaction during *M. tuberculosis* infection. Whole cell lysates were prepared from RAW 264.7 macrophages infected with mycobacterial strains as described above, immunoprecipitated with anti-p67^{phox} Ab, and probed with the anti-PPE2 Ab. Similar to in vitro experiments, PPE2 was also found to interact with p67^{phox} in infected macrophages when presented in the context of whole bacilli (Fig. 4G). Thus, our in vitro experiments using *M. tuberculosis* clearly suggest that *M. tuberculosis* PPE2 targets p67^{phox} to inhibit ROS generation in macrophages by inhibiting the formation of the active NADPH complex on the membrane.

ROS are shown to influence the secretion of proinflammatory cytokines (54). Because PPE2 inhibits ROS, we next examined the effect of PPE2 on cytokine production during mycobacterial infection. For this, peritoneal macrophages from BALB/c mice were infected with either WT CDC1551 or PPE2:KO or PPE2:KO:comp for 4 h at an MOI of 1:10. Culture supernatants were collected 24 h postinfection to measure various cytokines. It was observed that the levels of proinflammatory cytokines, like IL-1 β and TNF- α , were more in CDC1551- and PPE2:KO:comp-infected macrophages as compared with PPE2:KO-infected macrophages (Supplemental Fig. 2A, 2B). However, no significant changes were observed in the IL-10 level (Supplemental Fig. 2C). This suggests that PPE2 reduced the level of proinflammatory cytokines in macrophages.

PPE2 favors mycobacterial survival in macrophages by targeting p67^{phox}

As an innate effector function of macrophages, ROS are toxic for *M. tuberculosis*. Any defect in the assembly of NADPH oxidase can reduce ROS production and favor survival of bacilli (50, 51).

Therefore, we transfected RAW 264.7 macrophages with either p67^{phox} siRNA (p67^{phox} KD) or control siRNA followed by infection with WT *M. tuberculosis* CDC1551 or PPE2:KO or PPE2:KO:comp, and intracellular survival of bacilli was examined at various time points. We found that in control macrophages, WT CDC1551 or PPE2:KO:comp survived better than PPE2:KO at both 24 and 48 h time points (Fig. 5), indicating that PPE2 helps in the better survival of *M. tuberculosis*. However, PPE2:KO strain had higher CFU in p67^{phox} knock-down cells because of less NADPH-dependent ROS production in these cells. This also explains marginally higher CFUs for both WT CDC1551 and PPE2:KO:comp in p67^{phox} knock-down cells.

PPE2 possesses SH3-like domain

Domain prediction in the primary sequence of the proteins using knowledge-based sequence analysis servers and sequence alignment methods provides justifications for target-based approaches of protein interaction. Multiple sequence alignment with known eukaryotic SH3 domains and prokaryotic SH3-like domains revealed the presence of an SH3-like domain in PPE2 (aa 201–256) (Fig. 6A–C). Comparison of SH3-like domain of PPE2 with known eukaryotic SH3 domains allowed us to identify the conserved pattern of crucial amino acid residues with little variations. The SH3-like domain of PPE2 was found to be highly conserved with tryptophan (W) and proline (P) (Fig. 6B), which endows specificity and xP pockets. Other crucial aromatic amino acids of xP pocket (formed by aa 7, 55, 36, and 52, Fig. 6B), such as phenylalanine (F) and tyrosine (Y, after proline), were found to be less conserved in PPE2. However, the less conserved residues of PPE2 in SH3-like domain, like aspartic acid (D) and Isoleucine (I) in place of aromatic amino acid regions (F and Y), renders it incompetent in binding the class I type proline-rich region (PRR) ligands but is still capable of recognizing class II and nonconsensus ligands (55–58).

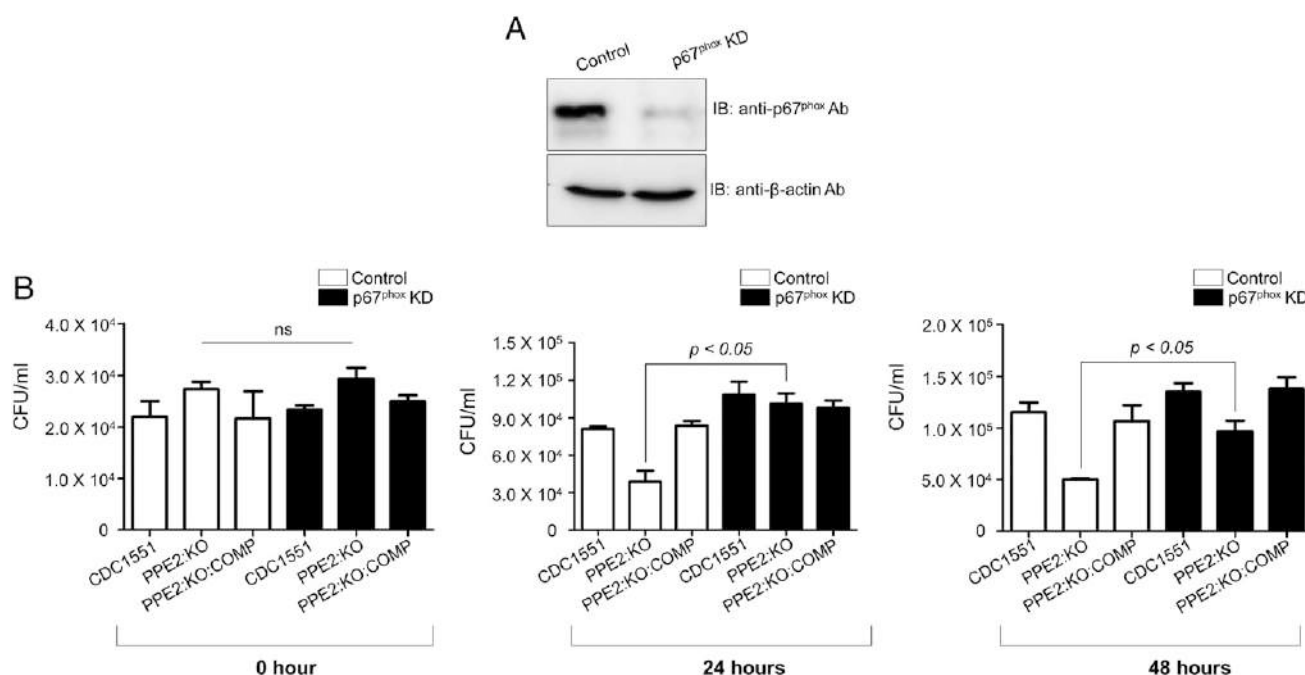


FIGURE 5. Intracellular survival of *M. tuberculosis* in macrophages in control and p67^{phox} knock-down macrophages. Macrophages were transfected with control siRNA or siRNA targeting p67^{phox}. After 24 h, expression of p67^{phox} was checked by Western blotting using anti-p67^{phox} Ab, and β -actin was used as a loading control (A). Macrophages were next infected with *M. tuberculosis* at an MOI of 1:10 for 4 h. Cells were lysed immediately (0 h) or after 24 and 48 h of culture. Intracellular survival of mycobacteria was measured by CFU enumeration (B). Data are mean \pm SEM of three independent experiments.

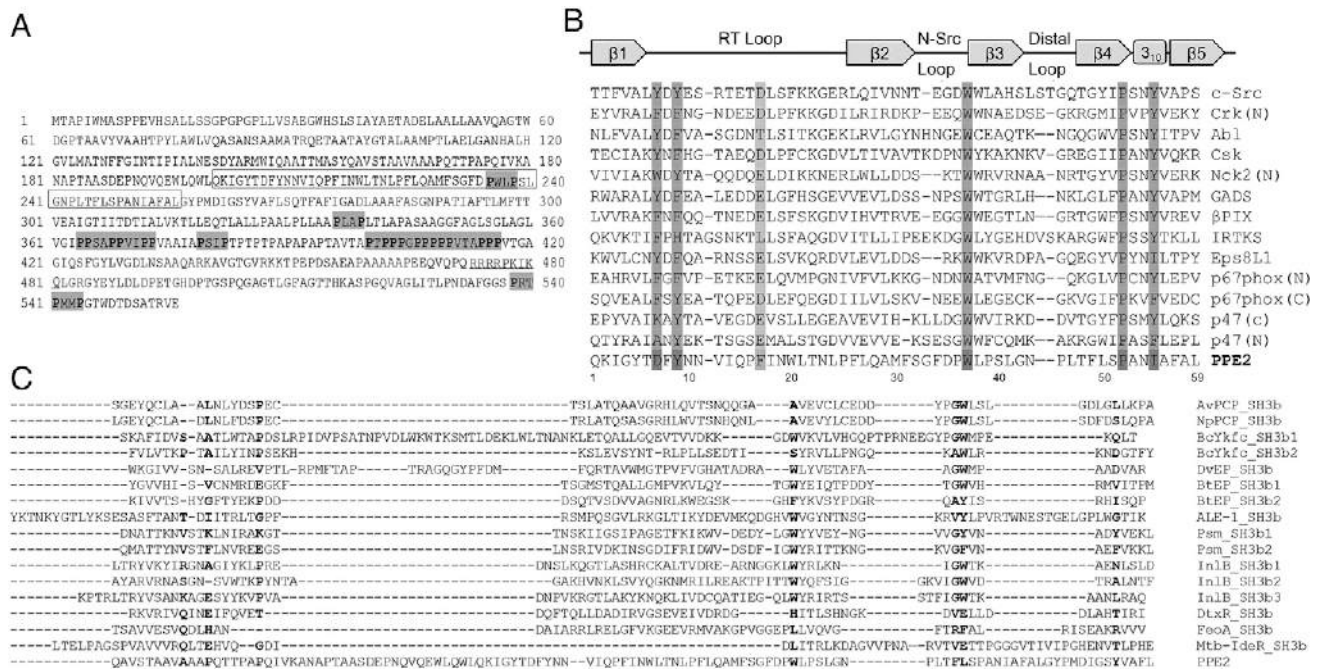


FIGURE 6. PPE2 possesses a SH3-like domain. **(A)** Amino acid sequences of PPE2 with SH3 domain are boxed, PxxP (PRRs) are in gray, and nuclear localization signal is underlined. FASTA sequence for PPE2 were obtained from TuberculList and UniProtKB databases, and p47^{phox} and p67^{phox} sequences were retrieved from UniProtKB. Pairwise multiple sequence alignment was used to identify a SH3-like domain in PPE2. **(B)** In amino acid sequence alignment (from 1 to 59 residues) between eukaryote SH3 domains with *M. tuberculosis* PPE2, key residues that form the two conserved xP pockets (amino acid residues 7 + 55 and 36 + 52) and the specificity pocket (aa 17) were highlighted in dark gray and light gray, respectively. The predicted SH3-like domain of PPE2 was aligned with conserved residues of other SH3 domain proteins at positions Y9, W36, and P52. Other positions D7, F17, and I55 are likely to form specificity binding properties toward unique PRRs. All the eukaryotic SH3 domain sequences used for the alignment (except PPE2) are of human origin. Common names of listed proteins are as follows: proto-oncogene tyrosine-protein kinase Src (C-Src), proto-oncogene c-Crk (Crk), Tyrosine-protein kinase ABL (Abl), NCK adaptor protein 2 (Nck2), GRB2-related adaptor downstream of Shc (GADS), β-p21-activated kinase-interacting exchange factor (βPIX), Bin/amphipysin/Rvs domain-containing protein (IRTKS), epidermal growth factor receptor kinase substrate 8-like protein 1 (EPS8L1), Neutrophil cytosol factor 2, also known as p67^{phox}, and Neutrophil cytosol factor 1, also known as p47^{phox}. **(C)** Amino acid sequence alignment between prokaryote SH3 domains (SH3b domains) with *M. tuberculosis* PPE2. *M. tuberculosis* PPE2 showed poor similarity with the other prokaryotic SH3-like domains. Similar residues are highlighted in bold. Sequences aligned in this study are obtained from the following sources: AvPCP of *Anabaena variabilis*, NpPCP of *Nostoc punctiforme*, BcYkfc of *Bacillus cereus*, DvEP of *Desulfovibrio vulgaris*, BtEP of *Bacteroides thetaiotaomicron*, ALB1 of *S. simulans*, Psm of *Clostridium perfringens* type A strain 101, InLB of *L. monocytogenes*, diphtheria toxin repressor of *C. diphtheriae*, ferrous iron-transport activating factor of *S. maltophilia*, IdeR of *M. tuberculosis*, and PPE2 of *M. tuberculosis*.

Because PPE2 protein is a proline-rich protein, we analyzed its sequence for the presence of PRRs. The conserved N-terminal (1–178 aa) and a variable C-terminal (179–556 aa) domains of PPE2 were analyzed for the presence of class I +XΦPXXP region (where “+” is a positively charged arginine (R) or lysine (L) residue, “X” is any amino acid, and symbol Φ refers to hydrophobic amino acid residues), class II XPXΦPX+ regions, and nonconsensus regions (59). We observed that the C-terminal region of PPE2 possesses 11 nonconsensus PxxP (PRRs), and also a class II consensus region was found in an inverse direction (+XPΦXPX) from 539 to 545 residues (RTPMMPG) (Fig. 6A).

Tryptophan 236 (W236) is an important residue responsible for PPE2–p67^{phox} interaction as W236A mutant did not inhibit ROS generation and also failed to interact with p67^{phox}

Sequence analysis of PPE2 for domain identification revealed the presence of SH3-like domain and PRRs with a PxxP motif (Fig. 7A). To understand which domain of PPE2 was responsible for its interaction with p67^{phox}, various mutations were generated in pRSET-A vector expressing PPE2 (residues, tyrosine 209 [Y209], tryptophan 236 [W236], and proline 249 [P249] were changed to alanine [Y209A, W236A, and P249A, respectively]) (Table I). Also, one disrupted PRR mutant was created by the deletion of residues from 540 to 543 (Δ540–543). All the recombinant proteins were purified using TALON beads as mentioned earlier (41).

We performed an ELISA-based in vitro binding assay in which a 96-well plate was coated with rp67^{phox} and incubated either WT or mutant PPE2 protein. The bound protein was detected by anti-PPE2 Ab (Fig. 7B). Similarly, in pull-down experiments, whole cell lysate prepared from macrophages was incubated with TALON-bound either WT or mutant PPE2 protein. Interaction of WT or mutant PPE2 using anti-p67^{phox} Ab was carried out using Western blotting (Fig. 7C). In both experiments, we observed that the rW236A protein failed to interact with p67^{phox}, whereas Y209A, P249A, and Δ540–543 exhibited interaction similar to PPE2-WT. Because the strength of the interaction was found to be weaker in the case of W236A mutant, we next examined whether the mutants could also affect PMA-induced ROS production in macrophages. Therefore, all the above-mentioned mutants were generated in pCDNA3.1-His-PPE2, and transfection in RAW 264.7 macrophages was performed (Table I). Expression of PPE2 in macrophages transfected with various mutants was validated by Western blotting after 24 h of transfection (Fig. 7D), and ROS measurement in these macrophages was carried out after stimulation with PMA (10 ng/ml) as mentioned before. We found that PPE2-WT, Y209A, P249A, and Δ540–543 were able to inhibit ROS except for W236A (Fig. 7E). These results indicate that W236 residue of PPE2 is critical for PPE2–p67^{phox} interaction and the inhibition of ROS production. Thus, it can be concluded that the SH3-like domain of PPE2 is critical for interaction with

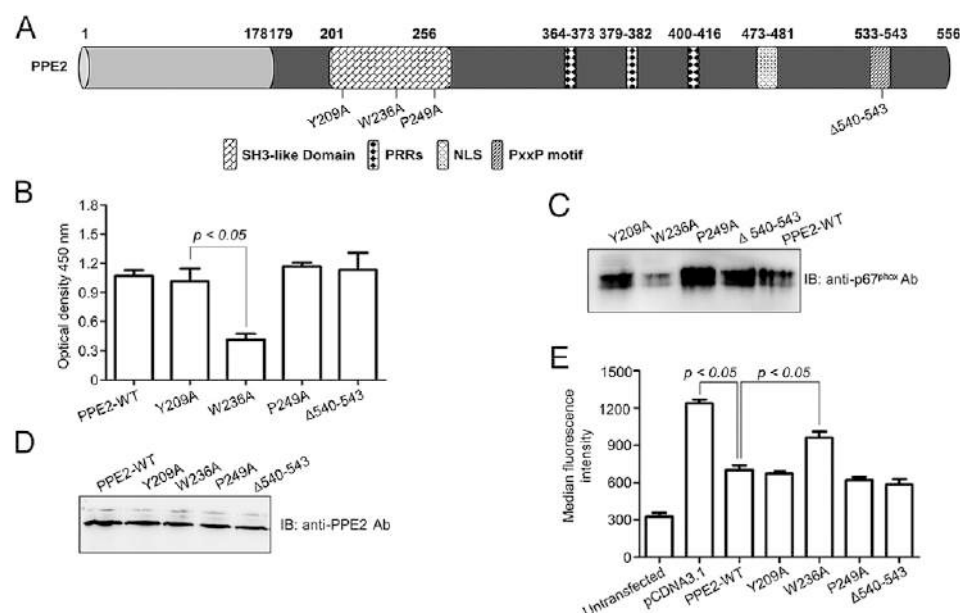


FIGURE 7. Tryptophan 236 in PPE2 is an important residue responsible for p67^{phox} interaction and the inhibition of ROS production. **(A)** Schematic representation of predicted domains present in PPE2. PPE2 has conserved N-terminal PPE2 (1–178 aa), and variable C-terminal PPE2 (179–556 aa). **(B)** In vitro analysis of the interaction of mutant rPPE2 proteins with p67^{phox} protein was performed by ELISA. Briefly, in 96-well microtiter plate, the rp67^{phox} protein was coated and incubated with recombinantly purified WT PPE2 or its various mutants (Y209A, W236A, P249A, and Δ540–543) overnight at 4°C to allow interaction with p67^{phox} protein. The plate was washed, and bound PPE2 protein was detected by Western blotting using mouse anti-PPE2 Ab and rabbit anti-mouse HRP conjugate, respectively. Data are mean ± SEM of three independent experiments. **(C)** In another experiment, whole cell lysate from unstimulated RAW 264.7 macrophages were incubated with TALON-bound recombinant WT PPE2 or its various mutants for overnight at 4°C. The bound p67^{phox} was detected by Western blotting using mouse anti-p67^{phox} Ab. Data are representative of three independent experiments. **(D and E)** RAW 264.7 macrophages were transfected with pCDNA3.1 expressing WT or various mutants of PPE2 (Y209A, W236A, P249A, and Δ540–543) or vector control alone. After 24 h, cells were either lysed, and the expression of PPE2 was checked by Western blotting using anti-PPE2 Ab **(D)** or stimulated with PMA (10 ng/ml) for the generation of ROS **(E)**. Levels of ROS production were measured by staining the cells with DCFH-DA dye, and fluorescence associated with DCFH-DA was measured by flow cytometry. Data are mean ± SEM of three independent experiments.

p67^{phox} subunit, and the tryptophan residue in the SH3-like domain of PPE2 plays an important role in this interaction.

Discussion

Oxidative burst is a characteristic innate effector function for the killing of several invading microorganisms by macrophages and neutrophils (60–62). ROS generation is an immediate response and represents the first line of defense of host against infection reservoirs (6–8). *M. tuberculosis* neutralizes the oxidative stress threat generated by macrophages using its own redox buffer

system or secretory virulence factors (41). As we found earlier that PPE2 can suppress NO production by inhibiting the transcription of *inos* in macrophages (41), we speculated that PPE2 may also play a role in NADPH oxidase-mediated ROS generation in macrophages. Interestingly, we observed that ROS generation in macrophages was suppressed by *M. tuberculosis* at the early time point (4 h) and more profoundly at the later time point (24 h). Earlier, using a surrogate bacterium *M. smegmatis*, we observed that at 1 h postinfection, PPE2 appears to be located predominantly in the endosome. However, at 6 h postinfection, it

Table I. List of primers used in this study

Primer Name	Primer Sequence
pCDNA3.1-His-PPE2-WT, <u>KpnI</u> , and <u>EcoRI</u>	Forward: 5'-ATATGGTACCATATGACCGCCCGGATCTGGA-3' Reverse: 5'-TTGAATTCTCACTCCACCCGGGTGCGTG-3'
pRSETA-PPE2-WT, <u>SacI</u> , and <u>EcoRI</u>	Forward: 5'-CGAGAGCTCAATGACCGCCCGGATCTGGATGG-3' Reverse: 5'-GCAGAATTCTCACTCCACCCGGGTGCGTGAGT-3'
pRSETA-PPE2 N-terminal, <u>NheI</u> , and <u>EcoRI</u>	Forward: 5'-GCAGCTAGCATGACCGCCCGGATCTGGATGG-3' Reverse: 5'-CGTGAATTCTCACTGGGGGGGTGGGGTGGTCTG-3'
pRSETA-PPE2 C-terminal, <u>BamHI</u> , and <u>EcoRI</u>	Forward: 5'-GCAGGATCCAAATGGTGAAAGCCAACGCGCCG-3' Reverse: 5'-CGTGAATTCTCACTCCACCCGGGTGCGTGAGT-3'
Y209A	Forward: 5'-CGGGTATACCGACTTCGCGAACAACGTTATACAACC-3' Reverse: 5'-GGTTGTATAACGTTGTTTCGCGAAGTCGGTATACCCG-3'
W236A	Forward: 5'-GTTTTCGGATTGATCCGGCGCTGCCCTCGCTGGGTAATC-3' Reverse: 5'-GATTACCCAGCGAGGCGAGCCGGGATCAAATCCGGAAAAC-3'
P249A	Forward: 5'-ACGCAATGTTGGCCGCGCTTAGGAAGGTTAG-3' Reverse: 5'-CTAACCTTCCTAAGCGCGGCAACATGTGCGT-3'
del-PxxP-540-543	Forward: 5'-CCAGGTTCCGGGGCGTGGGCTGCC-3' Reverse: 5'-GGCAGCCACGCCCCGAACCTGG-3'

Restriction enzymes and restriction sites are underlined.

is predominantly located in the cytoplasm and nucleus (41). This explains our inability to detect PPE2-mediated significant inhibition of ROS production as early as 4 h postinfection. ROS production was found to be significantly decreased at 24 h postinfection as by that time, a significant amount of PPE2 builds up in the cytoplasm. We were also able to detect PPE2–p67^{phox} interaction at the same time point of 24 h. Macrophages infected with *M. tuberculosis* PPE2:KO strain resulted in higher ROS generation and NADPH oxidase activity as compared with those infected with WT *M. tuberculosis* strain, indicating an active participation of PPE2 in ROS inhibition. Intracellular survival assay of *M. tuberculosis* in p67^{phox} knock-down macrophages showed that WT *M. tuberculosis* CDC1551 and *M. tuberculosis* PPE2:KO:comp survived better than *M. tuberculosis* PPE2:KO in control macrophages. Our results support the view that PPE2 can favor bacterial survival inside macrophages by interacting and sequestering p67^{phox} and the subsequent inhibition of ROS production. Also, we found that the secretion of proinflammatory cytokines, TNF- α and IL-1 β , were reduced in the presence of PPE2, and IL-10 levels were unchanged. Thus, PPE2 may influence the cytokine production to establish a positive infection.

NADPH oxidase complex assembly at the membrane is responsible for ROS generation (62, 63). We found that NADPH oxidase activity was reduced in the presence of PPE2. This reduction in NADPH oxidase activity occurs because of a defect in NADPH oxidase assembly (2). It has been shown earlier that PPE2 protein is translocated to the cytosol (41); thus, it can interact with the cytosolic p67^{phox} subunit, disrupting NADPH oxidase complex assembly. We observed a direct interaction of PPE2 with p67^{phox} subunit only but not with p47^{phox}, p40^{phox}, or Rac1. It is known that C-terminal SH3 domain of p67^{phox} interacts with a terminal PRR of p47^{phox} with a binding affinity of $K_d = 20$ nm (47, 63–65). The binding affinity of PPE2–p67^{phox} complex derived from our ITC experiment was of $K_d = 12$ nm, and therefore, affinity of PPE2 to p67^{phox} is higher than p67^{phox}–p47^{phox}. Thus, based on our ITC and pull-down experiments, it is likely that PPE2 preferably interacts with the free p67^{phox} to inhibit the formation of p67^{phox}–p47^{phox} complex. Consequently, sequestration of p67^{phox} by PPE2 prevents the subsequent recruitment of cytosolic p67^{phox} and p47^{phox} subunits to the membrane. Such unavailability of cytosolic subunits at the membrane causes a reduction of the functional assembly of NADPH oxidase complex, resulting in reduced NADPH oxidase activity and lesser ROS generation. This initial inhibition of ROS generation can help the bacterium to avoid the first line of host defense.

An SH3-like domain and several PRRs were identified in the C-terminal region of PPE2. SH3-like domain of PPE2 shows a regular and conserved pattern of eukaryotic Src homology, and similarities of residues can contribute to the formation of specificity toward unique PRR ligands. Most important conserved residues of SH3 domain (W36 and P52, Fig. 6B) were found to be well aligned and conserved with the residues of PPE2. In prokaryotes, sporadic occurrence of SH3-like domains (SH3b) is reported (66–68). Notable examples of prokaryotes with SH3-like domains are diphtheria toxin repressor (66, 69) from *Corynebacterium diphtheriae*, iron-dependent repressor (IdeR) 70 from *M. tuberculosis*, and ferrous iron-transport activating factor from *Stenotrophomonas maltophilia* (68). In *M. tuberculosis*, IdeR is known to have SH3-like-fold structure (70). But, SH3-like domain of PPE2 appears to be rare examples of bacterial proteins, in which it shows higher similarity toward the eukaryotic SH3 domains rather than bacterial (SH3b) domains (Fig. 6B, 6C). In most of the examples, conserved residues of SH3 domain (W36 and P52) together form a “specificity zone,” and neighboring residues facilitate precise

and selective interaction with ligands like PxxP (48, 56, 59). Site-directed mutagenesis-based studies revealed the loss in the interaction of PPE2 with p67^{phox} when tryptophan residue at 236 position was mutated to alanine. Accordingly, ROS generation was higher in macrophages transfected with the W236A mutant as compared with the macrophages transfected with WT PPE2, indicating that PPE2 interacts with p67^{phox} through its SH3 domain. It appears that the W236A mutation alters the specificity zone in such a way that PPE2 could only weakly interact with p67^{phox}, resulting in poorer ROS inhibition in macrophages.

Although it is widely accepted that ROS-mediated killing is nonspecific and rapid, it also promotes or helps in the establishment of adaptive immunity indirectly (71, 72). NADPH oxidase-mediated ROS generation in dendritic cell phagosome optimizes the pH required for cross-presentation of Ag (72, 73). But in gp91^{phox}–/– dendritic cells, ROS generation, as well as Ag processing, are shown to be compromised because of the alkaline environment of the phagosome (7). A similar school of thought also debate on the issue of Ag presentation or cross-presentation by MHC class I cells and escape of *Mycobacterium* sp. from phagosomes (74, 75). Neutrophils can also kill phagocytosed bacteria in NADPH oxidase-dependent manner (62). Because in vitro and in vivo studies on mycobacterial escape from phagosome to cytosol are not in concordance because of technical limitation and unavailability of the proper model system, it is extremely difficult to comprehend whether ROS generation has any direct effect on the processing and presentation of mycobacterial Ag. Nonetheless, *Mycobacterium*'s nonconventional choice of macrophage as its niche and granuloma formation indicates that it evades oxidative killing very effectively (76–78). Also, mouse knockout for NADPH oxidase are found to be susceptible to multiple infections and face early death (79), supporting the fact that the production of ROS is crucial for defense against several pathogens (80, 81). Use of drugs that release either NO or ROS donor like 2,3-dihydro-1,4-benzoquinones are already in trials as antimycobacterial agents (82).

Our study delineates the mechanism of ROS inhibition and highlights the potential of a PPE family protein, PPE2 protein, as a virulence factor used by the bacterium to avoid oxidative stress inside the hostile macrophage environment. Thus, PPE2 may be an important target for the development of a novel drug to fight against the sly foe *M. tuberculosis*.

Acknowledgments

The authors are extremely thankful to Dr. Laura Baciou (Laboratoire de Chimie Physique, Université Paris Sud) for providing p67^{phox} and p47^{phox} clones.

Disclosures

The authors have no financial conflicts of interest.

References

- World Health Organization. 2017. Global Tuberculosis Report (WHO). <http://apps.who.int/iris/bitstream/10665/259366/1/9789241565516-eng.pdf>. Accessed: September 18, 2018.
- Babior, B. M. 2004. NADPH oxidase. *Curr. Opin. Immunol.* 16: 42–47.
- Pizzolla, A., M. Hultqvist, B. Nilsson, M. J. Grimm, T. Eneljung, I. M. Jonsson, M. Verdreng, T. Kelkka, I. Gertsson, B. H. Segal, and R. Holmdahl. 2012. Reactive oxygen species produced by the NADPH oxidase 2 complex in monocytes protect mice from bacterial infections. *J. Immunol.* 188: 5003–5011.
- Novais, F. O., B. T. Nguyen, D. P. Beiting, L. P. Carvalho, N. D. Glennie, S. Passos, E. M. Carvalho, and P. Scott. 2014. Human classical monocytes control the intracellular stage of *Leishmania braziliensis* by reactive oxygen species. *J. Infect. Dis.* 209: 1288–1296.
- Hussain Bhat, K., and S. Mukhopadhyay. 2015. Macrophage takeover and the host-bacilli interplay during tuberculosis. *Future Microbiol.* 10: 853–872.
- Fang, F. C. 2011. Antimicrobial actions of reactive oxygen species. *MBio* 2: e00141–11.
- Molteni, C. G., N. Principi, and S. Esposito. 2014. Reactive oxygen and nitrogen species during viral infections. *Free Radic. Res.* 48: 1163–1169.

8. De Groote, M. A., U. A. Ochsner, M. U. Shiloh, C. Nathan, J. M. McCord, M. C. Dinauer, S. J. Libby, A. Vazquez-Torres, Y. Xu, and F. C. Fang. 1997. Periplasmic superoxide dismutase protects *Salmonella* from products of phagocyte NADPH-oxidase and nitric oxide synthase. *Proc. Natl. Acad. Sci. USA* 94: 13997–14001.
9. Gallois, A., J. R. Klein, L. A. Allen, B. D. Jones, and W. M. Nauseef. 2001. *Salmonella* pathogenicity island 2-encoded type III secretion system mediates exclusion of NADPH oxidase assembly from the phagosomal membrane. *J. Immunol.* 166: 5741–5748.
10. Songsunthong, W., M. C. Higgins, H. G. Rolán, J. L. Murphy, and J. Meccas. 2010. ROS-inhibitory activity of YopE is required for full virulence of *Yersinia* in mice. *Cell. Microbiol.* 12: 988–1001.
11. Cifani, N., B. Pompili, M. Anile, M. Patella, D. Diso, F. Venuta, G. Cimino, S. Quattrucci, E. G. Di Domenico, F. Ascenzioni, and P. Del Porto. 2013. Reactive-oxygen-species-mediated *P. aeruginosa* killing is functional in human cystic fibrosis macrophages. *PLoS One* 8: e71177.
12. Pollock, J. D., D. A. Williams, M. A. Gifford, L. L. Li, X. Du, J. Fisherman, S. H. Orkin, C. M. Doerschuk, and M. C. Dinauer. 1995. Mouse model of X-linked chronic granulomatous disease, an inherited defect in phagocyte superoxide production. *Nat. Genet.* 9: 202–209.
13. Röhm, M., M. J. Grimm, A. C. D'Auria, N. G. Almyroudis, B. H. Segal, and C. F. Urban. 2014. NADPH oxidase promotes neutrophil extracellular trap formation in pulmonary aspergillosis. *Infect. Immun.* 82: 1766–1777.
14. Deffert, C., M. G. Schappi, J. C. Pache, J. Cachat, D. Vesin, R. Bisig, X. Ma Mulone, T. Kelkka, R. Holmdahl, I. Garcia, et al. 2014. *Bacillus calmette-guerin* infection in NADPH oxidase deficiency: defective mycobacterial sequestration and granuloma formation. *PLoS Pathog.* 10: e1004325.
15. Noubade, R., K. Wong, N. Ota, S. Rutz, C. Eidenschenk, P. A. Valdez, J. Ding, I. Peng, A. Sebrell, P. Caplazi, et al. 2014. NRROS negatively regulates reactive oxygen species during host defence and autoimmunity. *Nature* 509: 235–239.
16. Adams, L. B., M. C. Dinauer, D. E. Morgenstern, and J. L. Krahenbuhl. 1997. Comparison of the roles of reactive oxygen and nitrogen intermediates in the host response to *Mycobacterium tuberculosis* using transgenic mice. *Tuber. Lung Dis.* 78: 237–246.
17. Manca, C., S. Paul, C. E. Barry, III, V. H. Freedman, and G. Kaplan. 1999. *Mycobacterium tuberculosis* catalase and peroxidase activities and resistance to oxidative killing in human monocytes *in vitro*. *Infect. Immun.* 67: 74–79.
18. Paiva, C. N., and M. T. Bozza. 2014. Are reactive oxygen species always detrimental to pathogens? *Antioxid. Redox Signal.* 20: 1000–1037.
19. Firmani, M. A., and L. W. Riley. 2002. *Mycobacterium tuberculosis* CDC1551 is resistant to reactive nitrogen and oxygen intermediates *in vitro*. *Infect. Immun.* 70: 3965–3968.
20. Koo, M. S., S. Subbian, and G. Kaplan. 2012. Strain specific transcriptional response in *Mycobacterium tuberculosis* infected macrophages. *Cell Commun. Signal.* 10: 2.
21. Kim, B. H., A. R. Shenoy, P. Kumar, R. Das, S. Tiwari, and J. D. MacMicking. 2011. A family of IFN- γ -inducible 65-kD GTPases protects against bacterial infection. *Science* 332: 717–721.
22. Roca, F. J., and L. Ramakrishnan. 2013. TNF dually mediates resistance and susceptibility to mycobacteria via mitochondrial reactive oxygen species. *Cell* 153: 521–534.
23. Paik, S., S. Choi, K. I. Lee, Y. W. Back, Y. J. Son, E. K. Jo, and H. J. Kim. 2019. *Mycobacterium tuberculosis* acyl carrier protein inhibits macrophage apoptotic death by modulating the reactive oxygen species/c-Jun N-terminal kinase pathway. *Microbes Infect.* 21: 40–49.
24. Dhandayuthapani, S., Y. Zhang, M. H. Mudd, and V. Deretic. 1996. Oxidative stress response and its role in sensitivity to isoniazid in mycobacteria: characterization and inducibility of ahpC by peroxides in *Mycobacterium smegmatis* and lack of expression in *M. aurum* and *M. tuberculosis*. *J. Bacteriol.* 178: 3641–3649.
25. Vilchère, C., T. Hartman, B. Weinrick, and W. R. Jacobs, Jr. 2013. *Mycobacterium tuberculosis* is extraordinarily sensitive to killing by a vitamin C-induced Fenton reaction. *Nat. Commun.* 4: 1881.
26. Venkataraman, V., Y. K. Dayaram, M. T. Talaue, and N. D. Connell. 2005. Glutathione and nitrosoglutathione in macrophage defense against *Mycobacterium tuberculosis*. *Infect. Immun.* 73: 1886–1889.
27. Betz, B. E., A. K. Azad, J. D. Morris, M. V. S. Rajaram, and L. S. Schlesinger. 2011. β -Glucans inhibit intracellular growth of *Mycobacterium bovis* BCG but not virulent *Mycobacterium tuberculosis* in human macrophages. *Microb. Pathog.* 51: 233–242.
28. Lee, H. J., H. J. Ko, and Y. J. Jung. 2016. Insufficient generation of mycobactericidal mediators and inadequate level of phagosomal maturation are related with susceptibility to virulent *Mycobacterium tuberculosis* infection in mouse macrophages. *Front. Microbiol.* 7: 541.
29. Jaeger, T., H. Budde, L. Flöhé, U. Menge, M. Singh, M. Trujillo, and R. Radi. 2004. Multiple thioredoxin-mediated routes to detoxify hydroperoxides in *Mycobacterium tuberculosis*. *Arch. Biochem. Biophys.* 423: 182–191.
30. Guimarães, B. G., H. Souchon, N. Honoré, B. Saint-Joanis, R. Brosch, W. Shepard, S. T. Cole, and P. M. Alzari. 2005. Structure and mechanism of the alkyl hydroperoxidase AhpC, a key element of the *Mycobacterium tuberculosis* defense system against oxidative stress. *J. Biol. Chem.* 280: 25735–25742.
31. Nambi, S., J. E. Long, B. B. Mishra, R. Baker, K. C. Murphy, A. J. Olive, H. P. Nguyen, S. A. Shaffer, and C. M. Sasseti. 2015. The oxidative stress network of *Mycobacterium tuberculosis* reveals coordination between radical detoxification systems. *Cell Host Microbe* 17: 829–837.
32. Kumar, A., A. M. Balakrishna, W. Nartey, M. S. S. Manimekalai, and G. Grüber. 2016. Redox chemistry of *Mycobacterium tuberculosis* alkylhydroperoxide reductase E (AhpE): structural and mechanistic insight into a mycoredoxin-1 independent reductive pathway of AhpE via mycothiol. *Free Radic. Biol. Med.* 97: 588–601.
33. Edwards, K. M., M. H. Cynamon, R. K. Voladri, C. C. Hager, M. S. DeStefano, K. T. Tham, D. L. Lakey, M. R. Bochan, and D. S. Kernodle. 2001. Iron-cofactored superoxide dismutase inhibits host responses to *Mycobacterium tuberculosis*. *Am. J. Respir. Crit. Care Med.* 164: 2213–2219.
34. Saini, V., B. M. Cumming, L. Guidry, D. A. Lamprecht, J. H. Adamson, V. P. Reddy, K. C. Chinta, J. H. Mazorodze, J. N. Glasgow, M. Richard-Greenblatt, et al. 2016. Ergothioneine maintains redox and bioenergetic homeostasis essential for drug susceptibility and virulence of *Mycobacterium tuberculosis*. *Cell Rep.* 14: 572–585.
35. Colangeli, R., A. Haq, V. L. Arcus, E. Summers, R. S. Magliozzo, A. McBride, A. K. Mitra, M. Radjainia, A. Khajo, W. R. Jacobs, Jr., et al. 2009. The multifunctional histone-like protein Lsr2 protects mycobacteria against reactive oxygen intermediates. *Proc. Natl. Acad. Sci. USA* 106: 4414–4418.
36. Cooper, A. M., B. H. Segal, A. A. Frank, S. M. Holland, and I. M. Orme. 2000. Transient loss of resistance to pulmonary tuberculosis in p47^{phox} mice. *Infect. Immun.* 68: 1231–1234.
37. Rosenberger, C. M., and B. B. Finlay. 2002. Macrophages inhibit *Salmonella typhimurium* replication through MEK/ERK kinase and phagocyte NADPH oxidase activities. *J. Biol. Chem.* 277: 18753–18762.
38. Fishbein, S., N. van Wyk, R. M. Warren, and S. L. Sampson. 2015. Phylogeny to function: PE/PPE protein evolution and impact on *Mycobacterium tuberculosis* pathogenicity. *Mol. Microbiol.* 96: 901–916.
39. Honaker, R. W., R. L. Leistikow, I. L. Bartek, and M. I. Voskuil. 2009. Unique roles of DosT and DosS in DosR regulon induction and *Mycobacterium tuberculosis* dormancy. *Infect. Immun.* 77: 3258–3263.
40. Homolka, S., S. Niemann, D. G. Russell, and K. H. Rohde. 2010. Functional genetic diversity among *Mycobacterium tuberculosis* complex clinical isolates: delineation of conserved core and lineage-specific transcriptomes during intracellular survival. *PLoS Pathog.* 6: e1000988.
41. Bhat, K. H., S. Srivastava, S. K. Kotturu, S. Ghosh, and S. Mukhopadhyay. 2017. The PPE2 protein of *Mycobacterium tuberculosis* translocates to host nucleus and inhibits nitric oxide production. *Sci. Rep.* 7: 39706.
42. Khan, N., S. S. Rahim, C. S. Boddupalli, S. Ghousunnissa, S. Padma, N. Pathak, D. Thiagarajan, S. E. Hasnain, and S. Mukhopadhyay. 2006. Hydrogen peroxide inhibits IL-12 p40 induction in macrophages by inhibiting c-rel translocation to the nucleus through activation of calmodulin protein. *Blood* 107: 1513–1520.
43. Fulciniti, M., S. Amin, P. Nanjappa, S. Rodig, R. Prabhala, C. Li, S. Minville, Y. T. Tai, P. Tassone, H. Avet-Loiseau, et al. 2011. Significant biological role of spl1 transactivation in multiple myeloma. *Clin. Cancer Res.* 17: 6500–6509.
44. Daniel, P. M. 2017. The correlation of plasma proteins binding capacity and flavopiridol cellular and clinical trial studies. *Biomed. Spectrosc. Imaging* 6: 59–73.
45. Bhat, K. H., A. Ahmed, S. Kumar, P. Sharma, and S. Mukhopadhyay. 2012. Role of PPE18 protein in intracellular survival and pathogenicity of *Mycobacterium tuberculosis* in mice. *PLoS One* 7: e26201.
46. Gluschko, A., M. Herb, K. Wiegmann, O. Krut, W. F. Neiss, O. Utermöhlen, M. Krönke, and M. Schramm. 2018. The β_2 integrin mac-1 induces protective Lc3-associated phagocytosis of *Listeria monocytogenes*. *Cell Host Microbe* 23: 324–337.e5.
47. Lejal, N., S. Truchet, E. Bechor, E. Bouguyon, V. Khedkar, N. Bertho, J. Vidic, P. Adenot, S. Solier, E. Pick, and A. Slama-Schwok. 2018. Turning off NADPH oxidase-2 by impeding p67^{phox} activation in infected mouse macrophages reduced viral entry and inflammation. *Biochim. Biophys. Acta Gen. Subj.* 1862: 1263–1275.
48. Ostuni, M. A., M. Gelinotte, T. Bizouarn, L. Baciou, and C. Houée-Levin. 2010. Targeting NADPH-oxidase by reactive oxygen species reveals an initial sensitive step in the assembly process. *Free Radic. Biol. Med.* 49: 900–907.
49. Lapouge, K., S. J. Smith, Y. Groemping, and K. Rittinger. 2002. Architecture of the p40-p47-p67^{phox} complex in the resting state of the NADPH oxidase. A central role for p67^{phox}. *J. Biol. Chem.* 277: 10121–10128.
50. Lam, G. Y., R. Fattouh, A. M. Muise, S. Grinstein, D. E. Higgins, and J. H. Brumell. 2011. Listeriolysin O suppresses phospholipase C-mediated activation of the microbicidal NADPH oxidase to promote *Listeria monocytogenes* infection. *Cell Host Microbe* 10: 627–634.
51. Smimov, A., K. P. Daily, and A. K. Criss. 2014. Assembly of NADPH oxidase in human neutrophils is modulated by the opacity-associated protein expression State of *Neisseria gonorrhoeae*. *Infect. Immun.* 82: 1036–1044.
52. Crowther, J. E., V. K. Kutala, P. Kuppasamy, J. S. Ferguson, A. A. Beharka, J. L. Zweier, F. X. McCormack, and L. S. Schlesinger. 2004. Pulmonary surfactant protein A inhibits macrophage reactive oxygen intermediate production in response to stimuli by reducing NADPH oxidase activity. *J. Immunol.* 172: 6866–6874.
53. Zielonka, J., M. Zielonka, A. Sikora, J. Adamus, J. Joseph, M. Hardy, O. Ouari, B. P. Dranka, and B. Kalyanaraman. 2012. Global profiling of reactive oxygen and nitrogen species in biological systems: high-throughput real-time analyses. *J. Biol. Chem.* 287: 2984–2995.
54. Verrall, A. J., M. Schneider, B. Alisjahbana, L. Apriani, A. van Laarhoven, V. A. C. M. Koeken, S. van Dorp, E. Diadani, F. Utama, R. F. Hannaway, et al. 2019. Early clearance of *Mycobacterium tuberculosis* is associated with increased innate immune responses. *J. Infect. Dis.*
55. Karimi, G., C. Houée Levin, M. C. Dagher, L. Baciou, and T. Bizouarn. 2014. Assembly of phagocyte NADPH oxidase: a concerted binding process? *Biochim. Biophys. Acta* 1840: 3277–3283.
56. Meijles, D. N., L. M. Fan, B. J. Howlin, and J. M. Li. 2014. Molecular insights of p47^{phox} phosphorylation dynamics in the regulation of NADPH oxidase activation and superoxide production. *J. Biol. Chem.* 289: 22759–22770.

57. Mizrahi, A., Y. Berdichevsky, Y. Ugolev, S. Molshanski-Mor, Y. Nakash, I. Dahan, N. Alloul, Y. Gorzalczany, R. Sarfstein, M. Hirshberg, and E. Pick. 2006. Assembly of the phagocyte NADPH oxidase complex: chimeric constructs derived from the cytosolic components as tools for exploring structure-function relationships. *J. Leukoc. Biol.* 79: 881–895.
58. Khan, A. A. 2014. *In silico* prediction of *Escherichia coli* proteins targeting the host cell nucleus, with special reference to their role in colon cancer etiology. *J. Comput. Biol.* 21: 466–475.
59. Saksela, K., and P. Permi. 2012. SH3 domain ligand binding: what's the consensus and where's the specificity? *FEBS Lett.* 586: 2609–2614.
60. Vazquez-Torres, A., J. Jones-Carson, P. Mastroeni, H. Ischiropoulos, and F. C. Fang. 2000. Antimicrobial actions of the NADPH phagocyte oxidase and inducible nitric oxide synthase in experimental salmonellosis. I. Effects on microbial killing by activated peritoneal macrophages *in vitro*. *J. Exp. Med.* 192: 227–236.
61. Laroux, F. S., X. Romero, L. Wetzler, P. Engel, and C. Terhorst. 2005. Cutting edge: MyD88 controls phagocyte NADPH oxidase function and killing of gram-negative bacteria. *J. Immunol.* 175: 5596–5600.
62. Uchiyama, S., S. Döhrmann, A. M. Timmer, N. Dixit, M. Ghochani, T. Bhandari, J. C. Timmer, K. Sprague, J. Bubeck-Wardenburg, S. I. Simon, and V. Nizet. 2015. Streptolysin O rapidly impairs neutrophil oxidative burst and antibacterial responses to group A *Streptococcus*. *Front. Immunol.* 6: 581.
63. Hata, K., K. Takeshige, and H. Sumimoto. 1997. Roles for proline-rich regions of p47^{phox} and p67^{phox} in the phagocyte NADPH oxidase activation *in vitro*. *Biochem. Biophys. Res. Commun.* 241: 226–231.
64. Mizuki, K., R. Takeya, F. Kuribayashi, I. Nobuhisa, D. Kohda, H. Nunoi, K. Takeshige, and H. Sumimoto. 2005. A region C-terminal to the proline-rich core of p47^{phox} regulates activation of the phagocyte NADPH oxidase by interacting with the C-terminal SH3 domain of p67^{phox}. *Arch. Biochem. Biophys.* 444: 185–194.
65. de Mendez, I., A. G. Adams, R. A. Sokolic, H. L. Malech, and T. L. Leto. 1996. Multiple SH3 domain interactions regulate NADPH oxidase assembly in whole cells. *EMBO J.* 15: 1211–1220.
66. Wang, G., G. P. Wylie, P. D. Twigg, D. L. Caspar, J. R. Murphy, and T. M. Logan. 1999. Solution structure and peptide binding studies of the C-terminal src homology 3-like domain of the diphtheria toxin repressor protein. *Proc. Natl. Acad. Sci. USA* 96: 6119–6124.
67. Bilwes, A. M., L. A. Alex, B. R. Crane, and M. I. Simon. 1999. Structure of CheA, a signal-transducing histidine kinase. *Cell* 96: 131–141.
68. Su, Y. C., K. H. Chin, H. C. Hung, G. H. Shen, A. H. Wang, and S. H. Chou. 2010. Structure of *Stenotrophomonas maltophilia* FeoA complexed with zinc: a unique prokaryotic SH3-domain protein that possibly acts as a bacterial ferrous iron-transport activating factor. *Acta Crystallogr. Sect. F Struct. Biol. Cryst. Commun.* 66: 636–642.
69. Wylie, G. P., V. Rangachari, E. A. Bienkiewicz, V. Marin, N. Bhattacharya, J. F. Love, J. R. Murphy, and T. M. Logan. 2005. Prolylpeptide binding by the prokaryotic SH3-like domain of the diphtheria toxin repressor: a regulatory switch. *Biochemistry* 44: 40–51.
70. Feese, M. D., B. P. Ingason, J. Goranson-Siekierke, R. K. Holmes, and W. G. Hol. 2001. Crystal structure of the iron-dependent regulator from *Mycobacterium tuberculosis* at 2.0-Å resolution reveals the Src homology domain 3-like fold and metal binding function of the third domain. *J. Biol. Chem.* 276: 5959–5966.
71. Sareila, O., T. Kelkka, A. Pizzolla, M. Hultqvist, and R. Holmdahl. 2011. NOX2 complex-derived ROS as immune regulators. *Antioxid. Redox Signal.* 15: 2197–2208.
72. Mantegazza, A. R., A. Savina, M. Vermeulen, L. Pérez, J. Geffner, O. Hermine, S. D. Rosenzweig, F. Faure, and S. Amigorena. 2008. NADPH oxidase controls phagosomal pH and antigen cross-presentation in human dendritic cells. *Blood* 112: 4712–4722.
73. Savina, A., C. Jancic, S. Hugues, P. Guernonprez, P. Vargas, I. C. Moura, A. M. Lennon-Duménil, M. C. Seabra, G. Raposo, and S. Amigorena. 2006. NOX2 controls phagosomal pH to regulate antigen processing during cross-presentation by dendritic cells. *Cell* 126: 205–218.
74. Harrieff, M. J., G. E. Purdy, and D. M. Lewinson. 2012. Escape from the phagosome: the explanation for MHC-I processing of mycobacterial antigens? *Front. Immunol.* 3: 40.
75. Houben, D., C. Demangel, J. van Ingen, J. Perez, L. Baldeón, A. M. Abdallah, L. Caleechurn, D. Bottai, M. van Zon, K. de Punder, et al. 2012. ESX-1-mediated translocation to the cytosol controls virulence of mycobacteria. *Cell. Microbiol.* 14: 1287–1298.
76. Lee, J., T. Repasy, K. Papavinasundaram, C. Sasseti, and H. Kornfeld. 2011. *Mycobacterium tuberculosis* induces an atypical cell death mode to escape from infected macrophages. *PLoS One* 6: e18367.
77. Corleis, B., D. Korb, R. Wilson, J. Bylund, R. Chee, and U. E. Schaible. 2012. Escape of *Mycobacterium tuberculosis* from oxidative killing by neutrophils. *Cell. Microbiol.* 14: 1109–1121.
78. Alves, C. M., D. A. Silva, A. E. Azzolini, C. M. Marzocchi-Machado, Y. M. Lucisano-Valim, M. C. Roque-Barreira, and J. R. Mineo. 2013. Galectin-3 is essential for reactive oxygen species production by peritoneal neutrophils from mice infected with a virulent strain of *Toxoplasma gondii*. *Parasitology* 140: 210–219.
79. Yang, C. T., C. J. Cambier, J. M. Davis, C. J. Hall, P. S. Crosier, and L. Ramakrishnan. 2012. Neutrophils exert protection in the early tuberculous granuloma by oxidative killing of mycobacteria phagocytosed from infected macrophages. *Cell Host Microbe* 12: 301–312.
80. McCaffrey, R. L., J. T. Schwartz, S. R. Lindemann, J. G. Moreland, B. W. Buchan, B. D. Jones, and L. A. Allen. 2010. Multiple mechanisms of NADPH oxidase inhibition by type A and type B *Francisella tularensis*. *J. Leukoc. Biol.* 88: 791–805.
81. Vlahos, R., J. Stambas, and S. Selemidis. 2012. Suppressing production of reactive oxygen species (ROS) for influenza A virus therapy. *Trends Pharmacol. Sci.* 33: 3–8.
82. Baptista, R., D. M. Fazakerley, M. Beckmann, L. Baillie, and L. A. J. Mur. 2018. Untargeted metabolomics reveals a new mode of action of pretomanid (PA-824). *Sci. Rep.* 8: 5084.